ON ENHANCING THE PERFORMANCE OF ION DRAG ELECTROHYDRODYNAMIC (EHD) MICROPUMPS

ON ENHANCING THE PERFORMANCE OF ION DRAG ELECTROHYDRODYNAMIC (EHD) MICROPUMPS

BY

MD. KAMRUL RUSSEL, B.Sc., M.A.Sc.

A Thesis
Submitted to the School of Graduate Studies
in Partial Fulfillment of the Requirements
for the Degree
Doctor of Philosophy
McMaster University

DOCTOR OF PHILOSOPHY (2016) McMaster University

(Mechanical Engineering) Hamilton, Ontario, Canada

TITLE	On enhancing the performance of ion drag electrohydrodynamic (EHD) micropumps
AUTHOR	Md. Kamrul Russel B.Sc., Mechanical Engineering, Bangladesh University of Engineering & Technology (BUET) M.A.Sc., Mechanical Engineering, McMaster University
SUPERVISOR	Professor \ Chan Y. Ching Department of Mechanical Engineering
SUPERVISOR	Professor \ Ponnambalam (Ravi) Selvaganapathy Department of Mechanical Engineering
NUMBER OF PAGES	xiii, 147

ABSTRACT

Electrohydrodynamic (EHD) micropumps have been developed and used in many diverse applications such as in microscale liquid cooling and various microfluidic systems. The objective of this research is to investigate different methods of enhancing the performance of ion drag EHD micropumps. In particular, the effect of electrode surface topology, applied electric field and doping agent in the dielectric liquid were investigated. The effect of 3D sharp features on the electrodes on charge injection in HFE 7100 as dielectric fluid was studied under an applied DC electric field. Micro and nano-scale features with high aspect ratio were developed on smooth copper electrodes by chemical etching or through electrophoretic deposition of single walled carbon nanotube (SWCNT). The spacing between the electrodes was kept at 250 μm. A reduction factor of 5 was achieved for SWCNT electrodes compared to the smooth case for the onset of charge injection. This study was then extended to determine its effects on the performance of ion drag EHD micropumps with 100 pairs of interdigitated electrodes. The emitter electrodes (20 μm) were half the width of the collector electrodes (40 μm), with one pump having an inter-electrode spacing of 120 μm and the other with 40 μm. Each micropump had a width of 5 mm and a height of 100 μm. SWCNT was deposited on the emitter electrodes of the micropump to generate a maximum static pressure of 4.7 kPa at 900 V, which is a 5 fold increase compared to the pump with smooth electrodes. Flow rate at no back pressure condition was improved by a factor of 3. The effect of Ferrocene as a doping agent in the working fluid HFE 7100 was studied under DC voltages. A maximum static pressure of 6.7 kPa was achieved at 700 V with 0.2% weight based doping agent, 11 times higher than when there was no doping agent at the same

applied voltage. When there was no back pressure the pump generated a maximum flow rate of 0.47 mL/min at 700 V with 0.05% doping agent which is 9 times greater than with no doping agent. The effect of pulsed voltage on the performance of ion drag EHD micropump has been studied to exploit the displacement current at the sudden change of applied voltage magnitude. A range of pulse repetition rate and duty cycle were found to significantly enhance the pump performance. Static pressure generation was up to 75% and 88% greater at an optimal pulse repetition rate and duty cycle, respectively, compared to the average of the two DC levels. The effect of external flow on the discharge characteristics of an injection micropump was studied with DC volts. Higher discharge current and lower threshold voltage for the onset of charge injection in case of co-flow compared to the static case was observed. There was an optimum flow rate to generate maximum current for both co and counter-flow cases.

ACKNOWLEDGEMENTS

The author would like to acknowledge his gratitude and respect to his supervisors Dr. Ponnambalam (Ravi) Selvaganapathy and Dr. Chan Y. Ching for their supervision, guidance, motivation and support throughout the course of his studies and stay at McMaster University. The author is grateful to Dr. Daniel Ewing, a great scientist and mentor, for his teaching of critical thinking on analytical and technical issues in last many years. The author is also grateful to members of the supervisory committee, Dr. Leyla Soleymani and Dr. James S. Cotton for their valuable guidance, suggestions and critical comments during the course of the study.

The author is also thankful to the technicians in the Mechanical Engineering department Joe Verhaeghe, J. P. Talon, Mark Mackenzie, Ron Lodewyks, John Colenbrander, Michael Lee, Dan Wright who provided valuable help at many points during this thesis. The author is also thankful to Doris Stevanovic and Zhilin Peng of CEDT, department of Engineering Physics, for their training and suggestions in microfabrication.

The author would like to express his gratitude to all his friends and colleagues in his research laboratories: Centre for Advanced Micro Electro Fluidics (CAMEF) and Thermal Management Research Laboratory (TMRL) for their continuous support throughout the course of his graduate programs. The author also would like to express his sincere gratitude to his parents, who always encouraged and supported him in all his difficulties. The support from his wife Zakia and son Zaayan is priceless to the author without which it would had been impossible to accomplish many achievements.

TABLE OF CONTENTS

ABSTRACT ..... **iii**
ACKNOWLEDGEMENTS ..... **v**
TABLE OF CONTENTS ..... **vi**
LIST OF FIGURES ..... **viii**
LIST OF TABLES ..... **xii**
Chapter 1 ..... **1**
Introduction **1**
1.1 Motivation and Research Objectives 5
1.2 Thesis Outline 6
1.3 A Note to the Reader 9
1.4 References 10
Chapter 2 ..... **14**
Effect of electrode surface topology on charge injection characteristics in dielectric liquids: an experimental study **14**
2.1 Introduction 16
2.2 Experimental Methodology 19
2.3 Results and Discussion 24
2.4 Conclusions 32
2.5 References 34
Chapter 3 ..... **37**
Electrohydrodynamic injection micropump with composite gold and single-walled carbon nanotube electrodes **37**
3.1 Introduction 39
3.2 Fabrication and Experimental Methodology 43
3.3 Results and Discussion 49
3.4 Conclusion 60
3.5 References 62
Chapter 4 ..... **67**

Effect of doping ferrocene in the working fluid of electrohydrodynamic (EHD) micropump..... 67
4.1 Introduction 69
4.2 Experimental Methodology 74
4.3 Results and Discussion 79
4.4 Conclusions 88
4.5 References 90
Chapter 5 95
Ion drag electrohydrodynamic (EHD) micro-pumps under a pulsed voltage..... 95
5.1 Introduction 97
5.2 Microfabrication & Experimental Methodology 103
5.3 Results and Discussion 106
5.4 Conclusion 121
5.5 References 122
Chapter 6 126
Effect of external fluid flow on discharge characteristics in a dielectric liquid with planar electrode configuration..... 126
6.1 Introduction 127
6.2 Experimental Facility 130
6.3 Results and Discussion 132
6.4 Conclusions 139
6.5 References 140
Chapter 7 142
Summary and Conclusions..... 142
7.1 Summary and Conclusions 142
7.2 Research Contributions 145
7.3 Recommendations for Future Work 146

LIST OF FIGURES

Fig. 2.1: Typical current-voltage (I-V) characteristics in a dielectric liquid. I-Ohmic; II-Quasi Ohmic; III-Injection; IV-Breakdown..... 17

Fig. 2.2: Schematic of the experimental facility..... 20

Fig. 2.3: Schematic of different surface configurations of the copper electrode pair (SWCNT(S) and SWCNT(E) refer to SWCNT deposited on a smooth and etched surface respectively). 21

Fig. 2.4: SEM images of different electrode surfaces. 23

Fig. 2.5: I-V characteristics of different applied polarity for etched-etched configuration. E1 and E2 refer to the two different etched electrodes. Δ E2 negative-E1 ground, □ E1 negative-E2 ground, ◊ E2 positive-E1 ground and ○ E1 positive-E2 ground. 25

Fig. 2.6: I-V characteristics of different applied polarity to smooth-etched configuration. ○ Etched negative-Smooth ground, □ Etched positive-Smooth ground, Δ Smooth negative-Etched ground and ◊ Smooth positive-Etched ground..... 26

Fig. 2.7: I-V characteristics of different combinations of parallel Cu electrode surfaces 250 μm apart. x Smooth-Smooth, ○ Etched-Etched, Δ Smooth-Etched, ◊ SWCNT (on smooth)-Smooth and □ SWCNT (on etched)-Smooth configuration..... 28

Fig. 3.1: Schematic of (a) ion drag EHD micropump (the total number of electrode pairs is 100 but only 5 pairs are shown for reference) and (b) dimensional specifications (not to scale). d_{ec} = 120 and 40 μm for the two different pumps. 44

Fig. 3.2: SEM images of electrodes with (a) no deposition and (b) SWCNT deposited. Scale bar = 2 μm. 45

Fig. 3.3: Schematic of the experimental facility (a) electric connections with the top view of the micropump electrodes (b) static pressure head measurement with the side view of the electrodes (c) flow velocity measurement at a back pressure equivalent to a height of Δh. (The number of electrode pairs is 100 but only 5 pairs are shown in the schematic as reference only.)..... 47

Fig. 3.4: I-V characteristics for ○ smooth electrodes and □ SWCNT deposited on emitter electrodes at static condition for the pump with inter-electrode spacing of 120 μm. 50

Fig. 3.5: Static pressure generated at different applied voltage for ○ smooth electrodes and □ SWCNT deposited on emitter electrodes for the pump with inter-electrode spacing of 120 μm. 52

Fig. 3.6: Static pressure generated at different input power for ○ smooth electrodes and □ SWCNT deposited on emitter electrodes for the pump with inter-electrode spacing of 120 μm. 53

Fig. 3.7: Flow rate at no back pressure condition at different applied voltage for ○ smooth electrodes and □ SWCNT deposited on emitter electrodes for the pump with inter-electrode spacing of 120 μm. 55

Fig. 3.8: Pressure vs flow characteristics of the pump with ○ smooth electrodes and □ SWCNT deposited on emitter electrodes at an applied voltage of 1100 volts with inter-electrode spacing of 120 μm..... 56

Fig. 3.9: I-V characteristics for ○ smooth electrodes and □ SWCNT deposited on emitter electrodes at static condition for the pump with inter-electrode spacing of 40 μm. 57

Fig. 3.10: Static pressure generated at different applied voltage for ○ smooth electrodes and □ SWCNT deposited on emitter electrodes for the pump with inter-electrode spacing of 40 μm. 58

Fig. 3.11: Static pressure generated at different input power for ○ smooth electrodes and □ SWCNT deposited on emitter electrodes for the pump with inter-electrode spacing of 40 μm. 59

Fig. 4.1: Schematic of the cross section of the pump with key dimensions (not to scale). The total number of electrode pairs is 100 but only 2 pairs are shown for reference..... 75

Fig. 4.2: Schematic of the experimental facility (a) electric connections with the top view of the micropump electrodes (b) static pressure head measurement with the side view of the electrodes (c) flow velocity measurement facility at a back pressure

equivalent to a height of Δh. (the number of electrode pairs is 100 but only 5 pairs are shown in the schematic for clarity) 77

Fig. 4.3: Variation of current with applied DC voltage for (*white square*) HFE-0.0, (*white circle*) HFE-0.05, (*white diamond*) HFE-0.1 and (*white triangle*) HFE-0.2 80

Fig. 4.4: Variation of static pressure with applied DC voltage for (*white square*) HFE-0.0, (*white circle*) HFE-0.05, (*white diamond*) HFE-0.1 and (*white triangle*) HFE-0.2 82

Fig. 4.5: Static pressure at an applied voltage of 600 V over time for HFE-0.05 83

Fig. 4.6: Power consumption to generate pumping pressure for (*white square*) HFE-0.0, (*white circle*) HFE-0.05, (*white diamond*) HFE-0.1 and (*white triangle*) HFE-0.2 84

Fig. 4.7: Variation of flow rate of HFE-0.0 (*open symbols*) and HFE- 0.05 (*filled symbols*) with applied DC voltage for back pressure of (*white square*, *black square*) 0 Pa, (*white circle*, *black circle*) 145 Pa, (*white diamond*, *black diamond*) 290 Pa and (*plus*) 726 Pa, (*black down-point triangle*) 580 Pa, (*black left-point triangle*) 1016 Pa..... 86

Fig. 4.8: Pump characteristic curve of pressure vs flow rate for (*black triangle*) HFE-0.0 and (*black circle*) HFE-0.05 at an applied voltage of 1.41 * V_{th} 87

Fig. 5.1: Schematic of (a) EHD micropump and (b) cross sectional view (dimensions not 104

Fig. 5.2: Experimental current response to a step voltage of 800 V DC with time. 107

Fig. 5.3: Variation of □ current and ○ static pressure with applied DC voltage for HFE-7100 as working fluid. 108

Fig. 5.4: (a) Time trace of the current of one complete cycle (sampling rate 200 KSa/sec). (b & c) zoomed in view of the transient current. D_C = 50%, V_L = 700 V and V_H = 800 V for f = 0.1 Hz. 111

Fig. 5.5: Variation of current as a function of pulse repetition rate with D_C = 50 %, □ pulse magnitude of 100 V (V_L = 700V & V_H = 800 V) and ○ pulse magnitude of 200 V (V_L = 700V & V_H = 900 V). Current at an applied DC voltage of — - — 700 V, – – 800 V and — 900 V. 113

Fig. 5.6: Variation of pressure as a function of pulse repetition rate with D_C = 50 % for □ V_L = 700V & V_H = 800 V, ○ V_L = 700V & V_H = 900 V and Δ V_L = 400V & V_H = 500 V..... 114

Fig. 5.7: Ratio of displacement (I_{dis}) to the average of the steady current of the half cycle of a pulse voltage ($I_{avg\_steady\_pulse}$) with D_C = 50 %, V_L = 700V and V_H = 800 V at different pulse repetition rate (f). 117

Fig. 5.8: Variation of current with duty cycle for with f = 0.1 Hz, V_L = 700 V and V_H = 800 V. (Steady state current at an applied DC voltage of – – 700 V and — 800 V are also presented for comparison.). 119

Fig. 5.9:Variation of pressure with duty cycle for with f = 0.1 Hz, V_L = 700V and V_H = 800 V. (Pressure at an applied DC voltage of – – 700V and — 800V are also presented for comparison)..... 120

Fig. 6.1: Schematic of (a) interdigitated electrodes and (b) cross sectional view (dimensions not to scale). 131

Fig. 6.2: Discharge characteristics in HFE 7100 with applied DC voltage at *Re* of: (circle) 0, (triangle) 1.31, (square) 2.61, (diamond) 5.19, (cross) 7.85, (down point triangle) 10.43 and (pentagon) 13.1. (a) Open symbols for co-flow and (b) filled symbols for counter-flow direction..... 134

Fig. 6.3:Discharge current at different flow rates within conduction regime. (square) 100V, (circle) 300V and (triangle) 500V. Open symbols represent co-flow, filled symbols represent counter-flow..... 136

Fig. 6.4: Discharge current at different flow rates within injection regime. (square) 1300V, (circle) 1400V and (triangle) 1500V. Open symbols represent co-flow, filled symbols represent counter-flow. 138

LIST OF TABLES

Table 2.1: Properties of HFE 7100 at 25 °C 20
Table 2.2: Threshold voltage and slope of I-V curve for different electrode configurations 30
Table 3.1: Properties of HFE 7100 at 25 °C [28] 48
Table 4.1: Properties of HFE-7100 at 25 °C (El-Genk and Bostanci 2003) 75
Table 4.2: Properties of ferrocene (Sigma-Aldrich) 75
Table 5.1: Properties of HFE-7100 110
Table 6.1: Threshold voltage and slope of I-V curve at different Reynolds number at *co-flow* condition 133
Table 6.2: Threshold voltage and slope of I-V curve at different Reynolds number at *counter-flow* condition 133

NOMENCLATURE

Symbols

DC	Direct current
D_C	Duty cycle (%)
E	Electric field (Vm^{-1})
f	Pulse repetition rate (Hz)
h	Height of the liquid level in inlet or outlet tube of the pump (m)
I	Electric current (μAmps, nAmps)
j	Electric current density (Am^{-2})
k	Ionic mobility of charges in dielectric liquid ($m^2V^{-1}s^{-1}$)
L_c	Characteristic length (m)
M	Ratio of EHD to ionic mobility
P	Pressure (Pa)
P_{in}	Input power (mWatts)
q	Charge density (Cm^{-3})
Q	Liquid flow rate (μL/min, mL/min)
Re	Reynolds number
R_z	Mean peak to valley roughness (μm)
t	Time (s, min)
t_{diff}	Time constant of viscous diffusion (s)
w	Fluid local velocity due to applied electric field (m/s)
W	External flow felocity (m/s)
Δ	Difference

Greek Symbols

ε	Electric permittivity of dielectric liquid (F/m)
v	Kinematic viscosity of dielectric liquid (m^2/s)
ρ	Density of dielectric liquid (Kgm^{-3})
σ	Conductivity of dielectric liquid ($Sm^{-1} = \Omega^{-1}m^{-1}$)
τ	Charge relaxation time (s)

Subscripts

c	Critical
dis	Displacement
H	High
L	Low
max	Maximum
opt	Optimum
ss	Steady state
th	Threshold

Chapter 1
Introduction

Thermal management of electronic devices is becoming increasingly more challenging due to high heat dissipation rates as the circuit packaging density and number of transistors increase. For example, high performance chips used in military defense are currently dissipating over 1000 W/cm^2 (Mudawar 2001; Ebadian and Lin 2011) and the heat flux in such electronics is expected to exceed 2500 W/cm^2 in the near future (Ebadian and Lin 2011). Conventional cooling techniques which typically use natural and forced convection with heat pipes in these applications are becoming inadequate due to their limits to transfer and dissipate heat.

A detailed literature survey is presented by Ebadian and Lin (2011), where electronics were classified based on their heat dissipation: (i) high heat flux (HHF): 10^2 – 10^3 W/cm^2, (ii) ultra-high heat flux (UHF): 10^3 – 10^4 W/cm^2 and (iii) extreme heat flux (HHF): $>10^4$ W/cm^2. Thermal management of electronics dissipating HHF has been performed using heat pipes, mini/micro-channel liquid cooling, porous material, jet impingement, spray cooling and flow boiling. Review papers on mini/micro-channel cooling under single and two phase flow conditions can be found in Bertsch et al. (2008), Cheng et al. (2009), Roday and Jensen (2009) and Kandlikar (2012) and on jet impingement, porous material and spray cooling in Kim (2007), Weigand and Spring (2011), Smakulski and Pietrowicz (2016). A review of HHF thermal management was

performed by Agostini et al. (2007) and Kandlikar et al. (2007) where multiple cooling techniques such as single and two phase liquid flow in microchannels, porous media and jet impingement, spray cooling are discussed. Examples include, but not limited to, first microchannel liquid cooling of 790 Wcm^{-2} by Tuckerman and Pease (1981) for HHF application, spray cooling with modified surface topology by Pais et al. (1992) of 1.2 $kWcm^{-2}$ and jet impingement cooling by Silverman et al. (2006) of 2 $kWcm^{-2}$for UHF applications. Ebadian and Lin (2011) suggested single phase cooling as the most viable method for practical HHF applications, while two phase cooling being most promising for future HHF electronic devices.

Of the many available cooling mechanisms, microchannel (hydraulic diameter ≤ 1 mm (Mehendale, Jacobi et al. 2000)) liquid cooling is most promising for electronic packaging, as the working fluid is not physically in contact with the chip. It is also of interest due to their high surface area to volume ratio, higher heat transfer capability, low acoustic noise and compact design (Khan and Fartaj 2011). A significant amount of research has been done on microchannel liquid cooling since the first study on HHF applications by Tuckerman and Pease (1981). The parameters studied include channel geometry, material and working fluid for laminar and turbulent flows to find the corresponding friction factor and heat transfer coefficient. Additional information can be found in the recent review papers by Khan and Fartaj (2011) and Dixit and Ghosh (2015).

In any liquid cooling application the pump is a key component to drive the working fluid through the microchannel. In the laminar flow regime (which is the case

for most microfluidic devices), an order-of-magnitude decrease in the hydraulic diameter of the channel requires an increase in the pressure difference by two orders of magnitude to maintain a constant average flow velocity (Laser and Santiago 2004). There are various types of micro-pumps which can be broadly divided into two categories according to the manner and means to produce fluid flow and pressure: (i) mechanical and (ii) non-mechanical micro-pumps (Laser and Santiago 2004; Abhari, Jaafar et al. 2012). The mechanical micro-pumps need a mechanical actuator or a pumping mechanism while the non-mechanical ones have no moving parts and add/transform non-mechanical energy into kinetic momentum to drive the working fluid through the microchannel (Abhari, Jaafar et al. 2012). Examples of mechanical and non-mechanical micro-pumps would be ones that use a diaphragm and magnetohydrodynamic (MHD) or electrohydrodynamic (EHD) as the pumping mechanisms, respectively. These micropumps have been subdivided further into categories based on their actuation principle and discussed in depth in the review paper by Iverson and Garimella (2008) and Abhari et. al (2012) .

EHD micro-pumps are advantageous over other existing types since it is compact, has no moving parts, consumes lower power, are easier to control the fluid flow/pressure difference via controlling the applied electric potential. In EHD micro-pumps, space charges are introduced into the dielectric liquid which experiences the electric body force along the applied electric field. A dielectric liquid is defined as a material in which equal, but opposite, charged monopoles or dipoles are separated by neutral entities (Crowley 1991). Space charge can be produced because of inhomogeneities in the fluid, or through

dissociation or direct charge injection. These three mechanisms of the generation of space charge are associated with induction, conduction and injection EHD pumping respectively. The working dielectric liquid in induction type micro-pump has spatial variation in electrical conductivity and/or permittivity. Gradients in electrical conductivity can be obtained in several dielectric and some polar liquids by anisotropic heating or cooling of those liquids (Melcher and Firebaugh 1967) as their electrical conductivity is temperature dependent. On the other hand, sudden jumps in electrical permittivity and electrical conductivity can be obtained through the use of layers of non-mixing fluids (Melcher 1966) or suspended particles or bubbles (Wawzyniak, Seyed-Yagoobi et al. 2000) in the fluid. Conduction micro-pumps work on the principle of electric conduction of pure dielectric liquid which is associated with a reversible process of dissociation-recombination between a neutral electrolytic species (AB) and its corresponding positive (A^+) and negative (B^-) ions as (Atten and Seyed-Yagoobi 2003): $AB \leftrightarrow A^+ + B^-$. Dissociation and recombination rates are in dynamic equilibrium until a certain low applied electric field (typically ~ 1kV/cm) is reached; beyond which the rate of dissociation increases as the field increases while that of recombination remains constant being independent of the applied electric field (Castellanos 1998). These charges generated by dissociation are redistributed due to the applied electric field which results in heterocharge layers in the vicinity of the electrodes. The attraction between the electrode and the charges within the heterocharge layer induces a fluid motion near the electrode from the liquid side to the electrode side (Al Dini 2005). In injection micropumps, charges are injected at the metal-liquid interface directly from (to) metal

electrode to (from) dielectric liquid by electron tunneling when applied electric field is beyond a threshold value. These charges interact with the neutral molecules due to the applied field and drag the liquid along the electric field lines. A detailed review including working principles and applications of these kinds of EHD micropumps has been performed by Laser and Santiago (2004) and Abhari et al. (2012).

1.1 Motivation and Research Objectives

Induction pumping for compact electronics cooling is not applicable as it requires gradients in fluid permittivity or conductivity. Conduction pumping is not promising either in terms of pressure head generation to ensure a continuous supply of the dielectric liquid through the cooling circuit. Injection based ion-drag EHD pumping shows promising features and can be improved further to enhance the pump performance. The limitation of such micropumps is insufficient pumping head and flow rate for practical applications. In this thesis the primary objective is to investigate methods that can improve the performance of injection EHD micropumps.

Injection of electrons (which in turn reflects the amount of charges available) at the liquid-metal interface from (to) metal electrode to (from) the liquid, depends on the energy barrier set by the electrode material and the liquid under consideration and presents an excellent research scope. This energy barrier can be reduced by intensifying the electric field by modifying the electrode surface or by adding doping agent to the base liquid. More charges can be added to the liquid by exploiting the displacement current

due to the sudden change in applied voltage level when pulsed voltages, instead of DC voltage is used. The specific objectives of this thesis are:

1. To study the effect of electrode surface topology on charge injection characteristics in dielectric liquids and corresponding EHD micropump performance
2. To study the effect of doping agent on discharge characteristics and performance of an EHD micropump
3. To study the effect of pulsed voltage on an ion drag EHD micro-pump
4. To study the effect of fluid flow on charge injection in a dielectric liquid.

1.2 Thesis Outline

The thesis consists of four articles that have been published and one article under preparation for submission that address the key objectives of this study. An introduction chapter and a final chapter with the overall conclusions and recommendations are included. Each chapter consisting of the journal articles are organized as:

Chapter 2: This chapter contains the first published journal article titled "Effect of electrode surface topology on charge injection characteristics in dielectric liquids: an experimental study". In this paper the presence of 3D sharp features on discharge characteristics has been studied. The micro/nano protrusions were developed on the base smooth electrode by chemical etching or electrophoretic deposition of single walled carbon nanotube (SWCNT). The SWCNT used in this study was from Sigma Aldrich with 40-60 wt% carbon content and 30-35 wt% metal content. Though its electrical

properties were not available, it could have same order of magnitude electrical conductivity as the base metal, copper. A reduction in the experimental threshold voltage and increase in the discharge current upon application of the SWCNT in this study indicates them to be conductive in nature. Further investigation of CNT conductivity on charge injection could indicate the importance between the conductivity vs the sharpness.

Presence of sharp micro/nano features with small tip radius of curvature has been found to reduce the metal work function in vacuum in previous studies (Xue, Wang et al. 2013). An increase in charge enhancement has been found as a result (Qian, Liu et al. 2008). Though an optimum aspect ratio to result in maximum enhancement was reported, a quantitative study of the sharpness to initiate lowering of work function was not studied in previous or present research.

Chapter 3: The second published journal article titled "Electrohydrodynamic injection micropump with composite gold and single-walled carbon nanotube electrodes" is presented in this chapter. This journal article is the application of the findings in Chapter 2 towards an EHD micropump to study pump performance. SWCNT was deposited on the emitter electrodes of the pump and a static pressure of 4.7 kPa was obtained at 900 V.

Chapter 4: The third published journal article titled "Effect of doping ferrocene in the working fluid of electrohydrodynamic (EHD) micropumps" is presented in chapter 4. In this study Ferrocene was added to the base dielectric liquid (HFE 7100) based on weight percentage fluid. HFE 7100 is selected as the working fluid due to its low viscosity and relatively high dielectric constant to result in low shear stress and high electric body force respectively. This fluid is a good candidate as a thermal fluid due to its thermal properties

and is environmentally friendly compared to CFCs. Ferrocene is an organometallic compound which has an Iron (Fe) molecule sandwiched between two cyclopentadienyl ($C_5H_5^-$) rings. Ferrocene, as a doping agent, was selected in this study as it dissolved in HFE 7100 homogeneously and loses an electron upon application of electric field due to redox reaction without destroying its molecular bond. Discharge characteristics and pump performance of an EHD micropump was studied with different percentage of doping agent below saturation point. A maximum static pressure of 6.7 kPa and flow rate of 0.47 mL/min with no back pressure condition was obtained at 700V. The static pressure generated in this study is the maximum to date for an ion drag EHD micropump.

Chapter 5: This chapter contains the fourth published journal article titled "Ion drag electrohydrodynamic (EHD) micro-pumps under a pulsed voltage". In this study the effect of pulse voltage on discharge characteristics and pump performance has been studied. Both conduction and injection regimes have been considered. Better pump performance was observed for certain range of pulse repetition rate and duty cycle.

Chapter 6: This chapter contains the article "Effect of external fluid flow on discharge characteristics in a dielectric liquid with planar electrode configuration". In this chapter the discharge characteristics of a planar micropump as a function of external fluid flow has been studied. This study is of importance when (i) the ion drag EHD micropump is used as a heat sink along with another external mechanical pump or (ii) such ion drag EHD micropump is used as a booster pump with as external mechanical pump and heat sink for cooling applications. In both cases the external flow due to the mechanical pump

will have effect on the discharge characteristics of the EHD pump. An increase in charge injection was observed when fluid flow was introduced through the EHD micropump.

1.3 A Note to the Reader

As this thesis consists of a number of journal articles, the reader might find repetitive material in it. Some material in the introduction, fabrication of the micropump, experimental facility and measurement methodology in some of the chapters contain significant repetition since the same facility was used in all experiments. It is worth mentioning that the introduction in each chapter emphasizes and discusses related references appropriate to that journal article.

1.4 References

Abhari, F., H. Jaafar, et al. (2012). "A comprehensive study of micropumps technologies." Int. J. Electrochem. Sci **7**: 9765-9780.

Agostini, B., M. Fabbri, et al. (2007). "State of the art of high heat flux cooling technologies." Heat Transfer Engineering **28**(4): 258-281.

Al Dini, S. A. S. (2005). Electrohydrodynamic induction and conduction pumping of dielectric liquid film: theoretical and numerical studies, Texas A&M University.

Atten, P. and J. Seyed-Yagoobi (2003). "Electrohydrodynamically induced dielectric liquid flow through pure conduction in point/plane geometry." Dielectrics and Electrical Insulation, IEEE Transactions on **10**(1): 27-36.

Bertsch, S. S., E. A. Groll, et al. (2008). "Review and comparative analysis of studies on saturated flow boiling in small channels." Nanoscale and Microscale Thermophysical Engineering **12**(3): 187-227.

Castellanos, A. (1998). Electrohydrodynamics, Springer Verlag Wien.

Cheng, P., G. Wang, et al. (2009). "Recent work on boiling and condensation in microchannels." Journal of heat transfer **131**(4): 043211.

Crowley, J. M. (1991). Fundamentals of applied electrostatics, Krieger Pub. Co.(Malabar, Fla.).

Dixit, T. and I. Ghosh (2015). "Review of micro-and mini-channel heat sinks and heat exchangers for single phase fluids." Renewable and Sustainable Energy Reviews **41**: 1298-1311.

Ebadian, M. and C. Lin (2011). "A review of high-heat-flux heat removal technologies." Journal of heat transfer **133**(11): 110801.

Iverson, B. D. and S. V. Garimella (2008). "Recent advances in microscale pumping technologies: a review and evaluation." Microfluidics and nanofluidics **5**(2): 145-174.

Kandlikar, S. G. (2012). "History, advances, and challenges in liquid flow and flow boiling heat transfer in microchannels: a critical review." Journal of heat transfer **134**(3): 034001.

Kandlikar, S. G. and A. V. Bapat (2007). "Evaluation of jet impingement, spray and microchannel chip cooling options for high heat flux removal." Heat Transfer Engineering **28**(11): 911-923.

Khan, M. G. and A. Fartaj (2011). "A review on microchannel heat exchangers and potential applications." International journal of energy research **35**(7): 553-582.

Kim, J. (2007). "Spray cooling heat transfer: the state of the art." International Journal of Heat and Fluid Flow **28**(4): 753-767.

Laser, D. J. and J. G. Santiago (2004). "A review of micropumps." Journal of micromechanics and microengineering **14**(6): R35.

Mehendale, S., A. Jacobi, et al. (2000). "Fluid flow and heat transfer at micro-and meso-scales with application to heat exchanger design." Applied Mechanics Reviews **53**(7): 175-193.

Melcher, J. R. (1966). "Traveling-Wave Induced Electroconvection." Physics of Fluids **9**: 1548.

Melcher, J. R. and M. S. Firebaugh (1967). "Traveling-Wave Bulk Electroconvection Induced across a Temperature Gradient." Physics of Fluids **10**: 1178.

Mudawar, I. (2001). "Assessment of high-heat-flux thermal management schemes." IEEE Transactions on Components and Packaging Technologies **24**(2): 122-141.

Pais, M., L. Chow, et al. (1992). "Surface roughness and its effects on the heat transfer mechanism in spray cooling." Journal of heat transfer **114**(1): 211-219.

Qian, X., H. Liu, et al. (2008). "Effect of aspect ratio on field emission properties of ZnO nanorod arrays." Nanoscale research letters **3**(8): 303.

Roday, A. P. and M. K. Jensen (2009). "A review of the critical heat flux condition in mini-and microchannels." Journal of Mechanical Science and Technology **23**(9): 2529-2547.

Silverman, I., A. Yarin, et al. (2006). "High heat-flux accelerator targets: Cooling with liquid metal jet impingement." International journal of heat and mass transfer **49**(17): 2782-2792.

Smakulski, P. and S. Pietrowicz (2016). "A review of the capabilities of high heat flux removal by porous materials, microchannels and spray cooling techniques." Applied Thermal Engineering **104**: 636-646.

Tuckerman, D. B. and R. Pease (1981). "High-performance heat sinking for VLSI." IEEE Electron device letters **2**(5): 126-129.

Wawzyniak, M., J. Seyed-Yagoobi, et al. (2000). "An experimental study of electrohydrodynamic induction pumping of a stratified liquid/vapor medium."

Journal Name: Journal of Heat Transfer; Journal Volume: 122; Journal Issue: 1; Other Information: PBD: Feb 2000: Medium: X; Size: page(s) 200-203.

Weigand, B. and S. Spring (2011). "Multiple jet impingement− a review." Heat Transfer Research **42**(2).

Xue, M., W. Wang, et al. (2013). "Understanding of the correlation between work function and surface morphology of metals and alloys." Journal of Alloys and Compounds **577**: 1-5.

Chapter 2

Effect of electrode surface topology on charge injection characteristics in dielectric liquids: an experimental study

Complete citation:

Russel, M.K., Selvaganapathy, P.R., Ching, C.Y., 2014. Effect of electrode surface topology on charge injection characteristics in dielectric liquids: an experimental study. *J. Electrostatics*. 72: 487-492.

Relative Contributions:

Russel M.K.: Performed all experiments, interpretation and analysis of the data and wrote the drafts of the manuscript including all figures and text.

Selvaganapathy P.R.: Co-supervisor of M.K. Russel and revised the initial drafts of the manuscript.

Ching C. Y.: Co-supervisor of M.K. Russel and was responsible for the final draft submittal to the journal.

Abstract

Micro/nano scale features are incorporated on an electrode surface to study its effect on the charge injection characteristics in HFE7100. These features are generated on a smooth surface by chemical etching of the electrodes or through electrophoretic deposition of single walled carbon nanotubes (SWCNT). The threshold voltage for charge injection was reduced by a factor of 5 and 2 for the SWCNT and etched electrodes respectively, when compared to the smooth electrode configuration. The presence of sharp features on the surface with high aspect ratio had a more dominant effect on enhancing the charge injection than the roughness.

2.1 Introduction

The current-voltage (I-V) characteristic of a dielectric liquid is nonlinear and typically shows four regions: (i) Ohmic (ii) low slope quasi-Ohmic (iii) injection and finally (iv) electric breakdown [1] as shown schematically in Fig. 2.1. At relatively low applied potentials (region I), the electrical characteristic is Ohmic due to the presence of minute amounts of impurities in the dielectric liquid. In this region, current flow through the dielectric liquid occurs via the dissociated molecules of the impurity while the dissociation and recombination process remains in dynamic equilibrium. In region (II), at higher potentials, the rate of dissociation becomes greater than that of recombination thus causing imbalance within the dielectric liquid. Current flow in region II occurs due to the dissociated ions and hetero-charges created at the electrodes. This region is bounded by the threshold potential above which there is a sudden increase in current due to charge injection by electron tunneling (region III). If the applied voltage is increased further, the dielectric liquid breaks down and this potential is known as the breakdown voltage of the particular liquid, which is generally avoided in practical applications.

The required potential for the onset of charge injection is typically known as the threshold voltage. The charge injection in region (III) depends on the energy barrier set by the electrode material and the dielectric liquid. The energy barrier is a function of various factors such as electrode material and surface topology (i.e., work function), dielectric liquid (ionization energy) and inter-electrode distance. The effect of dissimilar electrode materials [2-5], electrode size/geometry [2-10] and presence of macro/micro

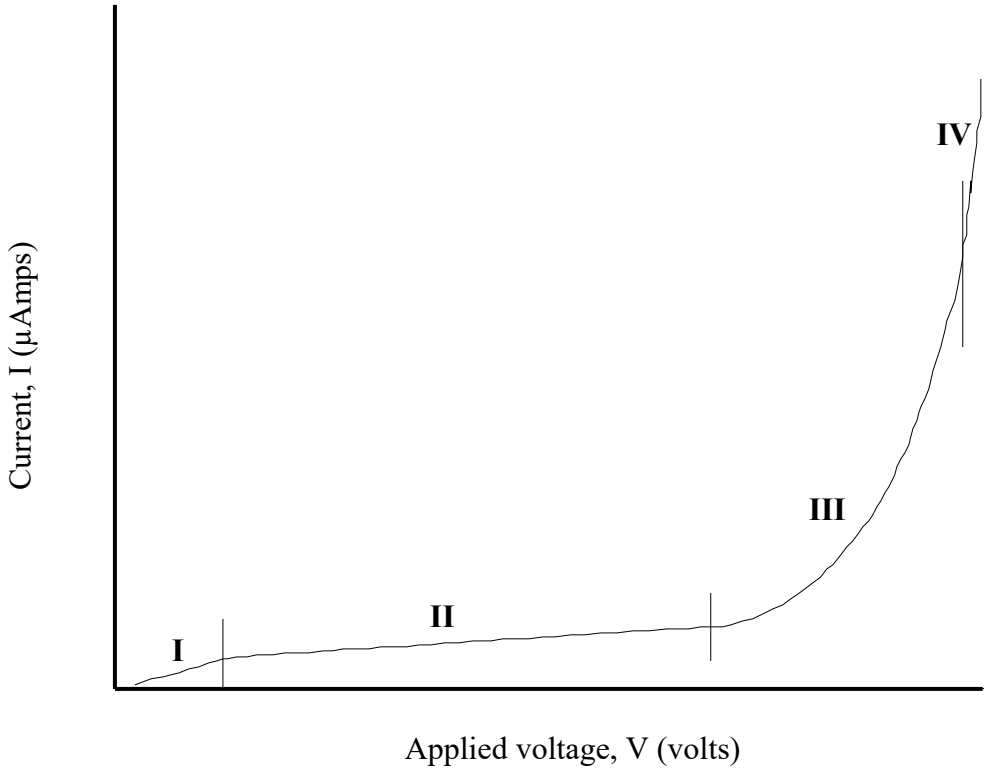

Fig. 2.1: Typical current-voltage (I-V) characteristics in a dielectric liquid. I-Ohmic; II-Quasi Ohmic; III-Injection; IV-Breakdown.

scale features on electrodes [7, 10, 11] on charge injection has been studied. Sharp geometrical features such as needles, razor and knife edges have been used on the emitter electrode to enhance charge injection [2-5, 8]. The tip radius of the sharp feature is an important parameter, as the surface electric field gradients increase with a decrease in the tip radius. The effect of sharp features on electrodes was compared to the case with smooth electrodes by Kazemi et al. [10] and Carvalho et al. [11]. Kazemi et al. [10] deposited nickel micro pillars with an aspect ratio (length of the major axis divided by the width of the minor axis [12]) of 0.5 onto gold planar electrodes. The I-V characteristics,

however, showed an increase rather than expected decrease in the threshold voltage for charge injection from the micro pillar electrodes compared to the planar electrodes with HFE 7100 as the working liquid. This could be because of sharper edges in the planar electrodes compared to the ones with the micro pillars. The threshold voltage for charge injection in air was reduced from 500 V to 10 V when copper nanorods with an aspect ratio of approximately 300 were grown onto one of two parallel electrodes by Carvalho et al. [11]. The I-V characteristics have also been measured at different inter-electrode spacing [3, 4, 7-11], applied polarity [3, 5, 8] and dielectric liquid [3, 4, 8] to study the effect of these parameters on the threshold voltage.

Numerical studies have been performed to determine the effect of electrode spacing, shape, size and tip radius on electric field enhancement [13, 14]. Kogut [13], in case of air, found for a rough surface with hemispherical structures on one electrode and the other being atomically smooth that the field enhancement factor, defined as the ratio of the electric field at the hemispherical tip to that of a smooth electrode, increased significantly when the radius of curvature of the hemisphere was reduced. This effect was much more significant compared to the effect of the inter-electrode distance. Edgcombe and Valdre [14] studied the electric field at the surface of a single tip field emitter for a variety of geometrical configurations and wide range of parameters in a vacuum. A maximum enhancement factor of 1600 is reported when the aspect ratio was approximately 800 for the planar electrode configuration with one cylindrical tip.

Heretofore, there have been no studies on charge injection from micro/nano structured electrodes into a dielectric liquid. Thus, the objective of this research is to

investigate the charge injection characteristics from nanostructures and hybrid micro/nano structures into a dielectric liquid. In particular, the charge injection from a chemically etched electrode surface and electrophoretically deposited single walled carbon nanotubes (SWCNT) onto smooth and etched surfaces were studied. The fabrication of the electrodes and experimental methodology is described in the next section, followed by a presentation and discussion of the results. The key conclusions are then finally presented.

2.2 Experimental Methodology

The current-voltage characteristics for different electrode surfaces using HFE 7100 as the working fluid were determined using the experimental facility shown schematically in Fig. 2.2. A housing consisting of two semi-circular cylindrical grooved parts (inset of Fig. 2.2) was 3D printed, and used to clamp two copper electrodes with nominal diameter of 0.25 inch to ensure proper alignment of the electrodes. The inter-electrode spacing was set to 250 μm using a spacer on the bottom part of the housing. A steady continuous supply of HFE 7100 at a rate of 8 mL/h was fed through the opening at the top using a syringe pump (Syringe infusion pump 22, Harvard Apparatus, accuracy ±0.35%) to compensate for any evaporation of the fluid during the tests. This ensured that the electrodes were completely immersed with a constant liquid level between the two electrodes. A 2 KV power supply (Trek 677B, accuracy ≤ 0.1% of full scale) and an ammeter (Keithley 2636 Source Meter, resolution of 1 fA, accuracy better than 0.06% of reading +40 pA) were used for the electrical measurements. The fluid used in this study is

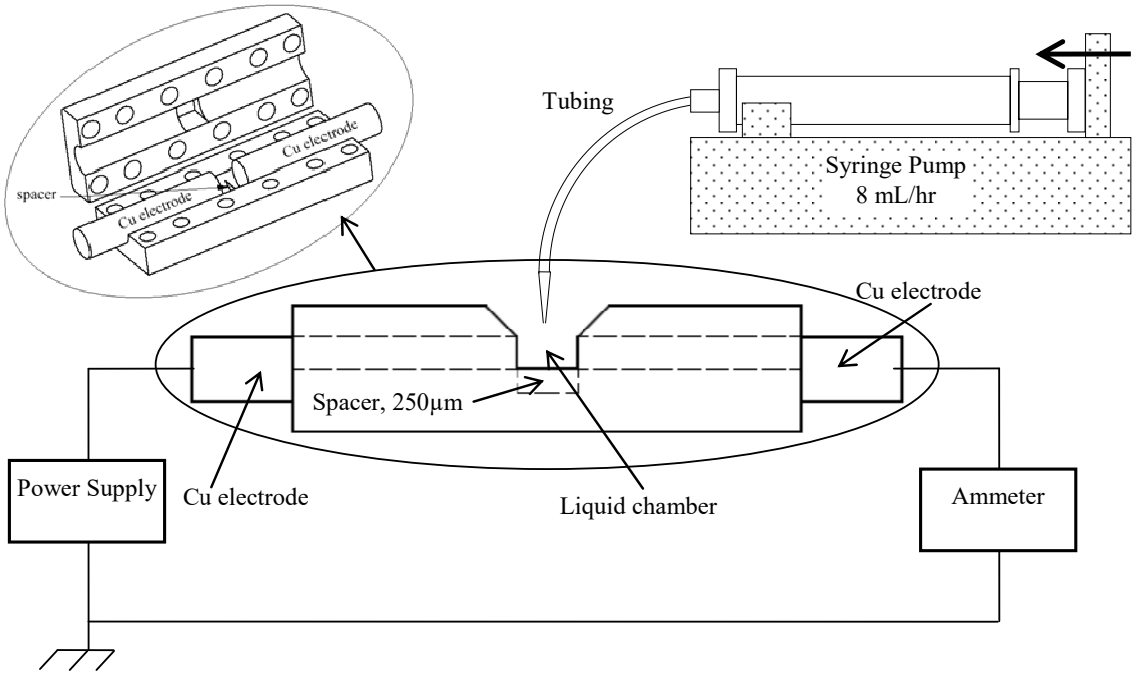

Fig. 2.2: Schematic of the experimental facility.

HFE 7100 from 3M and had been filtered using a 0.2 μm syringe filter. The fluid properties are presented in Table 2.1. This is a common thermal fluid and can be potentially used in many electronic cooling applications. For a given applied voltage, the current was recorded over time and averaged after reaching steady state. Steady state was assumed when fluctuations of the current with time was less than 10% and usually

Table 2.1: Properties of HFE 7100 at 25 °C

Property	Value
Density (Kg/m^3)	1481
Volume resistivity (Ω cm)	$3.29X10^9$
Dielectric constant, 100 Hz – 10 MHz	7.39
Dielectric strength (0.1 in gap)	28 kV (RMS)

achieved within 60 s. Each data point was repeated five times to ensure repeatability of the results.

Various surface configurations and their combinations were tested: (i) Smooth-Smooth, where both surfaces are smooth and mirror polished, (ii) Smooth-Etched, where one was chemically etched to produce micro-scale features (iii) Etched-Etched where both surfaces were chemically etched (iv) SWCNT(S)-Smooth where SWCNT was deposited on a mirror polished smooth surface to produce nano-scale features and the other surface being smooth and (v) SWCNT(E)-Smooth where SWCNT was deposited on a chemically etched surface. A schematic of these surface configurations is illustrated in Fig. 2.3, and is used to aid in the discussion of the results.

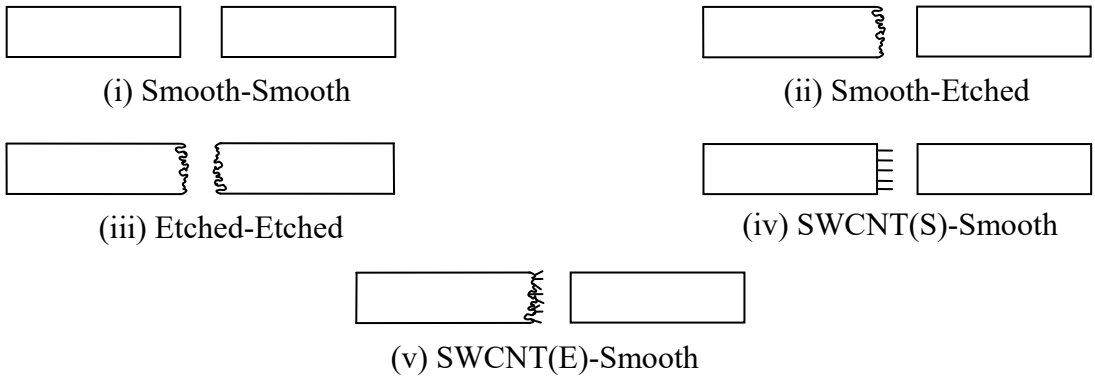

Fig. 2.3: Schematic of different surface configurations of the copper electrode pair (SWCNT(S) and SWCNT(E) refer to SWCNT deposited on a smooth and etched surface respectively).

The electrodes were fabricated from a 0.25 inch copper rod. The electrodes were first faced off and then polished using a series of sand paper followed by two very fine grit cloths (rated finish of 3 and 1 μm) coated with diamond particles. An alumina suspension is used as the final step to produce mirror polished surfaces which are used as the smooth electrodes in this study. For the etched surface, the smooth electrode was chemically etched following the technique by Pauric et al. [15]. SWCNT (1.3-1.5 nm individual diameter and 1-5 μm long, Sigma-Aldrich) was deposited on the smooth and etched copper surface by electrophoretic deposition following the technique proposed by Gao et al. [16]. The surface topology of the smooth and etched electrodes were quantified using a Zygo New View 5000 white light interferometer. The R_z roughness (mean peak to valley roughness over the evaluation area) of the smooth and etched electrodes were 0.58 and 2.28 μm, respectively. The topology of the SWCNT deposited smooth and etched electrodes were not measurable using the Zygo. Scanning electron microscopy (SEM) images of the different surfaces are presented in Fig. 2.4. The etched features of the etched surface (Fig. 2.4b) are clearly visible and distinguishable from the smooth surface (Fig. 2.4a). The SWCNT are visible on the surface in Fig. 2.4(c) and (d), with most of them in horizontal orientations; however, SWNCT are also present in vertical orientations as evidenced by the brighter dots in the SEM images of Fig. 2.4(c) and (d). The etched features are not very distinguishable in Fig. 2.4 (d) as the SWNCT obscure these features.

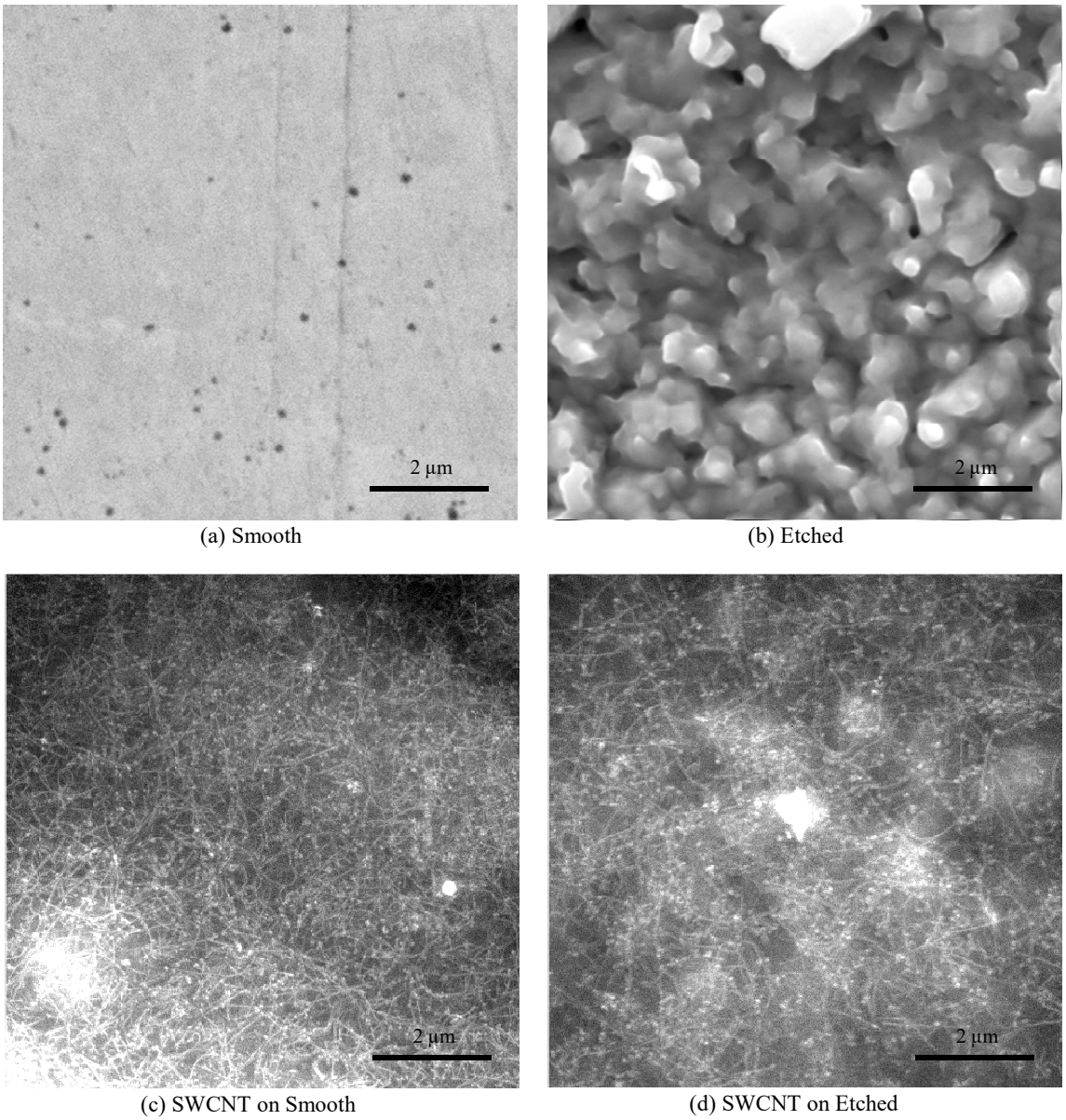

(a) Smooth (b) Etched

(c) SWCNT on Smooth (d) SWCNT on Etched

Fig. 2.4: SEM images of different electrode surfaces.

2.3 Results and Discussion

The current-voltage characteristics were obtained in HFE 7100 for the five different electrode configurations shown in Fig. 2.3. Configurations (i) and (iii) are considered symmetric as both electrodes have the same surface finish, while the other three configurations are considered asymmetric. The I-V characteristics of the Etched-Etched and Smooth-Etched as representative of the symmetric and asymmetric configurations are presented in Figs. 2.5 and 2.6, respectively. The results are shown for both a positive and negative polarity applied to one electrode while keeping the other grounded. For the negative and positive polarity, the charge injection is by field emission and field ionization, respectively [3]. The I-V characteristics for all cases are typical of discharge in a dielectric liquid as shown in Fig. 2.1. Two distinct regions are present: (i) a low slope region and (ii) a high slope injection region. The first and fourth regions (Ohmic and breakdown), which typically appear at very low and very high applied fields, are not of interest in this study and thus not examined. For the etched-etched configuration, the slope of the I-V curve, obtained from a linear fit to the data in the corresponding region, for both the field emission and ionization cases were similar in the low slope region (slope ~ 0.02 nAmp/V). The slopes, however, were very different in the high slope injection region for the two cases, with slopes of approximately 0.1 and 0.3 nAmp/V for the field ionization and emission, respectively. The transition from the low slope region to the high slope region is considered as the onset of charge injection, and the corresponding voltage is referred to as the threshold voltage. The threshold voltage in

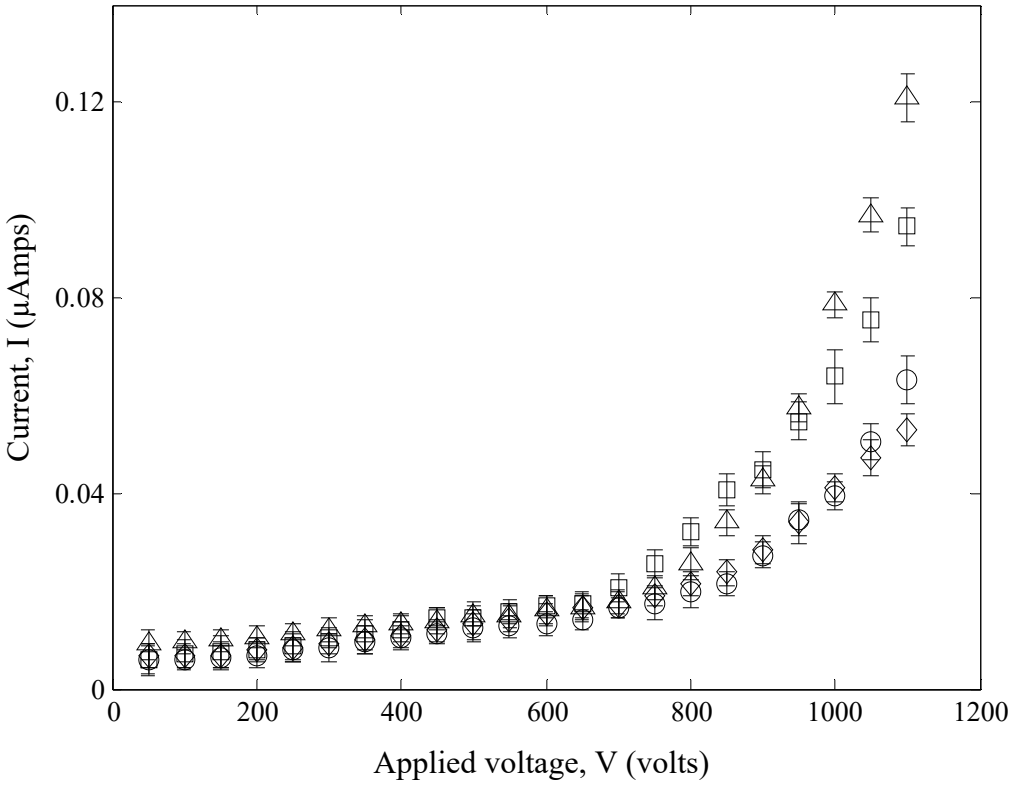

Fig. 2.5: I-V characteristics of different applied polarity for etched-etched configuration. E1 and E2 refer to the two different etched electrodes. Δ E2 negative-E1 ground, □ E1 negative-E2 ground, ◊ E2 positive-E1 ground and ○ E1 positive-E2 ground.

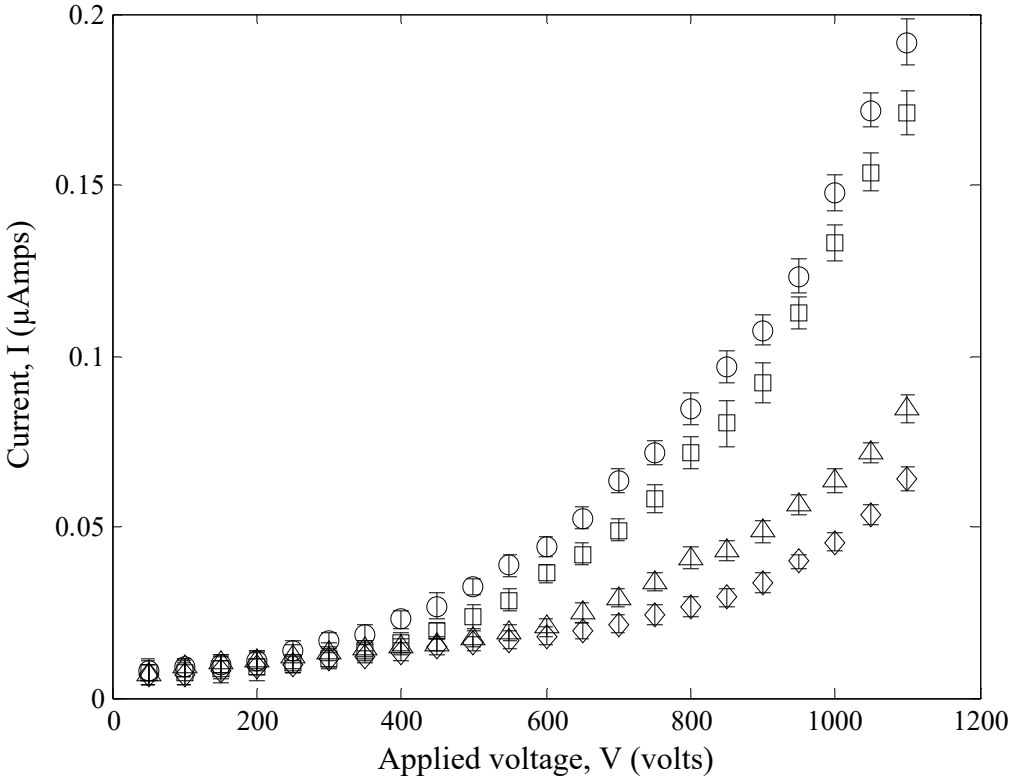

Fig. 2.6: I-V characteristics of different applied polarity to smooth-etched configuration. ○ Etched negative-Smooth ground, □ Etched positive-Smooth ground, Δ Smooth negative-Etched ground and ◊ Smooth positive-Etched ground.

this instance was determined from the intersection of the two linear fit lines to the two different regions. For any given configuration of the electrodes, the threshold voltage is lower for field emission than for field ionization which agrees with the studies of Butcher et al. [5] and Schmidt [17]. Charge injection due to field emission is controlled by the work function of the electrode material while that due to field ionization depends on the difference between the ionization energy of the dielectric liquid and the electrode work function [3]. The lower threshold voltage in case of field emission compared to field ionization is observed if the difference between the ionization energy and the work function is greater than the work function itself. Ionization energy of dielectric liquids is typically greater than the work function of the electrode materials [18]. For the symmetric etched-etched electrode configuration, the injection characteristics for field emission or ionization were similar for applied polarity to either electrode (Fig. 2.5). The small discrepancy in the charge injection region of the I-V curves for a negative polarity is likely due to small differences in the roughness of the two electrodes. For the asymmetric configuration of smooth-etched electrodes, a higher current from the etched surface compared to the smooth surface was observed at high voltages (positive or negative) within the injection region (Fig. 2.6). For instance, within the injection region the slope of the I-V curve for the etched electrode is 3 times that for the smooth electrode when negative polarity was applied. The threshold voltage for the etched electrode reduces by approximately 60 V from 600 V for the smooth electrode.

The I-V characteristics of all five configurations tested are presented in Fig. 2.7 to show the enhancement in charge injection for field emission or the reduction in threshold

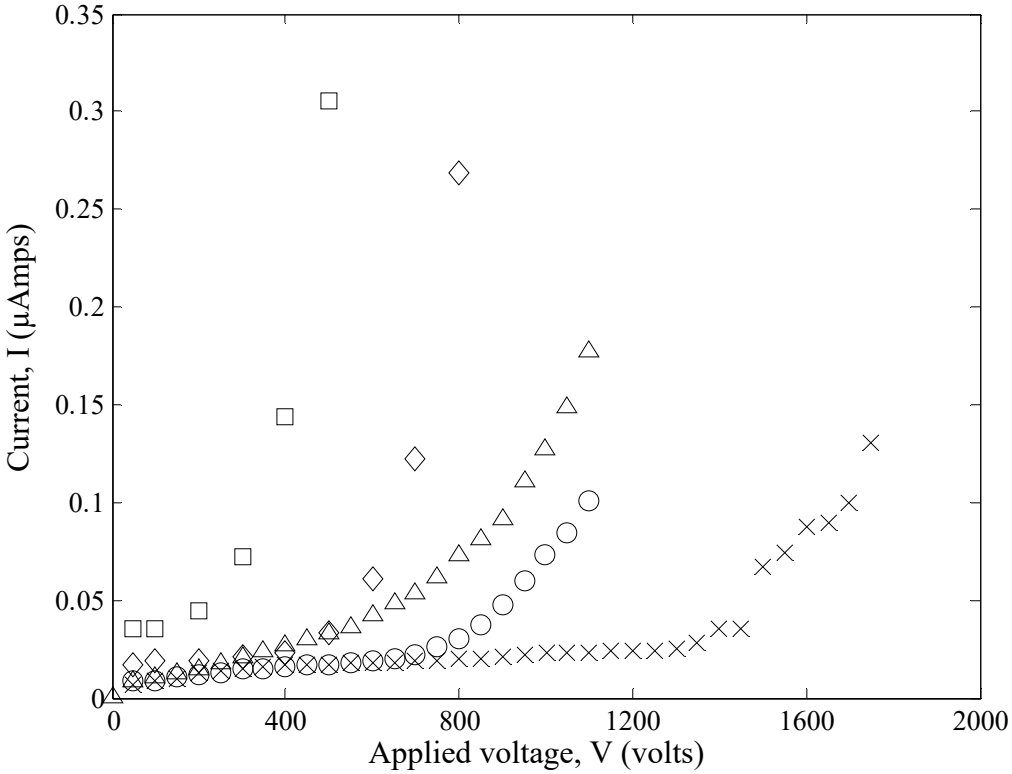

Fig. 2.7: I-V characteristics of different combinations of parallel Cu electrode surfaces 250 μm apart. x Smooth-Smooth, ○ Etched-Etched, Δ Smooth-Etched, ◊ SWCNT (on smooth)-Smooth and □ SWCNT (on etched) -Smooth configuration.

voltage when compared to the smooth-smooth case. For the symmetric configurations (smooth-smooth and etched-etched), the average of field emission results of both electrodes are considered and for the asymmetric configurations field emission result from the electrode with sharp asperities are considered. For all these cases the inter-electrode spacing was 250 μm. There is a significant reduction in the threshold voltage for charge injection for electrodes with sharp features compared to smooth electrodes. The threshold voltage reduces by a factor of 2.9 ± 0.2 (from 1560 ± 28 V to 540 ± 27 V) and 5.38 ± 0.17 (from 1560 ± 28 to 290 ± 4 V) in the smooth-etched and SWCNT(E)-

Smooth configurations compared to the smooth-smooth configuration. In general, higher charge injection and a lower threshold voltage was observed for the asymmetric configuration when compared to the symmetric configuration. This is likely because of the higher electric field gradients introduced by the asymmetry of the electrode pair. The deposition of SWCNT on the etched surface reduced the threshold voltage when compared to the etched surface alone. The slopes of the I-V curve within the injection region were steeper for the electrode surfaces with sharp features when compared to the smooth case. For example, the slopes are 0.2 and 1.2 nA/V for smooth-smooth and SWCNT(E)-smooth configurations, respectively. The threshold voltages for onset of charge injection and the slopes of the I-V curve within region II (quasi Ohmic) and III (injection) for the different configurations are summarized in Table 2.2. It is seen that the voltage required to generate the same amount of current after the onset of charge injection is significantly reduced by the introduction of sharp features. For example, the voltage required for 0.15 μA of current for smooth-smooth, smooth-etched and smooth-SWCNT deposited on etched configurations are approximately 1730, 1050 and 380 V respectively.

Two parameters that affect the threshold voltage for the onset of charge injection are: (i) asymmetry and (ii) surface roughness of the electrodes. The effect of asymmetry is evident in the I-V characteristics of the etched-etched and smooth-etched configurations (Fig. 2.7). Xue et al. [19] experimentally found that sharp micro/nano features at a rough surface resulted in a lower work function. At the tip of a micro/nano structure, an atom has lesser coordination atoms surrounding it than those at a flat surface

Table 2.2: Threshold voltage and slope of I-V curve for different electrode configurations

Electrode Configuration	Threshold voltage (V)	Slope in region II (nAmp/volt)	Slope in region III (nAmp/volt)
Smooth-Smooth	1560 ± 28	0.02 ± 0.0003	0.2 ± 0.064
Etched -Etched	940 ± 36	0.02 ± 0.005	0.2 ± 0.02
Smooth- Etched	540 ± 27	0.06 ± 0.004	0.3 ± 0.013
SWCNT(S)-Smooth	500 ± 14	0.03 ± 0.009	0.8 ± 0.1
SWCNT(E)-Smooth	290 ± 4	0.1 ± 0.02	1.2 ± 0.2

which causes the maximum electric field to occur at the tip of a sharp feature. Thus, when a potential sufficient to overcome the energy barrier is applied to the electrode, an electron from the atoms at the tip can readily escape and the atoms/nuclei have a weaker effect on it compared to a smooth surface. Liu et al. [20] performed a numerical study of different orientations/alignments and arrays (vertical, tilt, rainbow shaped and spiral) of CNT and showed that the electric field for a particular orientation is maximum at its tip; the one with the maximum aspect ratio produced the highest field. The current experimental results are in agreement with the findings of [19, 20] as seen in the higher current for the etched-etched (R_z = 2.28 μm) configuration compared to the smooth-smooth (R_z = 0.58 μm) configuration. The sharpness (e.g. aspect ratio and total number of feature) also plays an important role and could be more important than the roughness alone. For example, a surface with hemispherical features or needles may have the same peak to valley roughness but will result in different I-V characteristics. This is evident when comparing the smooth-smooth, smooth-etched and SWCNT(S)-smooth

configurations (Fig. 2.7). The SWCNT(S)-smooth configuration shows a smaller threshold voltage than the smooth-etched configuration, even though the roughness of the SWCNT deposited onto smooth electrode is expected to be similar to the smooth surface (the SEM images show that most of the SWCNT are deposited flat on to the surface) and significantly smaller than that of the etched electrode (R_z = 2.28 μm). The lower threshold voltage for the SWCNT(E)-smooth configuration compared to the smooth-etched case can be attributed to the presence of the SWCNT which increases the sharp features at the surface. The same is observed for the smooth-smooth and SWCNT(S)-smooth configuration. The significance of sharp features for charge injection can be evaluated by considering the charge density at the apex of a feature subject to high voltage. The protruding atoms at the sharp features are subject to a greater charge compared to a smooth surface [21]. This causes a greater local charge density and thus results in a greater electric field [22] at the protrusions when compared to an atomically smooth surface as observed by Liu et al. [20] in their numerical study. The electric field gradient at the apex of a sharp feature is also greater than that of a smooth surface which leads to a higher charge injection. Charge injection from a protruded sharp feature takes place once the applied potential overcomes the energy barrier set by the electrodes and the dielectric fluid, causing a local reduction in the electric field. The neighboring sharp feature with the high local charge density momentarily become active and thus maintains the injection level of charges.

2.4 Conclusions

An experimental study was performed to determine the effect of surface topology on the charge injection from parallel copper electrode surfaces in a dielectric liquid (HFE 7100). Surface modification of the electrodes was performed by chemical etching or electrophoretic deposition of SWCNT on the electrode surface, which produced electrodes with different roughness and sharpness at the micro/nano scales. Both field emission and field ionization experiments were performed with the former showing higher current and lower threshold voltage for charge injection. The results showed that sharp features on the electrode surface significantly reduced the threshold voltage and increased the charge injection. The effect of sharpness was more significant than the roughness alone for the current injection, threshold voltage and the slope of the I-V curve within the injection region. This is attributed to the higher charge density and greater electric field gradient at the sharp features. For the chemically etched surface, the threshold voltage was reduced by a factor greater than 2 while it was greater than 5 for SWCNT deposited on etched surface when compared to the smooth-smooth configuration. The slope of the I-V curve within the injection region for the SWCNT(E)-smooth configuration was 6 times of that for the smooth-smooth configuration. An asymmetric electrode configuration, where the two electrode surfaces were dissimilar showed a higher charge injection and lower threshold voltage compared to the symmetric case. The findings of this study would be useful in the design of the electrode geometry

in many electrohydrodynamic (EHD) applications involving single and two-phase fluid flow and heat transfer.

2.5 References

[1] S. Jeong, J. Seyed-Yagoobi, Experimental study of electrohydrodynamic pumping through conduction phenomenon, J. Electrost. 56 (2) (2002) 123-133.

[2] G. Coe, J. Hughes, P. Secker, High-current injection into liquid hexane using field emitters, Br. J. Appl. Phys. 17 (7) (1966) 885.

[3] K. Arii, W.F. Schmidt, Current injection and light emission in liquid argon and xenon in a divergent electric field, IEEE Trans. Electr. Insul. 1 (1984) 16-23.

[4] T. Takashima, R. Hanaoka, R. Ishibashi, A. Ohtsubo, I-V characteristics and liquid motion in needle-to-plane and razor blade-to-plane configurations in transformer oil and liquid nitrogen, IEEE Trans. Electr. Insul. 23 (4) (1988) 645-658.

[5] M. Butcher, A. Neuber, M. Cevallos, J. Dickens, H. Krompholz, Conduction and breakdown mechanisms in transformer oil, IEEE Trans. Plasma Sci. 34 (2) (2006) 467-475.

[6] G. Jorgenson, E. Will, Improved ion drag pump, Rev. Sci. Instrum. 33 (1962) 55.

[7] J. Darabi, M. Rada, M. Ohadi, J. Lawler, Design, fabrication, and testing of an electrohydrodynamic ion-drag micropump, J. Microelectromech. Syst. 11 (6) (2002) 684-690.

[8] P. Atten, M. Haidara, Electrical conduction and EHD motion of dielectric liquids in a knife-plane electrode assembly, IEEE Trans. Electr. Insul. 2 (1985) 187-198.

[9] P.Z. Kazemi, P.R. Selvaganapathy, C.Y. Ching, Effect of electrode asymmetry on performance of electrohydrodynamic micropumps, J. Microelectromech. Syst. 18 (3) (2009) 547-554.

[10] P.Z. Kazemi, P.R. Selvaganapathy, C.Y. Ching, Electrohydrodynamic micropumps with asymmetric electrode geometries for microscale electronics cooling, IEEE Trans. Dielectr. Electr. Insulation 16 (2) (2009) 483-488.

[11] D. Carvalho, S. Ghosh, R. Banerjee, P. Ayyub, Ultra-low breakdown voltage and origin of $1/f^2$ noise in metallic nanorod arrays, Nanotechnology 19 (2008) 445713.

[12] C.J. Murphy, N.R. Jana, Controlling the aspect ratio of inorganic nanorods and nanowires, Adv. Mater. 14 (1) (2002) 80.

[13] L. Kogut, The influence of surface topography on the electromechanical characteristics of parallel-plate MEMS capacitors, J. Micromechanics Microengineering 15 (5) (2005) 1068-1075.

[14] C. Edgcombe, U. Valdre, Microscopy and computational modelling to elucidate the enhancement factor for field electron emitters, J. Microsc. 203 (2) (2001) 188-194.

[15] A.D. Pauric, S.A. Baig, A.N. Pantaleo, Y. Wang, P. Kruse, Sponge-like porous metal surfaces from anodization in very concentrated acids, J. Electrochem. Soc. 160 (1) (2013) C12-C18.

[16] B. Gao, G. Yue, Q. Qiu, Y. Cheng, H. Shimoda, L. Fleming, O. Zhou, Fabrication and electron field emission properties of carbon nanotube films by electrophoretic deposition, Adv. Mater. 13 (23) (2001) 1770-1774.

[17] W.F. Schmidt, Electronic conduction processes in dielectric liquids, IEEE Trans. Electr. Insul. 5 (1984) 389-418.

[18] R. Bartnikas, Electrical Insulating Liquids, vol. 3, ASTM International, 1994.

[19] M. Xue, W. Wang, F. Wang, J. Ou, C. Li, W. Li, Understanding of the correlation between work function and surface morphology of metals and alloys, J. Alloys Compd. 577 (2013) 1-5.

[20] C. Liu, Y. Zheng, G. Ding, J. Wu, F. Zang, Numerical analysis in field emission characteristics of carbon nanotube field emitters and arrays, Proc. Institution Mech. Eng. Part N. J. Nanoeng. Nanosyst. 227 (1) (2013) 39-45.

[21] B. Gault, M.P. Moody, J.M. Cairney, S.P. Ringer, Field ion microscopy, in: Atom Probe Microscopy, Springer, 2012, pp. 9-28.

[22] S. Hudlet, M. Saint Jean, C. Guthmann, J. Berger, Evaluation of the capacitive force between an atomic force microscopy tip and a metallic surface, Eur. Phys. J. B-Condensed Matter Complex Syst. 2 (1) (1988) 5-10.

Chapter 3

Electrohydrodynamic injection micropump with composite gold and single-walled carbon nanotube electrodes

Complete citation:

Russel, M.K., Selvaganapathy, P.R., Ching, C.Y., 2015. Electrohydrodynamic injection micropump with composite gold and single-walled carbon nanotube electrodes. *J. MEMS*. 24: 1557-1564.

Copyright:

Relative Contributions:

Russel M.K.: Performed all experiments, interpretation and analysis of the data and wrote the drafts of the manuscript including all figures and text.

Selvaganapathy P.R.: Co-supervisor of M.K. Russel and revised the initial drafts of the manuscript.

Ching C. Y.: Co-supervisor of M.K. Russel and was responsible for the final draft submittal to the journal.

Abstract

The presence of microfeatures/nanofeatures with sharp asperities on the emitter electrodes of ion drag electrohydrodynamic (EHD) micropumps is likely to enhance the local electric field and charge injection significantly, and thus the pressure generation and flow rates. The objective of this paper is to investigate the performance of EHD micropumps with single walled carbon nanotubes (SWCNT) on the emitter electrodes. The micropumps had 100 pairs of planar electrodes where the width of the emitter and collector electrodes was 20 and 40 μm, respectively, with a cross-sectional domain of 100 μm × 5 mm. Two micropumps with interelectrode spacing of 120 and 40 μm were tested with a smooth emitter surface, and where SWCNT were electrophoretically deposited on the emitter electrodes using HFE7100 as the working fluid. The threshold voltage for charge injection lowered by a factor of 3 and 1.4 for the two pumps with SWCNT on the emitter electrodes compared with the smooth electrode case. The corresponding static pressure head increased by a factor 5, while the flow rate at no external back pressure increased by a factor 3 for the pump with interelectrode spacing of 120 μm. For the pump with interelectrode spacing of 40 μm, a maximum static pressure of 4.7 kPa was achieved at 900 V with SWCNT on the emitter electrode.

3.1 Introduction

Thermal management in electronic devices has become increasingly challenging due to higher circuit packaging densities. Mudawar [1] broadly identified two ranges of heat fluxes depending on the heat dissipation from the electronic chip: (i) high heat flux (10^2~10^3 W/cm^2) and (ii) ultra high heat flux (10^3~10^5 W/cm^2). Local thermal loads are often exacerbated since the heat dissipation is often unevenly distributed that can lead to very high local heat densities. Active cooling techniques, such as liquid cooling, have been studied and shown to achieve a cooling capacity up to 1 kW/cm^2 [2]. Microchannel liquid cooling has been studied since Tuckerman and Pease [3] dissipated 790 W/cm^2 using water as the cooling fluid in 50 μm × 302 μm microchannels. As the effective diameter of the microchannel decreases, the heat dissipation capacity increases due to the increase in the surface area associated with the cooling fluid over the same footprint of the electronic chip. However, the flow resistance in these channels also increases requiring higher external pressure heads to circulate the cooling fluid. A miniaturized pressure source, e.g., micropump integrated within the microchannels, can be used to overcome the resistance to the flow in these microchannels. Among various available micropumps [4], the ion drag/injection EHD micropump is particularly promising due to its small form factor, low power consumption, ability to work with dielectric heat transfer fluids, good controllability and absence of any moving parts.

The principles of ion drag pumping have been known since the late 1950's [5]. Since then, theoretical [6]–[9] and experimental [6], [7] studies have been performed to

better understand the pump characteristics. The first injection EHD micropump was fabricated by Richter et al. [10] where two parallel grid electrodes at a spacing of 350 μm were used to achieve a maximum pressure of 2480 Pa at an applied potential of 700 V using ethanol as the working fluid. The first planar electrodes for an ion drag EHD micropump was proposed by Ahn and Kim [11] with an inter electrode spacing of 100 μm. The spacing between each pair of electrodes was 200 μm. A maximum pressure head and flow rate of 240 Pa and 50 μL/min were reported using ethanol. The effect of fluid [10], [12], [13], microchannel height [14] and electrode design, such as spacing between electrodes and electrode pairs, asymmetry within the two adjacent electrode widths (i.e. 2D asymmetry) and 3D features on the electrodes (e.g. micropillars, microbumps) and their spatial spacing [14]–[19] on the performance of EHD micropumps have been studied. A higher pumping capacity and lower threshold voltage for the onset of charge injection has been reported when the inter-electrode spacing was reduced or asymmetry between the electrodes, both in 2D and 3D, were incorporated.

The longevity of ion drag EHD micropumps is important for practical applications, and has been studied previously [20], [21]. Bologa et al. [20] reported a stable pressure generation for over 400 hours with kerosene and transformer oil. A subsequent degradation beyond this time period was caused by several factors, such as, environmental temperature, pressure, gas content, humidity and fluid impurity. The reduction in pump performance was attributed to deposition of impurities or colloidal particles on the collector electrodes due to the high applied potential over time and hence reduced current. Filtration and degassing of the working fluid was found to increase the

longevity of the pump. Benetis [21] using HFE 7100 as the working fluid found that the pump performance over time degraded due to the degradation of the working fluid. The repeatability of his results improved from 50-100% to 20-30% when the working fluid was degassed and filtered before each experiment.

In general, the EHD pump performance depends on the applied electric field gradient [19] which fundamentally contributes to the charge injection. Charge injection primarily depends on the energy barrier set by the electrode materials, the dielectric liquid and the inter electrode spacing. One method to reduce the energy barrier is to lower the work function of the electrode material and thus improve the pump performance. This can be achieved by having sharp features with high aspect ratio such as nanotubes/rods on the electrodes [22]. These sharp features not only lower the energy barrier but also introduce fringing electric fields and thus increase the electric field gradient at their tips. Carvalho *et al.* [23] showed a reduction factor of 50 in the threshold voltage for the onset of charge injection in air when an electrode surface with vertical copper nanorods (aspect ratio of 300) was compared to a smooth electrode. Similar experiments in a dielectric liquid (HFE 7100) by Russel et al. [24] showed a reduction factor greater than 5 for randomly deposited single walled carbon nanotubes (SWCNT) on the electrodes. In their studies, the surface roughness was a secondary effect while the presence of sharp features with high aspect ratio had the primary effect in reducing the threshold voltage. An increase in current was observed by Dorsey and Davidson [25] in their study of ozone production in electrostatic air cleaners when there was dust accumulation on the flat collector electrodes, which could be attributed to an increase in the surface roughness. A

similar result for the effect of contaminants on the electrode surface on the ozone generation was later found by Tanasomwang and Lai [26]. In previous studies of 3D asymmetry within the electrodes in an ion drag micropump, the 3D features had an aspect ratio less than one [16], [18], [19]. The features in those studies were not sharp to produce significant enhancement in local electric field gradients.

The objective here is to investigate the effect of electrode sharp features on the performance of EHD micropumps. In particular, SWCNT was deposited onto the planar emitter electrodes of an ion drag EHD micropump to study the performance parameters such as the threshold voltage for charge injection, discharge current, and the pump characteristics using HFE 7100 as the working fluid. These results were compared against the case with smooth electrodes (i.e. with no SWCNT deposition). The fabrication of the micropump and experimental methodology is described in the next section, followed by a presentation and discussion of the results, and finally the conclusions of the study.

3.2 Fabrication and Experimental Methodology

The micropumps used in this study were similar to those used by Kazemi et al. [17]. A 240 nm layer of gold was deposited on a glass substrate with a thin layer (10 nm) of adhesive chromium in between to bind the gold layer to the glass. The micropump had 100 pairs of electrodes (emitters and collectors) lithographically patterned from the gold deposited glass substrate which acts as the bottom wall of a microchannel. The top and side walls (material: PDMS) of the microchannel is made out of a silicon mould and then bonded to the glass substrate. The electrodes in the micropump are of asymmetric planar configuration, where the width of the collector electrode was twice that of the emitter electrode (40 and 20 μm respectively). A schematic of the micropump with its dimensional specifications is shown in Figure 3.1. Two different pumps with inter electrode spacing (d_{ec}) of 120 and 40 μm and spacing between each pair of electrodes of 240 and 80 μm, respectively, were studied. This resulted in the total length of the pumps being 50 and 29 mm, respectively. The total thickness of the electrodes is 0.25 μm while the height and width of the micro channel were 100 μm and 5 mm respectively. The details of the fabrication procedures can be found in [17].

SWCNT (1.3-1.5 nm individual diameter and 1-5 μm long, Sigma-Aldrich) was deposited on the emitter electrodes by electrophoretic deposition prior to the bonding of the PDMS microfluidic channel onto the glass substrate containing the patterned electrodes following [27]. The SWCNT were first dispersed in methanol with a concentration of 0.01 mg/mL. A small amount (0.08 % v/v) of 1M sodium hydroxide was

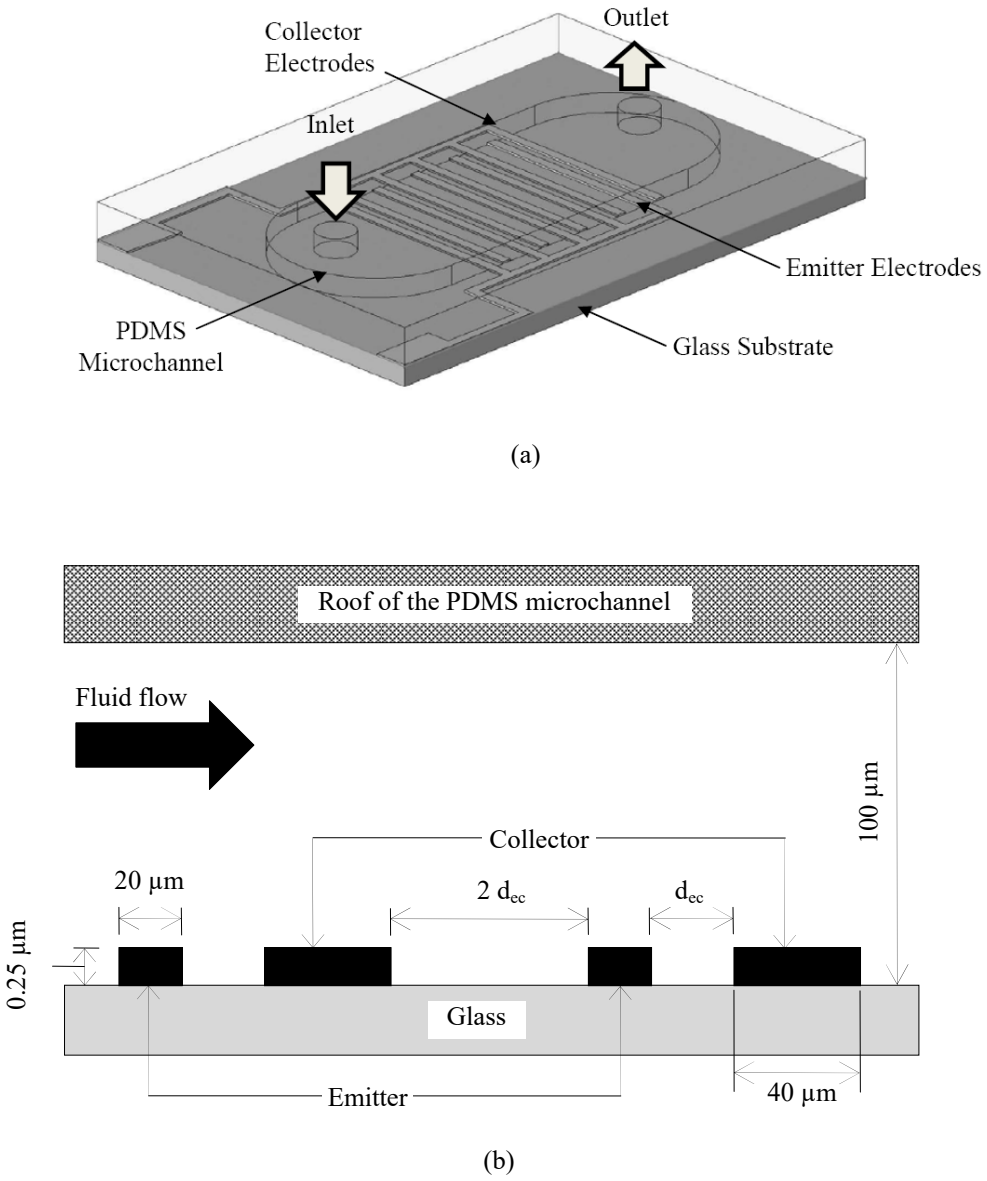

Fig. 3.1: Schematic of (a) ion drag EHD micropump (the total number of electrode pairs is 100 but only 5 pairs are shown for reference) and (b) dimensional specifications (not to scale). d_{ec} = 120 and 40 μm for the two different pumps.

added and then sonicated for 4 hours. The substrate with the micropump and another substrate with gold deposited on it (which is not patterned and acts as the counter electrode) were immersed into the suspension with a gap of 2 mm. A DC potential of 6 V was applied across the emitter electrodes of the micropump (positive terminal) and the counter electrode (grounded) for 1 minute. SEM images of the electrodes before and after the SWCNT deposited on them are presented in Figure 3.2. The electrophoretic method resulted in the deposition of a thin layer of randomly deposited SWCNT on the emitter electrodes of the micropump as seen in the SEM images. The nanotubes are mostly deposited horizontally flat onto the surface, though some at an angle to the surface can be observed. Transparent plastic tubing (ID = 1/16 inch) was connected to the inlet and

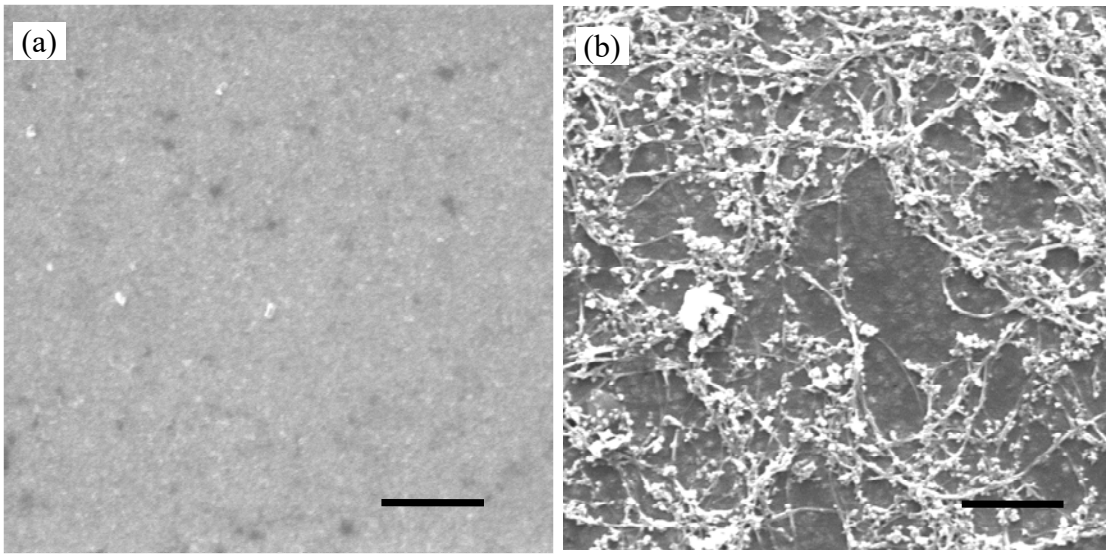

Fig. 3.2: SEM images of electrodes with (a) no deposition and (b) SWCNT deposited. Scale bar = 2 μm.

outlet of the micropump via glass tubing after bonding the PDMS microchannel to the glass substrate which contains the patterned electrodes.

A high voltage power supply (Trek 677 with capacity of 2 kV, accuracy ≤ 0.1% of full scale) was used with an ammeter (Keithley 2636 SourceMeter, resolution of 1 fA, accuracy better than 0.02% of reading + 25 nA) to record the current readings at different applied voltages as shown in Figure 3.3 (a). The current at an applied voltage was recorded over time and averaged after reaching steady state. The fluctuation in the current with time was less than 10 percent for a measurement period of 10 minutes. The static pressure head (no flow) generated for a given voltage was measured from the height difference between the inlet and outlet liquid columns as shown in Figure 3.3 (b) using a height gage (KBC tools, resolution 0.02mm). Before applying the voltage for each measurement, it was ensured that the two columns were at the same level.

The flow rates at different applied voltage and back pressure conditions were calculated from the cross sectional area and the average flow velocity through the long horizontal plastic tubing at the pump outlet. The flow velocity of the liquid in the downstream horizontal tubing was measured by tracking the liquid-air interface using a high speed digital camera capable of capturing 2000 frames/s (Figure 3.3 (c)). A series of successive frames was used to determine the displacement of the interface, and the velocity was determined from the ratio of the displacement to the time between the frames. The flow was assumed steady when the velocity did not change over time. The time required to reach steady state varied at different applied potential and back pressure conditions, and typically took 10 to 60 minutes. Each flow measurement experiment was

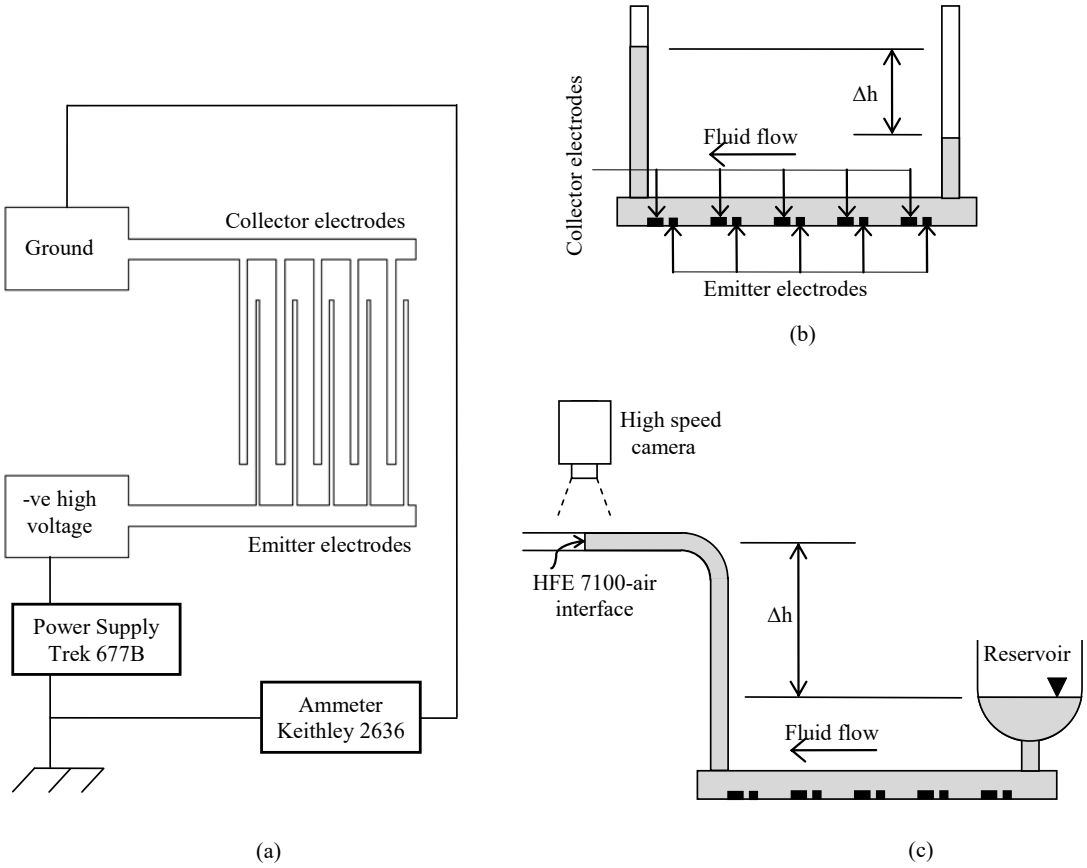

Fig. 3.3: Schematic of the experimental facility (a) electric connections with the top view of the micropump electrodes (b) static pressure head measurement with the side view of the electrodes (c) flow velocity measurement at a back pressure equivalent to a height of Δh. (The number of electrode pairs is 100 but only 5 pairs are shown in the schematic as reference only.)

performed at least 5 times to ensure repeatability of the results. A gravitational back pressure was applied by maintaining a corresponding height difference between the horizontally oriented section of the outlet tubing and the liquid level of the reservoir at the inlet of the pump as shown in Figure 3.3 (c). The liquid reservoir at the inlet had an inner diameter greater than 16 times that of the outlet tubing. The uncertainty of the flow velocity measurement was estimated as ±0.2 mm/s, which corresponds to an uncertainty

of ±14 to ±40 percent at the high and low flow rates. The working fluid is HFE 7100 and its properties are presented in Table 3.1 [28].

Table 3.1: Properties of HFE 7100 at 25 °C [28]

Property	Value
Boiling point (°C)	61
Viscosity (Kg/m.s)	$3.7X10^{-4}$
Specific heat (J/Kg.K)	1255
Density (Kg/m^3)	1481
Volume resistivity (Ω cm)	$3.29X10^{9}$
Dielectric constant, 100 Hz-10 MHz	7.39
Dielectric Strength (0.1 in. gap)	28 kV (RMS)

3.3 Results and Discussion

The pumps were tested in field emission mode with a negative voltage applied to the emitter electrodes while keeping the collector electrodes grounded. Operating in field emission is advantageous over field ionization due to higher charge injection and lower threshold voltage for the onset of charge injection [24], [29]–[32]. In field emission, electrons tunnel through the negative metal electrodes into the insulating liquid once sufficient energy is applied to overcome the barrier set by the metal-dielectric liquid interface [30], [31]. The electrons interact with certain neutral molecules of the liquid to ionize them. The ionized molecules then move along the applied electric field due to the electrophoretic force experienced by these charges. The motion is transmitted to the other neutral molecules due to viscosity which results in bulk fluid motion.

The maximum allowable operating voltage was initially determined from preliminary experiments where the electric potential was increased till electrical breakdown occurred (as evidenced by a spark across the electrodes). Subsequent tests were performed with new pumps and the voltage kept below this breakdown voltage. The variation of the discharge current with applied voltage for the 120 μm electrode spacing pumps with smooth and SWCNT deposited on emitter electrodes are presented in Figure 3.4 for a static or no flow condition. The relative uncertainty in the current was less than ±10 percent. The I-V characteristic has the typical trend of discharge in a dielectric liquid showing a low slope quasi-Ohmic region and a high slope injection region [24]. The low slope quasi-Ohmic region corresponds to the conduction mechanism [33], while the high

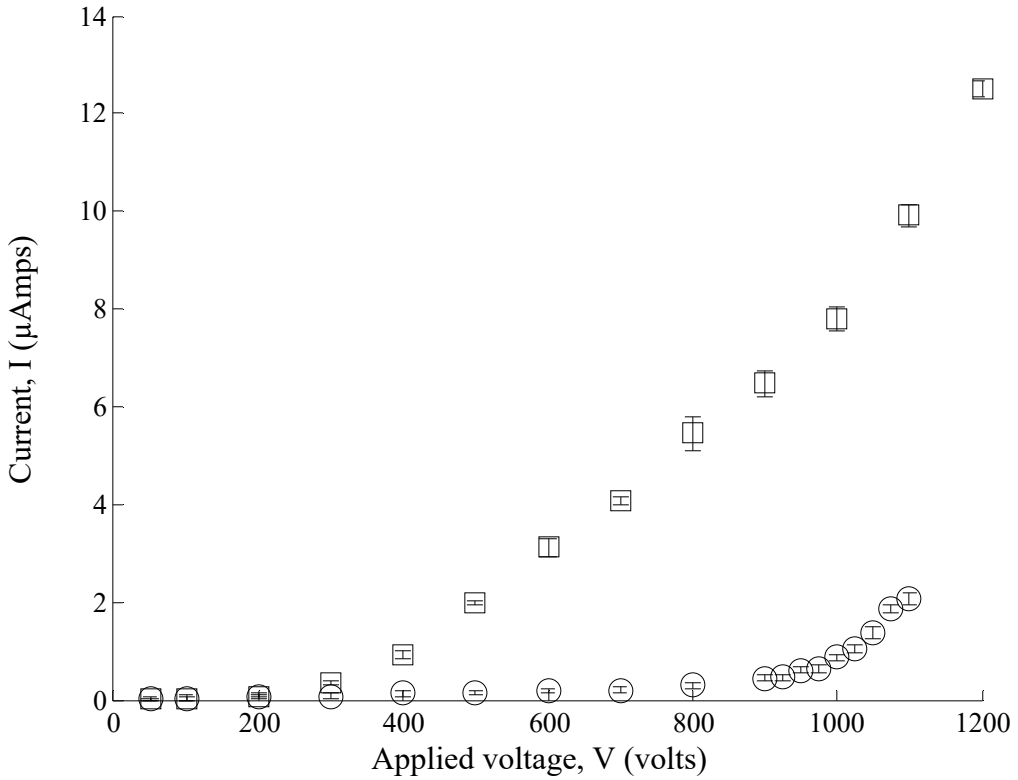

Fig. 3.4: I-V characteristics for ○ smooth electrodes and □ SWCNT deposited on emitter electrodes at static condition for the pump with inter-electrode spacing of 120 μm.

slope injection region corresponds to the ion injection mechanism. In the conduction region, the charges are produced by the dissociation of the fluid molecules and recombination of the generated ions. The rate of dissociation is greater than that of recombination, which induces layers of hetero-charges within the vicinity of the electrodes. Current flow in this region occurs due to the dissociated ions and hetero-charges created at the electrodes [34]. The threshold voltage for the onset of charge injection, estimated as the voltage where the low slope quasi-Ohmic region intersects with the steeper injection region [24], are approximately 900 and 340 V for the

micropumps with smooth and SWCNT deposited on emitter electrodes, respectively. The slopes of the I-V curves within the injection region were, however, similar for both cases. A higher injection current for a given applied voltage within the injection region was observed for the micropump with SWCNT compared to the smooth electrode case, as observed previously for SWCNT or nanorods [23], [24]. The higher injection current is likely because of the reduced work function of the electrode material due to the presence of the sharp features as found experimentally by Xue et al. [22]. An atom at the tip of a sharp structure is surrounded by fewer atoms compared to the one on a smooth surface. A higher charge density occurs at the tip of the sharp feature when a potential is applied which results in the maximum electric field at that location. Thus, when energy just above the energy barrier set by the electrode and the dielectric fluid is applied, an electron from the atoms at the tip can readily escape. On the other hand, a smooth surface is occupied by more neighboring atoms with uniformly shared free electrons which results in a comparatively stronger attraction between the electrons and the atoms. These results are consistent with those of Carvalho et al. [23] for injection in air and Russel et al. [24] for injection in HFE 7100. The reduction factor in the threshold voltage for the micropump with SWCNT is approximately 3. The effect of (i) the augmentation in the surface area or (ii) the decrease in the inter electrode spacing due to the introduction of the sharp features when compared to a smooth electrode, was considered by Kogut [35]. It was concluded that the presence of the sharp features with high aspect ratio had a primary effect on the charge injection enhancement while the other two parameters had a secondary effect.

The variation of the static pressure head generated at different applied voltages for the pump with inter-electrode spacing of 120 μm is presented in Figure 3.5 for both the smooth and SWCNT deposited emitter electrodes. The pressure-voltage characteristics are similar to the I-V characteristics when the two pumps are compared. No significant pressure is generated until 900 and 500 V for the pump with smooth and SWCNT deposited on the emitter electrodes. The pressure generation at an applied voltage is greater for the pump with SWCNT deposited on the emitter electrodes. For example, the

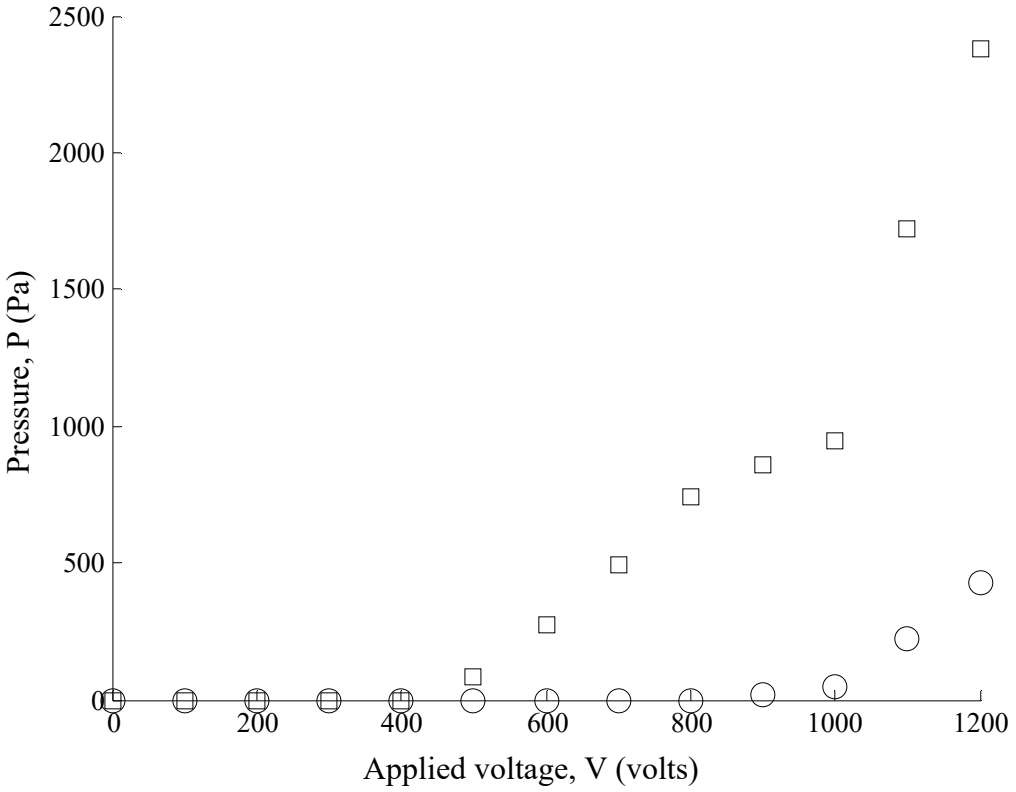

Fig. 3.5: Static pressure generated at different applied voltage for ○ smooth electrodes and □ SWCNT deposited on emitter electrodes for the pump with inter-electrode spacing of 120 μm.

pressure generation for this pump at 1200 V is more than 5 times that of the pump with smooth electrodes. This can be attributed to the enhancement in charge injection as seen in Figure 3.4; however, the enhancement in charge injection is greater than that observed in the pressure generation. The static pressure generated by this pump is plotted against the input power in Figure 3.6. The input power is an important parameter since for the no flow condition it reflects the Joule heating within the working fluid. The Joule heating is

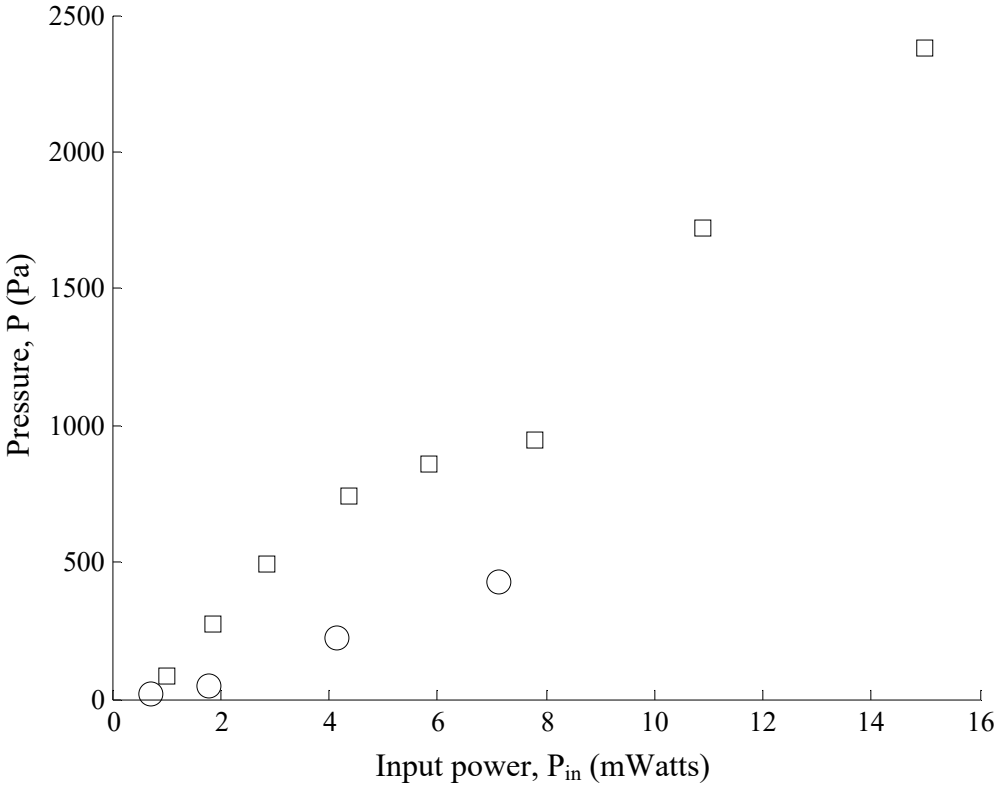

Fig. 3.6: Static pressure generated at different input power for ○ smooth electrodes and □ SWCNT deposited on emitter electrodes for the pump with inter-electrode spacing of 120 μm.

important in microscale cooling applications, since it is an additional parasitic heating that needs to be removed by the fluid. Here, the static pressure varies nearly linearly with the input power for both cases, similar to the findings of Kazemi et. al. [16]. Darabi et. al. [19], however, found a nonlinear relationship between the generated pressure and the power consumption for two of the four pumps tested in their study. The slope can be considered as one measure of the pump performance [16], with values of approximately 67 and 157 Pa/mW for the pump with smooth and SWCNT deposited on emitter electrodes, respectively.

The flow rate at different applied voltages with no back pressure ($\Delta h = 0$) is presented in Figure 3.7 for the pump with inter-electrode spacing of 120 μm. The flow rate increases with an increase of the applied voltage, with it being much more significant for the case where SWCNT was deposited on the emitter electrode. For instance, the maximum flow rate at 1300 V is 29 and 93 μL/min for the pump with smooth and SWCNT deposited electrodes, respectively. The higher flow rate in case of the latter pump can be directly attributed to the higher charge injection. The flow rates were also measured at different back pressures (by changing Δh) for a fixed applied voltage of 1100 V to determine the pump characteristic curve (plot of the pressure head vs flow rate). The variation of pressure head with the flow rate for this applied voltage is presented in Figure 3.8. There is an increase in the flow range, and an increase in the pressure with the SWCNT deposited micropump when compared to the smooth electrode case.

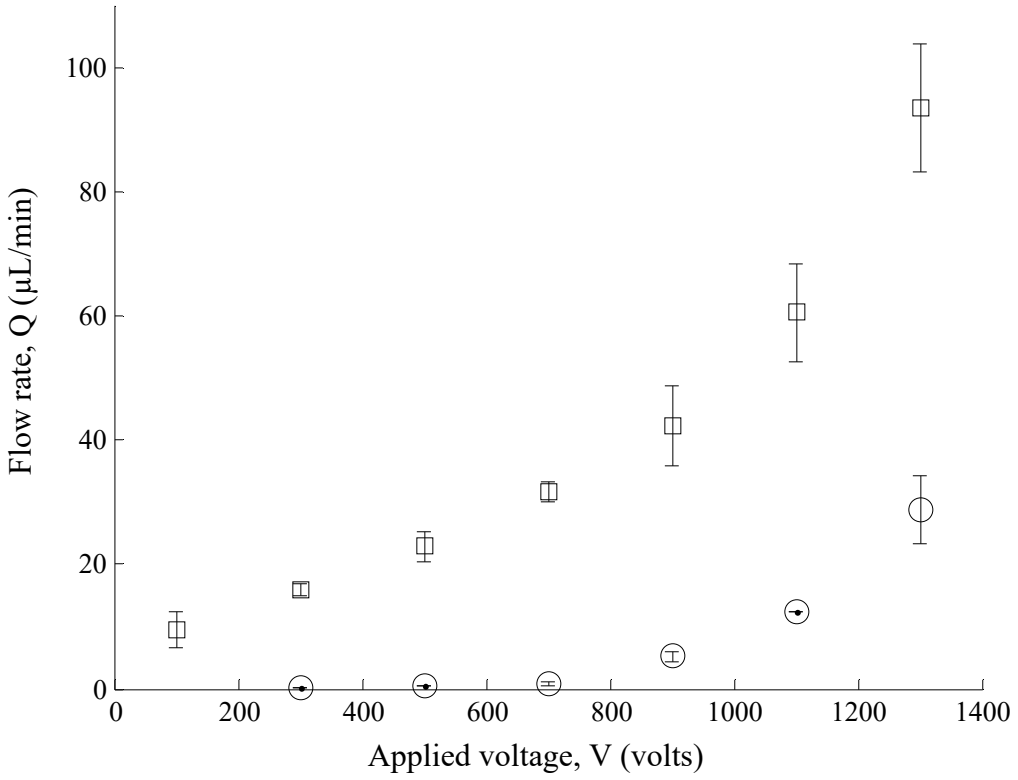

Fig. 3.7: Flow rate at no back pressure condition at different applied voltage for ○ smooth electrodes and □ SWCNT deposited on emitter electrodes for the pump with inter-electrode spacing of 120 μm.

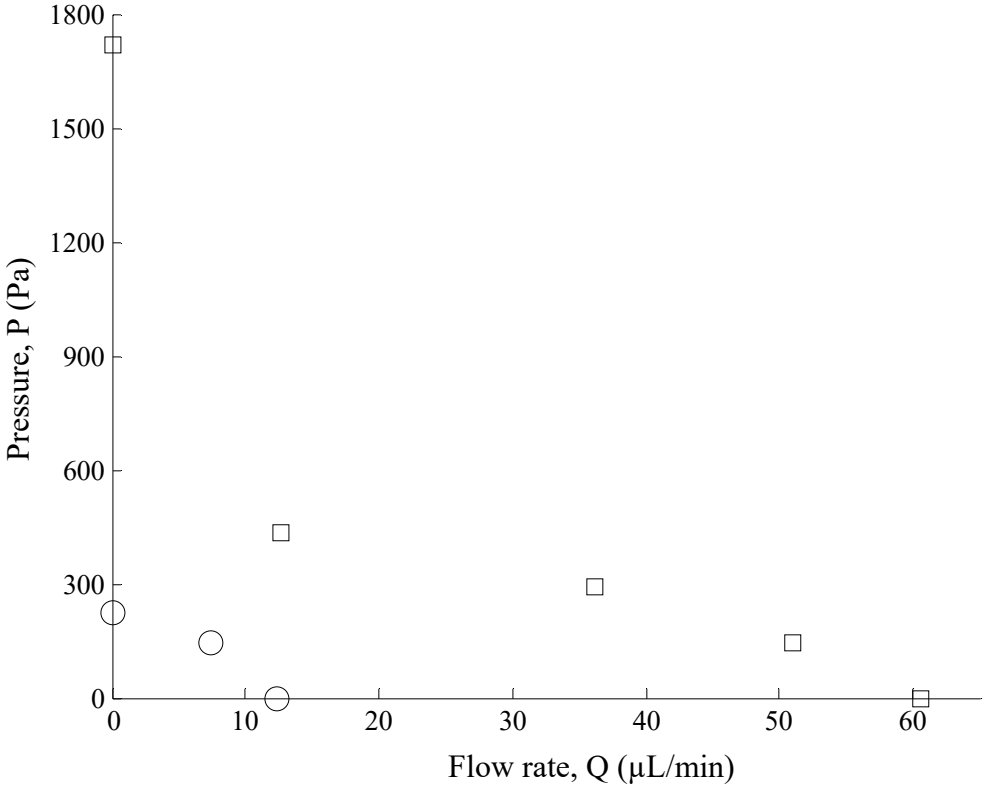

Fig. 3.8: Pressure vs flow characteristics of the pump with ○ smooth electrodes and □ SWCNT deposited on emitter electrodes at an applied voltage of 1100 volts with inter-electrode spacing of 120 μm.

The corresponding current and static pressure generation with the applied voltage for the micropump with inter-electrode spacing of 40 μm are presented in Figure 3.9 and Figure 3.10. As the inter-electrode spacing is reduced, the effective electric field increases which results in a higher charge injection as observed in Figure 3.9 for both the smooth and SWCNT deposited on emitter electrodes when compared to the pumps with inter-electrode spacing of 120 μm (Figure 3.4). This enhancement in charge injection is reflected as an improvement in pump performance as shown in Figure 3.10 in terms of the static pressure generated at the different applied voltages. For example, the static

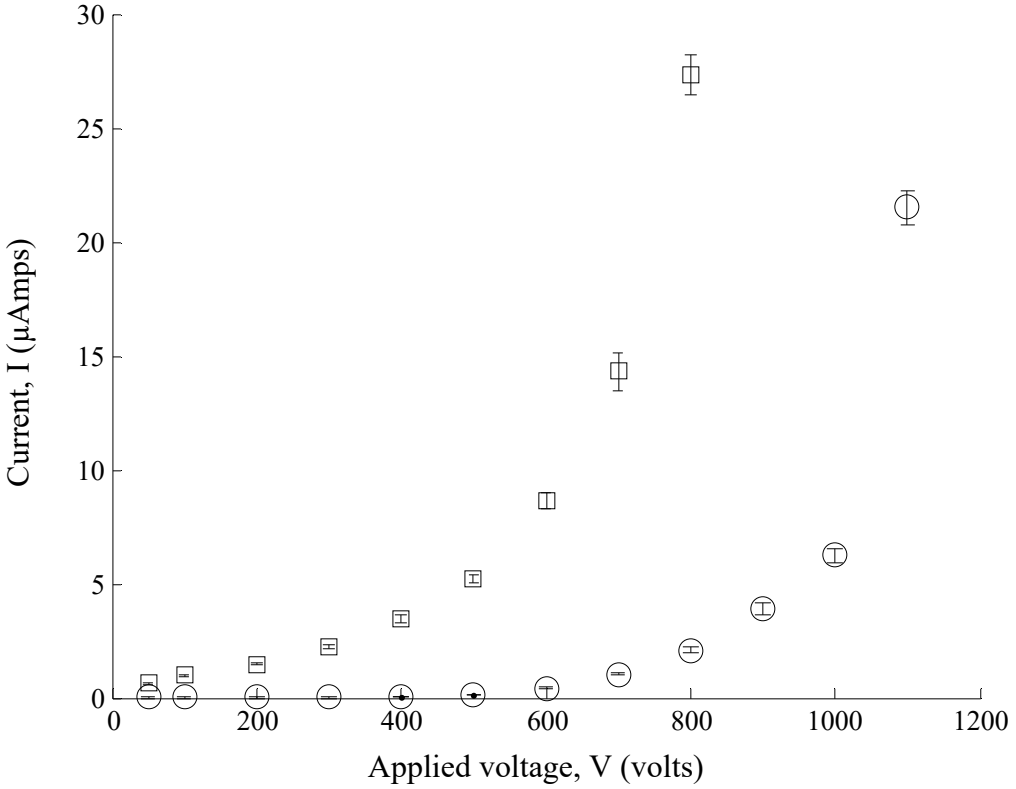

Fig. 3.9: I-V characteristics for ○ smooth electrodes and □ SWCNT deposited on emitter electrodes at static condition for the pump with inter-electrode spacing of 40 μm.

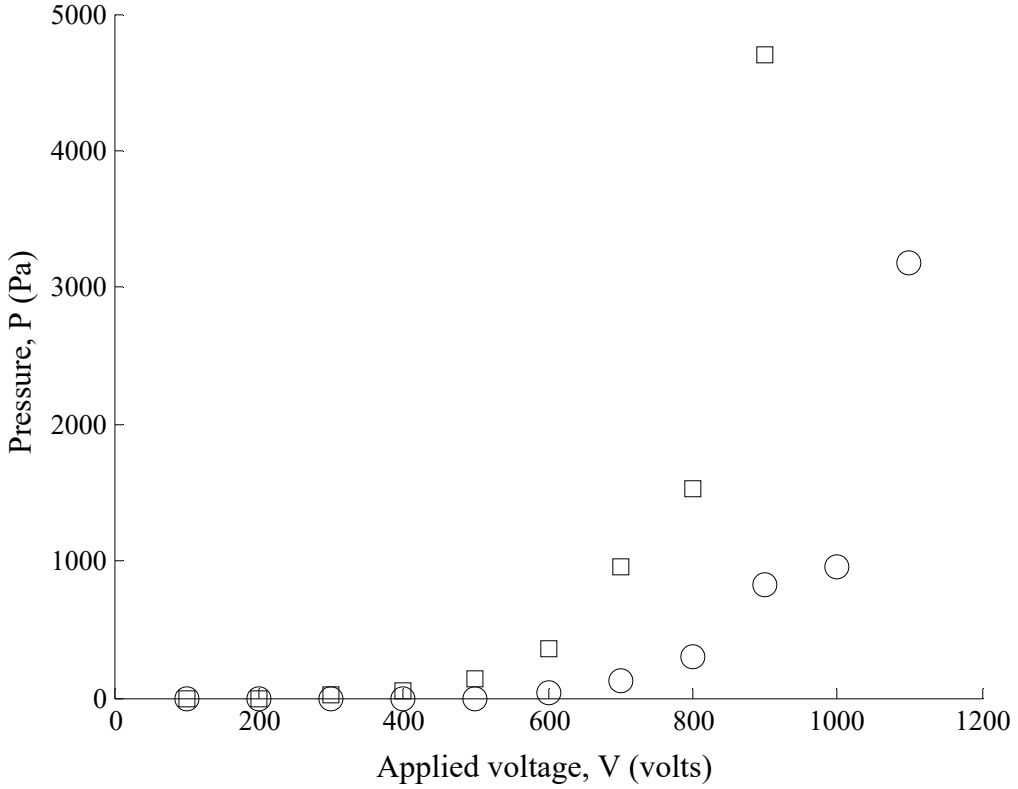

Fig. 3.10: Static pressure generated at different applied voltage for ○ smooth electrodes and □ SWCNT deposited on emitter electrodes for the pump with inter-electrode spacing of 40 μm.

pressure head generation improved by a factor greater than 12 and 5 when the inter electrode spacing reduced from 120 to 40 μm for the pumps with smooth electrodes and with SWCNT deposited on the emitter electrodes, respectively. A maximum static pressure of 4.7 kPa was obtained for the micropump with SWCNT deposited on emitter electrodes when the interelectrode spacing was 40 μm. The pressure generation with the input power is presented in Figure 3.11. The static pressure generation per unit power consumption was 131 and 211 Pa/mW for the pump with smooth and SWCNT deposited

electrodes when the inter-electrode spacing was 40 μm (Figure 3.11), which was an improvement by a factor of approximately 2 and 1.3 respectively.

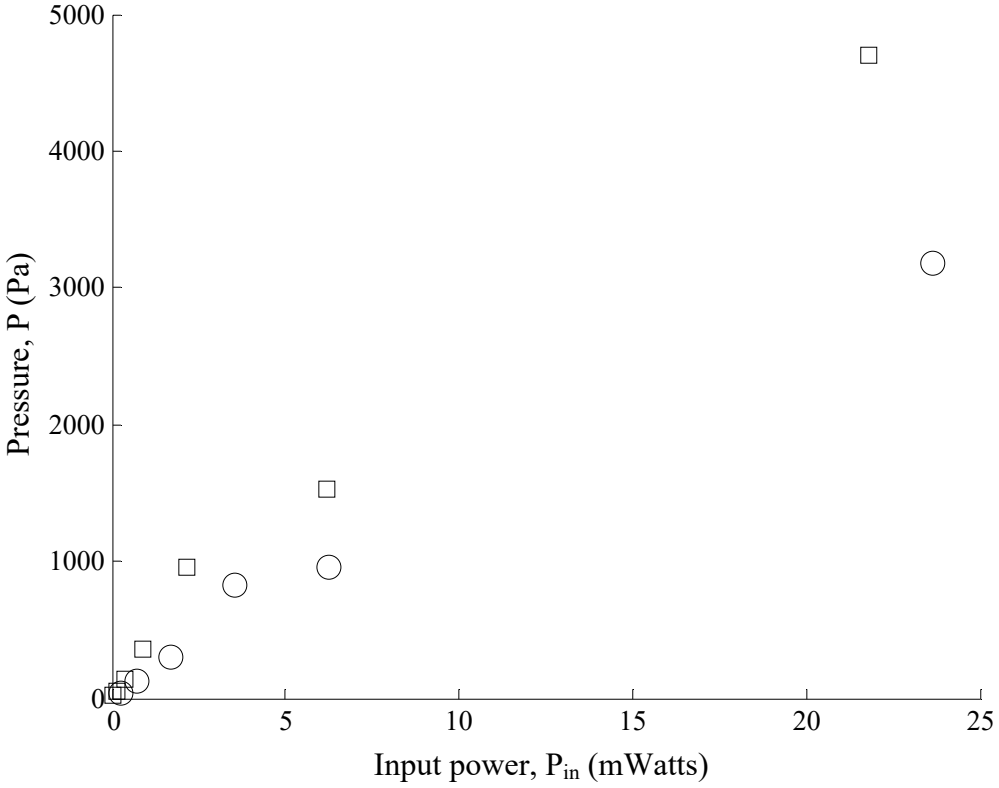

Fig. 3.11: Static pressure generated at different input power for ○ smooth electrodes and □ SWCNT deposited on emitter electrodes for the pump with inter-electrode spacing of 40 μm.

3.4 Conclusion

An experimental study was performed to determine the effect of nano structures (deposited on the emitter electrodes) on the charge injection, pressure generation and flow rate of an ion drag EHD micropump using HFE 7100 as the working dielectric liquid. SWCNT were deposited on the emitter electrodes by electrophoretic deposition. The pumps had a total of 100 pairs of electrodes, where the width of the emitter and collector electrodes was 40 and 20 μm, respectively. Two pumps with inter-electrode spacing of 120 and 40 μm were tested, where the spacing between each pair of electrodes was 240 and 80 μm, respectively. The width and height of the microchannel was 5 mm and 100 μm respectively, while the lengths of the two pumps were 50 and 29 mm respectively. A lower threshold voltage, higher current and greater static pressure and flow rate was obtained with the pump where SWCNT was deposited on the emitter electrode compared to the one with smooth electrodes. The threshold voltage was reduced by a factor of approximately 3 and 1.4 for the micropumps with SWCNT deposited on the emitter electrodes when compared to the one with smooth electrodes for inter-electrode spacing of 120 μm and 40 μm, respectively. A maximum pressure generation of 4.7 kPa was obtained at an applied voltage of 900 V for the pump with inter-electrode spacing of 40 μm when SWCNT was deposited on emitter electrodes. The maximum flow rate was improved by a factor of 3 for the pump with SWCNT deposited on the emitter electrodes when compared to the smooth electrode one. The input power

required to generate a set pressure head is lower for the pump with SWCNT deposited on the emitter electrode.

3.5 References

[1] I. Mudawar, "Assessment of high-heat-flux thermal management schemes," IEEE Trans. Compon. Packag. Technol., vol. 24, no. 2, pp. 122–141, Jun. 2001.

[2] L. Jiang, M. Wong, and Y. Zohar, "Forced convection boiling in a microchannel heat sink," J. Microelectromech. Syst., vol. 10, no. 1, pp. 80–87, Mar. 2001.

[3] D. B. Tuckerman and R. F. W. Pease, "High-performance heat sinking for VLSI," IEEE Electron Device Lett., vol. 2, no. 5, pp. 126–129, May 1981.

[4] B. D. Iverson and S. V. Garimella, "Recent advances in microscale pumping technologies: A review and evaluation," Microfluidics Nanofluidics, vol. 5, no. 2, pp. 145–174, Aug. 2008.

[5] O. M. Stuetzer, "Ion drag pressure generation," J. Appl. Phys., vol. 30, no. 7, pp. 984–994, 1959.

[6] O. M. Stuetzer, "Ion drag pumps," J. Appl. Phys., vol. 31, no. 1, pp. 136–146, 1960.

[7] G. V. Jorgenson and E. Will, "Improved ion drag pump," Rev. Sci. Instrum., vol. 33, no. 1, pp. 55–56, 1962.

[8] W. F. Pickard, "Ion drag pumping. II. Experiment," J. Appl. Phys., vol. 34, no. 2, pp. 251–258, 1963.

[9] J. Seyed-Yagoobi, J. E. Bryan, and J. A. Castaneda, "Theoretical analysis of ion-drag pumping," IEEE Trans. Ind. Appl., vol. 31, no. 3, pp. 469–476, May/Jun. 1995.

[10] A. Richter, A. Plettner, K. A. Hofmann, and H. Sandmaier, "A micromachined electrohydrodynamic (EHD) pump," Sens. Actuators A, Phys., vol. 29, no. 2, pp. 159–168, Nov. 1991.

[11] S.-H. Ahn and Y.-K. Kim, "Fabrication and experiment of a planar micro ion drag pump," Sens. Actuators A, Phys., vol. 70, nos. 1–2, pp. 1–5, Oct. 1998.

[12] J. M. Crowley, G. S. Wright, and J. C. Chato, "Selecting a working fluid to increase the efficiency and flow rate of an EHD pump," IEEE Trans. Ind. Appl., vol. 26, no. 1, pp. 42–49, Jan./Feb. 1990.

[13] J. E. Bryan and J. Seyed-Yagoobi, "Experimental study of ion-drag pumping using various working fluids," IEEE Trans. Elect. Insul., vol. 26, no. 4, pp. 647–655, Aug. 1991.

[14] V. Benetis, A. Shooshtari, P. Foroughi, and M. M. Ohadi, "A sourceintegrated micropump for cooling of high heat flux electronics," in Proc. 19th Annu. IEEE Semiconductor Thermal Meas. Manage. Symp., Mar. 2003, pp. 236–241.

[15] P. Foroughi, V. Benetis, M. Ohadi, Y. Zhao, and J. Lawler, "Design, testing and optimization of a micropump for cryogenic spot cooling applications," in Proc. 21st Annu. IEEE Semiconductor Thermal Meas. Manage. Symp., Mar. 2005, pp. 335–340.

[16] P. Z. Kazemi, P. R. Selvaganapathy, and C. Y. Ching, "Electrohydrodynamic micropumps with asymmetric electrode geometries for microscale electronics cooling," IEEE Trans. Dielect. Elect. Insul., vol. 16, no. 2, pp. 483–488, Apr. 2009.

[17] P. Z. Kazemi, P. R. Selvaganapathy, and C. Y. Ching, "Effect of electrode asymmetry on performance of electrohydrodynamic micropumps," J. Microelectromech. Syst., vol. 18, no. 3, pp. 547–554, Jun. 2009.

[18] P. Z. Kazemi, P. R. Selvaganapathy, and C. Y. Ching, "Effect of micropillar electrode spacing on the performance of electrohydrodynamic micropumps," J. Electrostatics, vol. 68, no. 4, pp. 376–383, Aug. 2010.

[19] J. Darabi, M. Rada, M. Ohadi, and J. Lawler, "Design, fabrication, and testing of an electrohydrodynamic ion-drag micropump," J. Microelectromech. Syst., vol. 11, no. 6, pp. 684–690, Dec. 2002.

[20] M. K. Bologa, I. A. Kozhukhar, A. V. Malakhov, and V. L. Balokhin, "Electrohydrodynamic pump service life," in Proc. IEEE 11th Int. Conf. Conduction Breakdown Dielect. Liquids (ICDL), Jul. 1993, pp. 561–565.

[21] V. Benetis, "Experimental and computational investigation of planar ion drag micropump geometrical design parameters," Ph.D. dissertation, Dept. Mech. Eng., Univ. Maryland, College Park, MD, USA, 2005.

[22] M. Xue, W. Wang, F. Wang, J. Ou, C. Li, and W. Li, "Understanding of the correlation between work function and surface morphology of metals and alloys," J. Alloys Compounds, vol. 577, pp. 1–5, Nov. 2013.

[23] D. Carvalho, S. Ghosh, R. Banerjee, and P. Ayyub, "Ultra-low breakdown voltage and origin of 1/f 2 noise in metallic nanorod arrays," Nanotechnology, vol. 19, no. 44, p. 445713, 2008.

[24] M. K. Russel, P. R. Selvaganapathy, and C. Y. Ching, "Effect of electrode surface topology on charge injection characteristics in dielectric liquids: An experimental study," J. Electrostatics, vol. 72, no. 6, pp. 487–492, Dec. 2014.

[25] J. A. Dorsey and J. H. Davidson, "Ozone production in electrostatic air cleaners with contaminated electrodes," IEEE Trans. Ind. Appl., vol. 30, no. 2, pp. 370–376, Mar./Apr. 1994.

[26] L. Tanasomwang and F. C. Lai, "Long-term ozone generation from electrostatic air cleaners," in Proc. 32nd IEEE Ind. Appl. Conf. IAS Annu. Meeting (IAS), Oct. 1997, pp. 2037–2044.

[27] B. Gao et al., "Fabrication and electron field emission properties of carbon nanotube films by electrophoretic deposition," Adv. Mater., vol. 13, no. 23, pp. 1770–1773, Dec. 2001.

[28] M. S. El-Genk and H. Bostanci, "Saturation boiling of HFE-7100 from a copper surface, simulating a microelectronic chip," Int. J. Heat Mass Transf., vol. 46, no. 10, pp. 1841–1854, May 2003.

[29] M. Butcher, A. Neuber, M. D. Cevallos, J. C. Dickens, and H. Krompholz, "Conduction and breakdown mechanisms in transformer oil," IEEE Trans. Plasma Sci., vol. 34, no. 2, pp. 467–475, Apr. 2006.

[30] W. F. Schmidt, "Electronic conduction processes in dielectric liquids," IEEE Trans. Elect. Insul., vol. EI-19, no. 5, pp. 389–418, Oct. 1984.

[31] B. Halpern and R. Gomer, "Field emission in liquids," J. Chem. Phys., vol. 51, no. 3, pp. 1031–1047, 1969.

[32] B. Halpern and R. Gomer, “Field ionization in liquids,” J. Chem. Phys., vol. 51, no. 3, pp. 1048–1056, 1969.

[33] P. Atten and J. Seyed-Yagoobi, “Electrohydrodynamically induced dielectric liquid flow through pure conduction in point/plane geometry,” IEEE Trans. Dielect. Elect. Insul., vol. 10, no. 1, pp. 27–36, Feb. 2003.

[34] S.-I. Jeong and J. Seyed-Yagoobi, “Experimental study of electrohydrodynamic pumping through conduction phenomenon,” J. Electrostatics, vol. 56, no. 2, pp. 123–133, Sep. 2002.

[35] L. Kogut, “The influence of surface topography on the electromechanical characteristics of parallel-plate MEMS capacitors,” J. Micromech. Microeng., vol. 15, no. 5, p. 1068, 2005.

Chapter 4

Effect of doping ferrocene in the working fluid of electrohydrodynamic (EHD) micropump

Complete citation:

Russel, M.K., Hasnain, S.M., Selvaganapathy, P.R., Ching, C.Y., 2016. Effect of doping ferrocene in the working fluid of electrohydrodynamic (EHD) micropump. *Microfluid Nanofluid*. 20 (8): 1-9.

Copyright:

Relative Contributions:

Russel M.K.: Performed all experiments, interpretation and analysis of the data and wrote the drafts of the manuscript including all figures and text.

Hasnain, S.M.: Assisted in performing experiments.

Selvaganapathy P.R.: Co-supervisor of M.K. Russel and revised the initial drafts of the manuscript.

Ching C. Y.: Co-supervisor of M.K. Russel and was responsible for the final draft submittal to the journal.

Abstract

The effect of doping ferrocene in the working fluid of electrohydrodynamic micropumps was investigated under the application of DC electric fields. The micropump consisted of 100 planar electrode pairs that were embedded along the bottom wall of a 100-micron-high, 5-mm-wide and 26-mm-long microchannel. The width of the emitter and collector electrodes was 20 and 40 μm, respectively, with inter-electrode spacing of 30 μm. A redox dopant, ferrocene, was diffused homogeneously into the working fluid HFE-7100 at 0.05, 0.1 and 0.2 % concentration by weight. The static pressure head generation and flow rate at different back pressure conditions were measured under different applied DC voltages. The current and pressure generated with the doped working fluid were significantly higher than with pure HFE-7100 under an applied DC field. A maximum static pressure of 6.7 kPa and flow rate of 0.47 mL/min at no back pressure were achieved at 700 V.

4.1 Introduction

Micropumps play an important role in many diverse applications such as in micromixers, 'Lab on Chip' devices and other biological applications (Amirouche et al. 2009; Bourouina et al. 1997; Noori et al. 2009). Another important application for micropumps is in thermal management of microelectronics via liquid cooling. Ion-drag EHD micropumps have been proposed in cooling of transformers, space power stations, high power underground cables and other similar electrical equipments (Bryan and Seyed-Yagoobi 1992). General Electric Co. (Schwabe et al. 1987) used an ion-drag pump in a transformer which enhanced the convective cooling of the transformer. Electrohydrodynamic (EHD) micropumps are particularly appealing for microelectronics cooling as they operate with no moving parts, are easily controllable and can be configured with low-form factors. Stuetzer (1959) first showed that high electric fields can cause flow of ions, and thus fluid flow from one electrode to another. He studied different electrode geometries and obtained a maximum static pressure of approximately 2 kPa with a needle-cylinder electrode configuration. Since then EHD pumps have been developed at the microscale (Ahn and Kim 1998; Darabi et al. 2002; Yang et al. 2004). Darabi et al. (2002) introduced 3D features on the electrodes and obtained 800 Pa of static pressure using HFE-7100 as the working fluid. Kazemi et al. (2009b) incorporated micropillars on the electrodes in their pumps and obtained a maximum static pressure of 2.24 kPa at an applied voltage of 900 V using HFE-7100 as the working fluid. Russel et al. (2014a, b) studied the effect of the electrode surface topology by depositing single

walled carbon nanotubes (SWCNT) on the electrodes. They observed an increase in the local electric field and obtained a static pressure of 4.7 kPa at an applied voltage of 900 V.

For EHD pumps to produce higher flow velocities, a working fluid with low viscosity and high dielectric constant is required. On the other hand, for greater pump efficiency, a fluid with lower electric conductivity and ionic mobility is desired. A low viscosity will provide lower shear resistance to the flow, while a low mobility will increase the breakdown potential of the fluid. A fluid with high dielectric constant is also desired to ensure better efficiency of the system (Crowley et al. 1990). A common working fluid used for micropump applications is Methoxynonafluorobutane (HFE-7100) with a chemical formula, $C_4F_9OCH_3$. HFE-7100 holds several advantages as it is CFC free and is already being used as an industrial refrigerant. Ion-drag injection pumps work on the principle of injecting charges at the metal/dielectric interface by electron tunneling (Schmidt 1984). Charge injection in the system could be by field emission (Halpern and Gomer 1969a) or field ionization (Halpern and Gomer 1969b) and depends on the energy barrier set by the electrode and the dielectric liquid. Energy barrier depends on the effective electric field, e.g., electrode design and configuration, inter-electrode spacing and work function of the electrode material and ionization energy of the working fluid. Electrode design, such as spacing and asymmetry between electrodes, or addition of 3D features on the electrodes, can affect the performance of EHD micropumps (Benetis et al. 2003; Darabi et al. 2002; Darabi and Wang 2005; Foroughi et al. 2005, 2010; Kazemi et al. 2009a, b, 2010). The effect of inter-electrode spacing between the emitter and

collector electrodes (Arii and Schmidt 1984; Atten and Haidara 1985; Darabi and Rhodes 2006; Kazemi et al. 2009a), work function (Butcher et al. 2006) and dielectric liquid type (Arii and Schmidt 1984; Atten and Haidara 1985) on charge injection has been studied.

One drawback of existing micropumps is the relatively low pressure head developed, which makes it difficult for use in practical applications where there is a large pressure drop across the microchannel heat sinks. Several studies on the effect of adding doping agent into the dielectric liquid on the fluid properties and flow velocity have been studied (Bohinsky and Seyed-Yagoobi 1990; Bryan and Seyed-Yagoobi 1991, 1992; Jayaram and Cross 1994; Pontiga and Castellanos 1996). Bryan and Seyed-Yagoobi (1991, 1992) found an increase in the electrical conductivity but decrease in the permittivity as the level of doping agent was increased in the working fluids dodecylbenzine (dielectric constant of 1.71) and Envirotemp 200. They used 'over based calcium sulfonate' as their doping agent. Bohinsky and Seyed-Yagoobi (1990) reported an increase in the electrical conductivity as the doping level increased but the kinematic viscosity remained the same. Bryan and Seyed-Yagoobi (1991, 1992) found a reduction in the velocity of the bulk liquid as the level of doping agent increased in dodecylbenzine while for Envirotemp 200 as the working fluid; there was an optimum doping level to generate the highest velocity. For example, the bulk velocity reduced by a factor of 3 when doping agent at 100 ppm was introduced to dodecylbenzine compared to no doping for a range of nominal applied field of 3–5 V/μm. No significant change in velocity was observed for higher doping level of 250 ppm when compared to 100 ppm. In case of undoped Envirotemp 200, no significant velocity was observed. As the level of doping

agent was increased the velocity increased up to a doping level of 750 ppm and decreased thereafter. Bohinsky and Seyed-Yagoobi (1990) also found an optimal level of doping in the working fluid n-Hexane and dodecylbenzene to generate a maximum velocity, while for Texaco 0600 such optimal doping level was not found. Jayaram and Cross (1994) studied the effect of adding anionic surfactant (dodecyl benzenesulfonic acid) as dopant into working fluids voltesso 35, norpar 12, norpar 13 and norpar 15. They reported an increase in the electric conductivity, apparent liquid velocity and steady state current as the doping level increased. Pontiga and Castellanos (1996) developed an analytical model to study the effect of levels of electrolyte solutions in nonpolar liquids to characterize the contribution of the dissociation and the injection current components of the total current. The total current within the quasi-Ohmic conduction regime or the injection regime increased as the dopant level increased. The dissociation component of the current within these regimes remained similar, indicating a significant increase in the injection current component as the doping level increased. Most of these studies have used ionic or polarizable groups as dopant molecules. There have been no studies on the use of redox active groups as dopant molecules in EHD micropumps.

The objective of this research is to investigate the effect of doping the working fluid with a redox dopant to enhance the injection strength and EHD mobility and thus the charge injection and pump performance. The pump configuration and electrode geometry were based on previous studies (Kazemi et al. 2009a, b, 2010). In this study, the working fluid HFE-7100 was doped with ferrocene at different percentage concentration by weight. Ferrocene is an organometallic compound with a Ferrous (Fe^{2+})

ion in the center of the molecular structure and two cyclopentadienyl rings ($C_5H_5^-$) giving it a chemical formula $Fe(C_5H_5)_2$ (Ewing and Cazes 2005; Zanello 2003). Under the application of an electric field, ferrocene will transform into Ferrocenium ($Fe(C_5H_5)_2^+$) through a redox reaction:

$$Fe(C_5H_5)_2 \leftrightarrow \left[Fe(C_5H_5)_2^+\right] + e^- \qquad (4.1)$$

The ionized molecules will move in the direction of the electric field and generate fluid flow through drag on the adjacent molecules. The potential advantages of doping HFE with ferrocene are additional charge availability and higher pressure generation. Ferrocene is also able to retain its molecular structure even when losing an electron, and thus there will be no decomposition of ferrocene under the applied electric potential.

4.2 Experimental Methodology

The micropump used in this study has 100 pairs of lithographically patterned gold electrodes in series embedded along the bottom glass wall of a microchannel. An asymmetric planar electrode configuration (with the width of the collector electrode being twice that of the emitter electrode) was used as this electrode configuration resulted in significantly higher pump performance when compared to a symmetric design (with the width of the emitter and collector being equal) (Kazemi et al. 2009b). For such an electrode design, the component of the net electric field in the flow direction increases due to the asymmetry of the electric field distribution. The thickness of the electrodes is 250 nm which have a 240-nm layer of gold deposited on a glass substrate with a thin layer (10 nm) of adhesive chromium in between to bind the gold layer to the glass. The details of the microfabrication can be found in (Kazemi et al. 2009b). The widths of the emitter and collector electrodes were 20 and 40 μm, respectively. The inter-electrode spacing was 30 μm, and the spacing between each pair of electrodes is 60 μm. The PDMS microchannel (26 mm long) was made out of a silicon mold and bonded to the glass substrate. A schematic of the cross-section of the pump with two pairs of electrodes with the principal dimensions is shown in Fig. 4.1.

The micropumps were tested with HFE-7100 alone and with ferrocene doped in HFE-7100 (by weight) as the working fluid under no flow and different back flow conditions. The properties of HFE-7100 and ferrocene are presented in Table 4.1 (El-Genk and Bostanci 2003) and Table 4.2, respectively. The weight-based saturation point

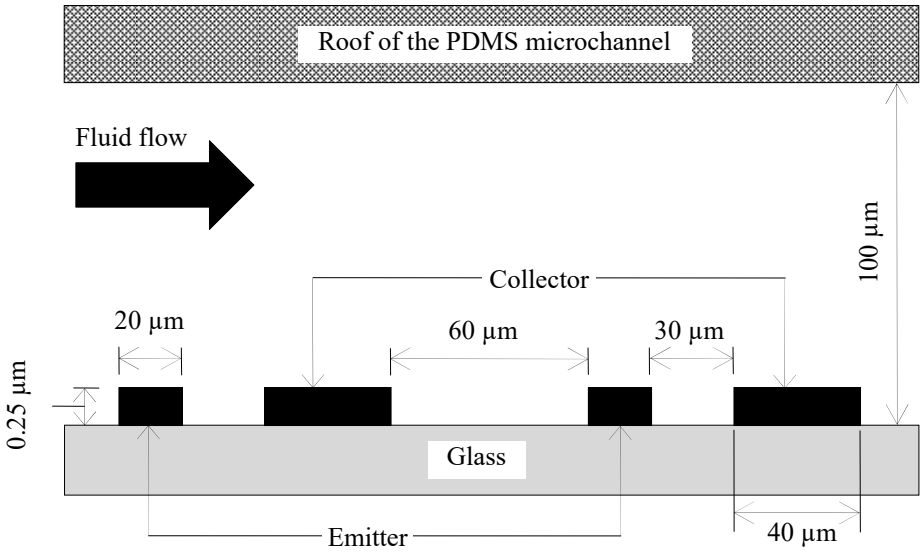

Fig. 4.1: Schematic of the cross section of the pump with key dimensions (not to scale). The total number of electrode pairs is 100 but only 2 pairs are shown for reference.

Table 4.1: Properties of HFE-7100 at 25 °C (El-Genk and Bostanci 2003)

Property	Value
Boiling point (°C)	61
Viscosity (Kg/ms)	$3.7X10^{-4}$
Specific heat (J/KgK)	1255
Density (Kg/m^3)	1481
Volume resistivity (Ω cm)	$3.29 X 10^9$
Dielectric constant, 100 Hz – 10 MHz	7.39
Dielectric strength (0.1 in. gap)	28 kV (RMS)

Table 4.2: Properties of ferrocene (Sigma-Aldrich)

Property	Value
Form	Powder, orange
Boiling point (°C)	249
Melting point (°C)	172-174
Density (Kg/m^3)	2690
Conductivity (S/cm)	$6X10^{-3}$
Molecular weight (gm/mol)	186.03

of ferrocene in HFE-7100 was estimated using a thermogravimetric analysis (TGA Q 5000 IR Thermogravimetric Analyzer, TA Instruments, sensitivity <0.1 μg, weighing accuracy ≤ ± 0.1 % of reading) and found to be 0.22 %. Three (0.05, 0.1 and 0.2 %) different percentage of ferrocene doped in HFE-7100 were tested and compared with the base case of HFE-7100 only. The HFE-ferrocene was sonicated for 5 min, and no particle aggregation was visible even after months.

A DC voltage was applied using a Trek 677 supply/amplifier (capacity of 2 kV, accuracy ≤0.1 % of full scale) that was connected to embedded emitter and collector electrode pads (Fig. 4.2a). An ammeter (Keithley 2636 SourceMeter, resolution of 1 fA, accuracy better than 0.02 % of reading + 25 nA) was used to record the current readings at different applied voltages. Short glass tubings of 1.5 mm diameter were connected to the inlet and outlet of the micropump that functioned as the fluidic interconnections. Transparent plastic tubing of 1/16 in. diameter was subsequently connected to the glass tubings. To determine the pressure generation, the plastic tubings were positioned vertically close to each other and the micropump was filled with the working fluid using a syringe so that the fluid level could be easily detected in both the inlet and outlet columns to ensure no entrapped bubbles. The fluid level in both the inlet and outlet columns was checked to be equal before turning on the power supply. The fluid level in both plastic tubings readily equalized indicating that surface tension effects were not dominant in the pressure measurement. The pressure head at no flow condition was determined at different applied voltages by measuring the difference in the fluid level in

the inlet and outlet columns (Fig. 4.2b) using a height gage (KBC tools, resolution 0.02 mm).

Fluid flow experiments with HFE-7100 and 0.05 % ferrocene doped in HFE-7100 were performed at different back pressure conditions for a range of applied potential.

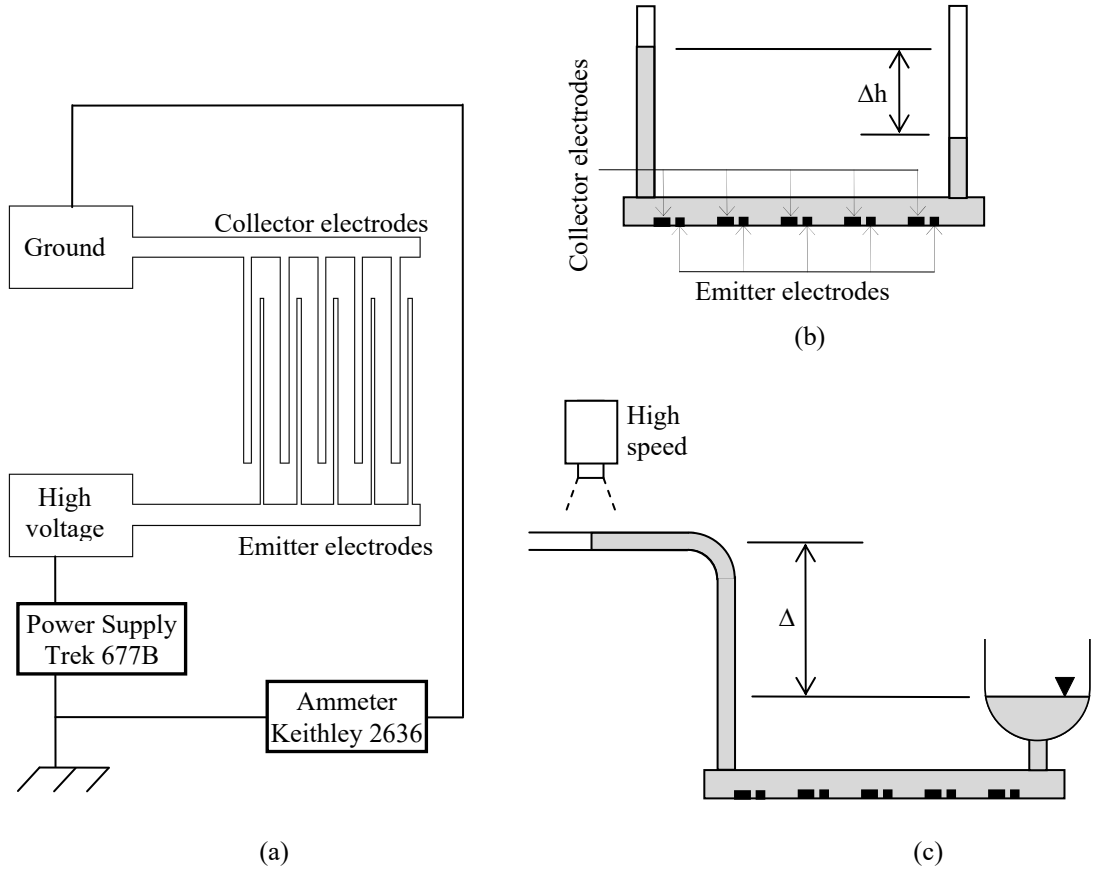

Fig. 4.2: Schematic of the experimental facility (a) electric connections with the top view of the micropump electrodes (b) static pressure head measurement with the side view of the electrodes (c) flow velocity measurement facility at a back pressure equivalent to a height of Δh. (the number of electrode pairs is 100 but only 5 pairs are shown in the schematic for clarity)

Flow rate was calculated from the cross-sectional area and the average flow velocity in the long horizontal plastic tubing downstream of the pump. The flow velocity was measured using a high-speed digital camera to image the moving liquid–air interface (Fig. 2c). Commercially, available image processing software was used to calculate the displacement and the time between a series of successive frames of the interface. The velocity of the interface was obtained from the ratio of the displacement to the time. A steady flow was assumed when the velocity did not change over time. The time required to reach steady flow was different at different applied potential and back pressure conditions and was typically between 10 and 60 min. Different back pressure conditions were applied by maintaining an equivalent height difference calculated using the properties of HFE-7100 between the horizontal downstream section of the outlet tubing and the liquid level of the reservoir at the inlet of the pump as shown in Fig. 2c. The ratio of the diameters of the reservoir at the inlet to the downstream outlet tubing was greater than 16. The uncertainty of the flow velocity measurement was estimated as ±0.2 mm/s, which corresponds to an uncertainty of ±20 to ±33 % at the high and low-flow rates. The results presented in the results and discussion section are average of five experiments and corresponding error bars in each figure represent the uncertainty in each set of results.

4.3 Results and Discussion

The tests were performed using HFE-7100 doped with ferrocene by 0.05, 0.1 and 0.2 % concentration by weight (hereafter known as HFE-x, where x = 0.05, 0.1 or 0.2 %) and were compared against the results obtained using HFE- 0.0 (here x = 0.0 %, indicating no doping). The maximum doping percentage of ferrocene was kept to 0.2 % as the saturation was found to be 0.22 % from thermogravimetric analysis. Negative voltages were applied to the emitter electrodes (i.e., field emission), while the collector electrodes were grounded in all the experiments performed as it was found from previous studies that field emission is advantageous over field ionization due to higher charge injection and lower threshold voltage for the onset of charge injection (Butcher et al. 2006; Halpern and Gomer 1969a, b; Russel et al. 2014a, b; Schmidt 1984). During the field emission process, electrons tunnel through the metal–liquid interface provided that sufficient energy is applied to overcome the energy barrier set by the electrodes and the liquid (Halpern and Gomer 1969a; Schmidt 1984). The voltage–current (I–V) characteristic at different applied voltage for the doped fluids is compared to HFE- 0.0 in Fig. 4.3 for a static/no flow condition. The results for all four liquids show the typical trend of discharge in a dielectric liquid with two distinct regimes: (1) a low slope quasi-Ohmic region and (2) a high slope injection region (Russel et al. 2014a, b). The low slope quasi-Ohmic region corresponds to conduction mechanism (Atten and Seyed-Yagoobi 2003), while the high slope region correspond to injection mechanism. Current flow within the low slope quasi-Ohmic region is due to the dissociated ions and heterocharges

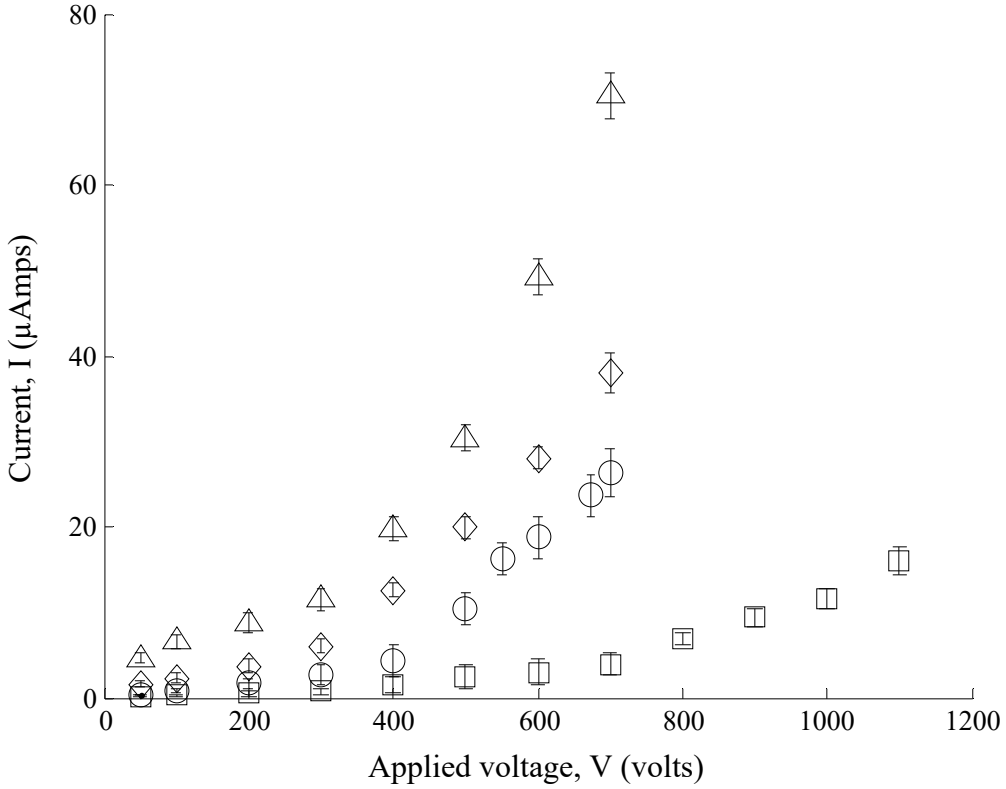

Fig. 4.3: Variation of current with applied DC voltage for (*white square*) HFE-0.0, (*white circle*) HFE-0.05, (*white diamond*) HFE-0.1 and (*white triangle*) HFE-0.2

generated at the electrodes (Jeong and Seyed-Yagoobi 2002). As the level of doping agent was increased the slope of the low slope quasi-Ohmic region increased, indicating an increase in the electric conductivity of the ferrocene doped liquid as observed previously (Bohinsky and Seyed-Yagoobi 1990; Bryan and Seyed-Yagoobi 1991, 1992; Jayaram and Cross 1994). As the level of doping increases, the additional electrons from the redox reaction (Eq. 4.1) increases and enhances the effective conductivity of the fluid. The higher current within the injection regime could be attributed to the higher injection strength (Pontiga and Castellanos 1996) or EHD mobility (Jayaram and Cross 1994) due

to the increase in the doping level. Jayaram and Cross (1994) in their study found that as the level of doping agent was increased the transient velocity of the fluid increased, which in turn enhanced the EHD mobility.

The threshold voltage for the onset of charge injection is typically estimated as the voltage where the low slope quasi-Ohmic region and the steeper injection region intersect (Russel et al. 2014a, b). The threshold voltages for HFE-0.0, HFE-0.05, HFE-0.1 and HFE-0.2 are 640 ± 30, 390 ± 20, 330 ± 20 and 290 ± 15 V, respectively. The doping with ferrocene is seen to increase the current for a given applied voltage. There is an increase in the total current as the level of doping increases over the range of the applied voltage, consistent with previous studies (Jayaram and Cross 1994; Park et al. 2009; Pontiga and Castellanos 1996). For example, the discharge current at 700 V is 3.9, 26.4, 39.9 and 70.5 μAmps for HFE-0.0, HFE-0.05, HFE- 0.1 and HFE-0.2, respectively. The enhancement in the current due to doping could be attributed to two factors: (1) the readily available additional electrons due to the redox reaction and (2) increase in the total charges compared to HFE-7100 due to the Ferrocenium ($Fe(C_5H_5)_2^+$) ions from ferrocene. The additional current contributed through the redox reaction directly influences the total current at an applied voltage. The other contributing factor in the increased current is the number of ions available in the fluid at an applied voltage. As the number of ion increases due to the increase in doping level of ferrocene, the Coulomb force increases compared to HFE-7100 which influences the EHD motion of the fluid and increases the efficiency of the charge transportation toward the collector electrodes.

The corresponding static pressure generation is shown in Fig. 4.4 and shows a similar trend as the I–V characteristics. The pressure generated with HFE-ferrocene is significantly higher than for HFE-7100 at the same applied voltage. Similar to the current, the pressure increases as the ferrocene percentage is increased. For example, the static pressure at 700 V for HFE-0.0, HFE-0.05, HFE-0.1 and HFE-0.2 are 0.6, 2.6, 4 and 6.7 kPa, respectively. It should be noted that the tests were performed for over 8 h with no significant degradation in the performance as shown in Fig. 4.5. The higher static

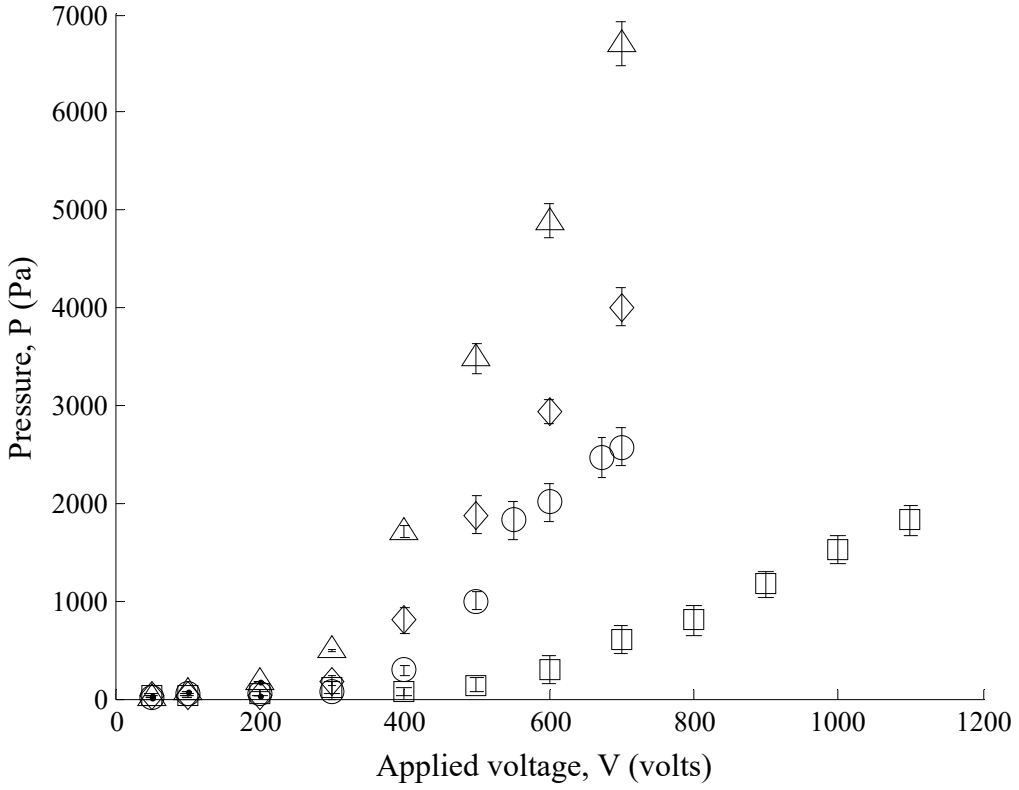

Fig. 4.4: Variation of static pressure with applied DC voltage for (*white square*) HFE-0.0, (*white circle*) HFE-0.05, (*white diamond*) HFE-0.1 and (*white triangle*) HFE-0.2

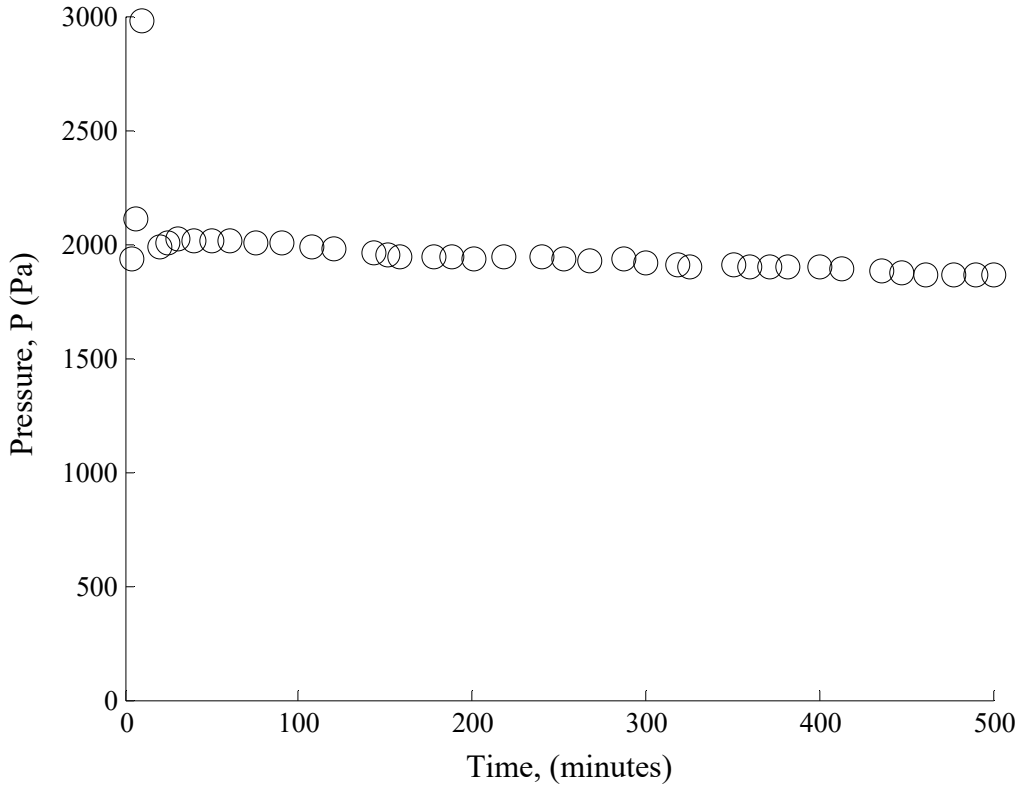

Fig. 4.5: Static pressure at an applied voltage of 600 V over time for HFE-0.05

pressure can be attributed to the higher number of charges within the liquid when ferrocene is doped into HFE-7100. To the best of the authors' knowledge, the 6.7 kPa of pressure generation with HFE-0.2 is the highest to date that has been reported for an EHD micropump. The input power requirement to generate unit pressure is an important pump performance characteristic (Kazemi et al. 2009b) and is presented in Fig. 4.6. The input power indicates the amount of Joule heating at static/no flow condition. The parabolic trend of the graphs show lesser power requirement as the doping level increases to generate a given pressure. For example, the slopes at 2 kPa static power generation are approximately 10, 4.5, 4.3 and 3.5 mW/kPa for HFE-0.0, HFE-0.05, HFE-0.1 and HFE-

0.2, respectively. The 3.5 mW/kPa for HFE-0.2 is much smaller than what has been reported before for EHD micropumps, where Kazemi et al. (2009b) obtained 5.6 mW/kPa. It is interesting to note that the power requirement for the range studied, decreases significantly (26 %, on average) for HFE-0.05 compared to HFE-0.0 but remained about the same (3 %, on average) when further ferrocene was added, e.g., from x = 0.05–0.1 or 0.1–0.2. This is due to the combined effect of increase in the static pressure and ion/charge when ferrocene was doped in HFE-7100 as described earlier.

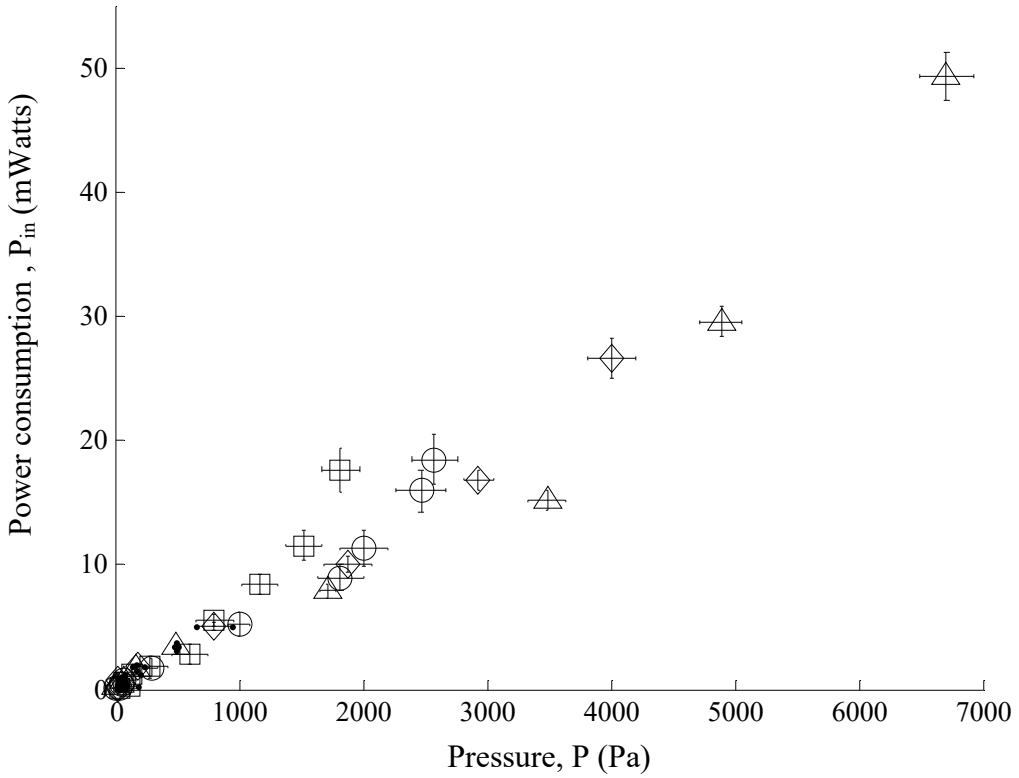

Fig. 4.6: Power consumption to generate pumping pressure for (*white square*) HFE-0.0, (*white circle*) HFE-0.05, (*white diamond*) HFE-0.1 and (*white triangle*) HFE-0.2

When a trace amount (e.g., 0.05 %) of doping agent is introduced to HFE-7100, the number of ions/charges at an applied electric field is greater compared to the case with no doping agent. The Coulomb force, thus, increases which enhances the mobility. The insignificant enhancement in this performance, e.g., static pressure generation per unit power requirement, might indicate that the mobility does not linearly increase as the doping level increases, as seen previously (Jayaram and Cross 1994). The power consumption per unit pressure generation trends in previous studies was found to be linear (Darabi et al. 2002; Kazemi et al. 2009b; Russel et al. 2014a, b); however, Darabi et al. (2002) found a nonlinear relation.

The flow rates at different applied voltage and back pressure conditions are presented in Fig. 4.7 for HFE-0.0 and HFE-0.05. Only the doping level of 0.05 % was tested here as a representative case, and similar results are expected for the other doping levels. The flow rate typically increased as the applied voltage was increased at a given back pressure condition or as the back pressure decreased at an applied voltage. The flow rate at a given back pressure condition and an applied voltage was greater for the doped liquid compared to HFE-7100. For example, at an applied potential of 700 V, the flow rates at a back pressure of 290 Pa are 0.021 and 0.16 mL/min for HFE-0.0 and HFE-0.05, respectively, while the corresponding flow rates at no back pressure conditions are 0.05 and 0.47 mL/min, respectively. Liquid flow at low applied voltage is also evident at greater back pressure conditions when the doping agent is added to the host liquid. The increase in the flow rate could be due to the higher EHD mobility due to the presence of ferrocene in HFE-7100 as explained by Jayaram and Cross (1994). As the transient

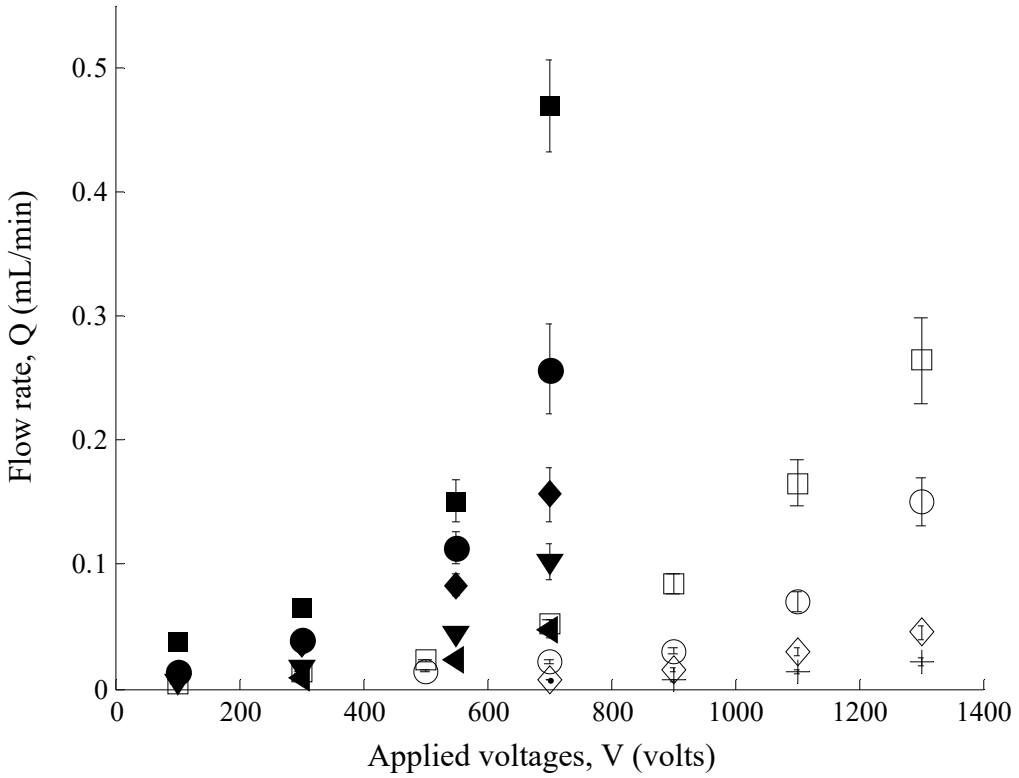

Fig. 4.7: Variation of flow rate of HFE-0.0 (*open symbols*) and HFE- 0.05 (*filled symbols*) with applied DC voltage for back pressure of (*white square*, *black square*) 0 Pa, (*white circle*, *black circle*) 145 Pa, (*white diamond*, *black diamond*) 290 Pa and (*plus*) 726 Pa, (*black down-point triangle*) 580 Pa, (*black left-point triangle*) 1016 Pa

velocity of the fluid increases due to the addition of doping agent, the ion transfer becomes more efficient. The additional Ferrocenium ions interact with the neutral molecules within the liquid due to the electric field and drag the liquid along the field.

Two pump characteristic curves of pressure head at different flow rates for HFE-0.0 and HFE-0.05 are presented in Fig. 8 at an applied potential of $1.41 \times V_{th}$. Here, V_{th} is the threshold voltage for the onset of charge injection, and a factor 1.41 is used so that the pump curves for both HFE-0.0 and HFE-0.05 are in the injection regime. In this case, the

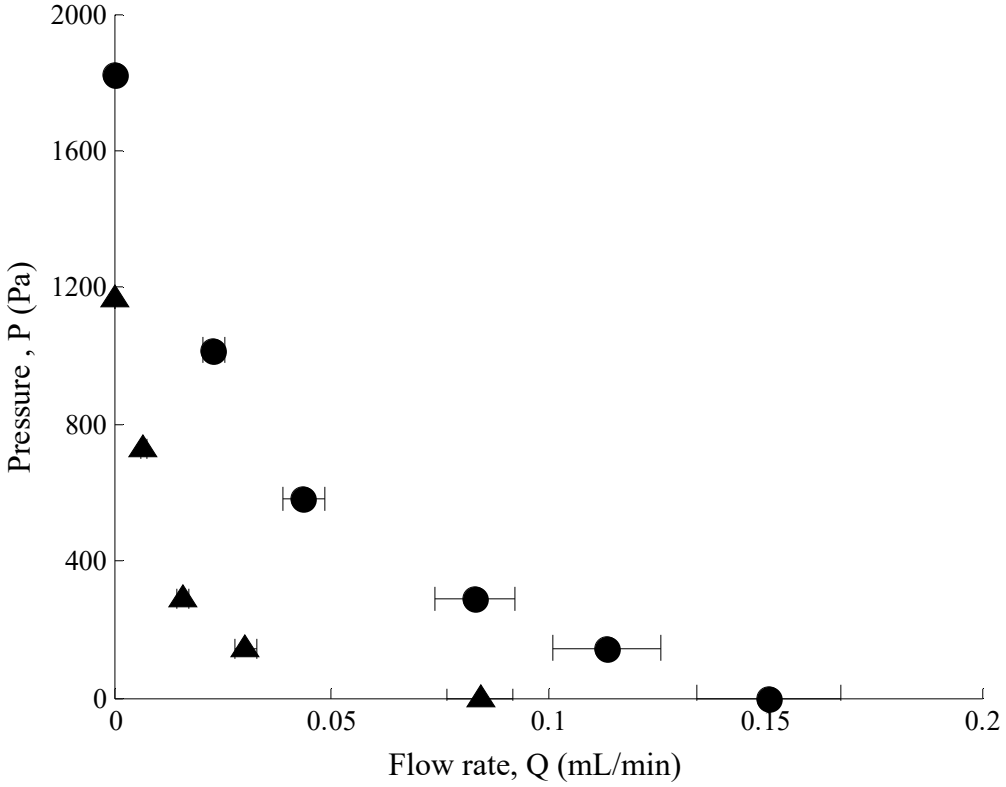

Fig. 4.8: Pump characteristic curve of pressure vs flow rate for (*black triangle*) HFE-0.0 and (*black circle*) HFE-0.05 at an applied voltage of 1.41 * V_{th}

applied voltages correspond to 900 and 550 V for HFE-0.0 and HFE-0.05, respectively. Both pump curves are nonlinear with a steeper decrease in the pressure with flow rate at low-flow conditions compared to the higher flow conditions. The pump characteristic curve for HFE-0.05 sits above the one for HFE-0.0 over the entire range of flow rates. The intersection of the fluid system curve with the pump characteristic curve provides the operating point for the system. It is clear that a greater performance is obtained with the ferrocene doped fluid, with a wider operating range.

4.4 Conclusions

The effect of doping the working fluid HFE-7100 with a redox dopant, ferrocene, on the performance of an EHD micropump was investigated. The micropump consisted of 100 planar electrode pairs that were embedded along the bottom wall of a 100-micron-high and 5 mm-wide microchannel, where the width of the emitter and collector electrodes was 20 and 40 microns, respectively. The micropump had an inter-electrode spacing of 30 microns. Experiments were performed with ferrocene doping levels of 0.05, 0.1 and 0.2 % by weight. The doping was found to improve the pump performance, both in terms of pressure generation and flow rates. The discharge current and static pressure generation increased with an increase in the ferrocene doping level. The discharge current and static pressure generation for the 0.2 % ferrocene concentration fluid were approximately 70 μAmps and 6.7 kPa at an applied potential of 700 V, compared to 3.9 μAmps and 0.6 kPa for the un-doped HFE-7100. The 6.7 kPa of pressure generation with 0.2 % ferrocene concentration fluid is the highest to date that has been reported for an EHD micropump. The tests were performed for over 8 h with no degradation in the pump performance. The flow rate under a no back pressure condition with 0.05 % ferrocene doped in HFE-700 was approximately 0.47 mL/min at 700 V, compared to 0.05 mL/min for the un-doped fluid. The pump characteristic curves of pressure head with flow rate for the 0.05 % ferrocene doped and un-doped fluid are nonlinear, with a steeper decrease in the pressure with flow rate at low-flow conditions

compared to the higher flow conditions. The overall pump performance with the 0.05 % ferrocene doped fluid is better, with a wider operating range.

4.5 References

Ahn S-H, Kim Y-K (1998) Fabrication and experiment of a planar micro ion drag pump. Sens Actuators A Phys 70:1–5

Amirouche F, Zhou Y, Johnson T (2009) Current micropump technologies and their biomedical applications. Microsyst Technol 15:647–666

Arii K, Schmidt WF (1984) Current injection and light emission in liquid argon and xenon in a divergent electric field. IEEE Trans Electr Insul EI-19(1):16–23

Atten P, Haidara M (1985) Electrical conduction and EHD motion of dielectric liquids in a knife-plane electrode assembly. IEEE Trans Electr Insul EI-20(2):187–198

Atten P, Seyed-Yagoobi J (2003) Electrohydrodynamically induced dielectric liquid flow through pure conduction in point/plane geometry. IEEE Trans Dielectr Electr Insul 10:27–36

Benetis V, Shooshtari A, Foroughi P, Ohadi M (2003) A source-integrated micropump for cooling of high heat flux electronics. In: Semiconductor thermal measurement and management symposium, 2003. Nineteenth annual IEEE, 2003. IEEE, pp 236–241

Bohinsky B, Seyed-Yagoobi J (1990) Induction electrohydrodynamic pumping-selecting an optimum working fluid. In: Industry applications society annual meeting, 1990. Conference record of the 1990 IEEE, 1990. IEEE, pp 795–801

Bourouina T, Bossebuf A, Grandchamp J-P (1997) Design and simulation of an electrostatic micropump for drug-delivery applications. J Micromech Microeng 7:186

Bryan J, Seyed-Yagoobi J (1991) Experimental study of ion-drag pumping using various working fluids. IEEE Trans Electr Insul 26:647–655

Bryan JE, Seyed-Yagoobi J (1992) An experimental investigation of ion-drag pump in a vertical and axisymmetric configuration. IEEE Trans Ind Appl 28:310–316

Butcher M, Neuber A, Cevallos MD, Dickens JC, Krompholz H (2006) Conduction and breakdown mechanisms in transformer oil. IEEE Trans Plasma Sci 34:467–475

Crowley JM, Wright GS, Chato JC (1990) Selecting a working fluid to increase the efficiency and flow rate of an EHD pump. IEEE Trans Ind Appl 26:42–49

Darabi J, Rhodes C (2006) CFD modeling of an ion-drag micropump. Sens Actuators A Phys 127:94–103

Darabi J, Wang H (2005) Development of an electrohydrodynamic injection micropump and its potential application in pumping fluids in cryogenic cooling systems. J Microelectromech Syst 14:747–755

Darabi J, Rada M, Ohadi M, Lawler J (2002) Design, fabrication, and testing of an electrohydrodynamic ion-drag micropump. J Microelectromech Syst 11:684–690

El-Genk MS, Bostanci H (2003) Saturation boiling of HFE-7100 from a copper surface, simulating a microelectronic chip. Int J Heat Mass Transf 46:1841–1854

Ewing G, Cazes J (2005) Ewing's analytical instrumentation handbook. Marcel Dekker, New York

Foroughi P, Benetis V, Ohadi M, Zhao Y, Lawler J (2005) Design, testing and optimization of a micropump for cryogenic spot cooling applications. In: Semiconductor thermal measurement and management symposium, 2005 IEEE twenty first annual IEEE, 2005. IEEE, pp 335–340

Foroughi P, Shooshtari A, Dessiatoun S, Ohadi MM (2010) Experimental characterization of an electrohydrodynamic micropump for cryogenic spot cooling applications. Heat Transf Eng 31:119–126

Halpern B, Gomer R (1969a) Field emission in liquids. J Chem Phys 51:1031–1047

Halpern B, Gomer R (1969b) Field ionization in liquids. J Chem Phys 51:1048–1056

Jayaram S, Cross J (1994) Effects of ionic impurities on EHD motion and conduction in nonpolar liquids. IEEE Trans Dielectr Electr Insul 1:1005–1015

Jeong S, Seyed-Yagoobi J (2002) Experimental study of electrohydrodynamic pumping through conduction phenomenon. J Electrostat 56:123–133

Kazemi PZ, Selvaganapathy PR, Ching CY (2009a) Effect of electrode asymmetry on performance of electrohydrodynamic micropumps. J Microelectromech Syst 18:547–554

Kazemi PZ, Selvaganapathy PR, Ching CY (2009b) Electrohydrodynamic micropumps with asymmetric electrode geometries for microscale electronics cooling. IEEE Trans Dielectr Electr Insul 16:483–488

Kazemi PZ, Selvaganapathy PR, Ching C (2010) Effect of micropillar electrode spacing on the performance of electrohydrodynamic micropumps. J Electrostat 68:376–383

Noori A, Selvaganapathy PR, Wilson J (2009) Microinjection in a microfluidic format using flexible and compliant channels and electroosmotic dosage control. Lab Chip 9:3202–3211

Park JK, Ryu JC, Kim WK, Kang KH (2009) Effect of electric field on electrical conductivity of dielectric liquids mixed with polar additives: DC conductivity. J Phys Chem B 113:12271–12276

Pontiga F, Castellanos A (1996) Electrical conduction of electrolyte solutions in nonpolar liquids. IEEE Trans Ind Appl 32:816–824

Russel M, Selvaganapathy P, Ching C (2014a) Effect of electrode surface topology on charge injection characteristics in dielectric liquids: an experimental study. J Electrostat 72:487–492

Russel M, Selvaganapathy PR, Ching CY (2014b) Electrohydrodynamic injection micropump with composite gold and single walled carbon nanotube electrodes. IEEE J Microelectromech Syst. doi:10.1109/JMEMS.2015.2421641

Schmidt WF (1984) Electronic conduction processes in dielectric liquids. IEEE Trans Electr Insul EI-19(5):389–418

Schwabe R, McMillen C, Sharbaugh A (1987) Electrohydrodynamic pumping in distribution transformers: final report. General Electric Co., Corporate Research and Development Center, Schenectady

Stuetzer OM (1959) Ion drag pressure generation. J Appl Phys 30:984–994

Yang L-J, Wang J-M, Huang Y-L (2004) The micro ion drag pump using indium-tin-oxide (ITO) electrodes to resist aging. Sens Actuators A Phys 111:118–122

Zanello P (2003) Inorganic electrochemistry: theory, practice and applications. Royal Society of Chemistry, London

Chapter 5

Ion drag electrohydrodynamic (EHD) micro-pumps under a pulsed voltage

Complete citation:

Russel, M.K., Selvaganapathy, P.R., Ching, C.Y., 2016. Ion drag electrohydrodynamic (EHD) micro-pumps under a pulsed voltage. *J. Electrostatics* 82: 48-54.

Copyright:

Relative Contributions:

Russel M.K.: Performed all experiments, interpretation and analysis of the data and wrote the drafts of the manuscript including all figures and text.

Selvaganapathy P.R.: Co-supervisor of M.K. Russel and revised the initial drafts of the manuscript.

Ching C. Y.: Co-supervisor of M.K. Russel and was responsible for the final draft submittal to the journal.

Abstract

The use of pulsed voltages to improve the performance of an Electrohydrodynamic (EHD) micropump with HFE7100 as the working fluid was investigated. The micropump consisted of 100 planar electrode pairs that were embedded along the bottom wall of a 100 μm high microchannel. The pressure generation was measured at different operating pulse voltage parameters. An optimum pulse repetition rate and duty cycle for the pump geometry and fluid was found for maximum static pressure. The maximum pressure at the optimum pulse repetition rate was 75% greater than the average of the pressures generated at the two DC voltage levels.

5.1 Introduction

Micropumps play an important role in many diverse applications such as in microfluidic and microscale liquid cooling systems [1]. Micropumps have been used in 'Lab on Chip' devices to sample, trap, separate, sort, treat, detect and analyze biofluid samples [2, 3]. Other applications of micropumps include micromixing, microdosing and thermal management of compact electronics and microscale liquid cooling solutions using microchannels [4-6]. Micropumps can be broadly classified into: (i) mechanical displacement and (ii) electro- or magneto-kinetic micropumps [1]. The former exerts force on the working fluid via a moving solid-fluid or fluid-fluid boundary, while the latter provides energy directly to the liquid to generate flow. Amongst the latter, electrohydrodynamic (EHD) micropumps are particularly appealing for electronic cooling applications as they operate with no moving parts, use non-conducting dielectric fluids, are amenable to local control and can be configured with low form factors. In EHD pumping, an electric body force is generated within the fluid by the interaction of electric fields with the charges in a dielectric fluid. Three different types of EHD pumps have been developed, which are distinguished by the manner in which the charges are introduced into the fluid: (i) Induction, (ii) Conduction, and (iii) Injection [7]. In induction EHD pumping, charges are induced due to a discontinuity or gradient of electrical conductivity. Typically, the fluid motion is generated by a travelling wave of electric field which interacts with the net zero induced charges within the bulk of the liquid [8, 9]. The working principle of conduction EHD micropump depends on the

impurities (if any) dissolved within the working fluid. When an electric field is applied, the impurities dissociate to produce ions that are attracted towards the oppositely charged electrode and form an electric double layer (EDL) around them. The double layer is generally thought to consist of two parts. The first is an immobile compact layer predominantly populated by counter ions, where the accumulated charge density is high and which typically extends to about 0.5 nm from the electrode. The second is a mobile diffuse layer which is populated by both co and counter ions and extends into the bulk of the solution to the order of 100 nm. Charges in the diffuse layer are mobile and its thickness depends on the bulk ionic concentration, i.e., the amount of impurities and the properties of the dielectric liquid [10]. At low applied electric field across asymmetric electrodes the dissociation rate of the impurities is greater than that of the recombination rate which generates layers of hetero-charges. Current flow and thus the fluid motion in these pumps are due to the dissociated ions and hetero-charges created at the electrodes [8, 11]. In injection or ion drag EHD micropumps, the charges are injected directly into/from the fluid at the electrode-fluid interface due to electron tunneling. The injected charges move along the electric field lines from the emitter to the collector electrode and drag the neutral molecules to generate fluid motion [8, 12]. Injection typically occurs at high applied electric field. Charge injection into/from a dielectric liquid occurs by either field emission [13] or field ionization [14] and depends on the energy barrier set by the electrode and the dielectric liquid. In field emission, electrons tunnel through the electrode-fluid interface from the negative electrode to the liquid while in field ionization electrons tunnel from the liquid molecule to the positive electrode. A higher injection

current and lower electric field requirement for the onset of charge injection was observed for field emission compared to field ionization [12-16], making the former method favorable for ion drag injection pumps.

One of the earliest investigations into EHD pumping was conducted by Stuetzer [17] where a high electric field caused the flow of ions from the electrode into the working fluid. Different electrode geometries such as planar, cylindrical, needle and spherical were investigated. The pressure was found proportional to the applied current. A maximum pressure of 2 kPa was obtained with a needle-cylinder electrode configuration and castor oil as the working fluid. Since then, EHD pumps have been developed at the micro-scale [18-20]. Darabi et al. [19] studied the effect of electrode surface topology by introducing 3D soldered bumps and reported about 700 Pa of static pressure generation at an applied voltage of 300 V using HFE 7100 as the working fluid. Kazemi et al. [21] improved the electrode design by introducing micropillars on the electrodes which resulted in a maximum static pressure of 2.24 kPa at an applied voltage of 900 V using HFE-7100 as the working fluid. Russel et al. [22] deposited single walled carbon nano-tubes (SWCNT) on gold electrodes to further increase the local electric field and hence charge injection and obtained a static pressure of 4.7 kPa at an applied voltage of 900 V.

Most studies on ion drag EHD pumps have been performed with applied DC electric fields. There have been little or no studies on the effect of a pulsed voltage on the performance of EHD pumps. However, there are several fundamental investigations on the application of a step voltage and its transient effect on electroconvection, current

behavior and charge generation [23-25]. Typically, the current rises sharply to a maximum (I_m) upon the application of the step voltage, followed by a gradual decrease to steady state (I_{ss}). The amount of time it takes to reach I_{ss} from I_m is called the transit time and indicates the time required for the slowest charge carriers to reach the collector electrode from the emitter. Within the transit time the electric field within the fluid continuously changes and cannot come to an electrostatic equilibrium. Once transit time elapses the effect of change in voltage level disappears and the total current would be contributed only due to the injection current. The difference between the transient maximum and the steady state current depends on the magnitude of the applied electric field.

This difference (I_m - I_{ss}) is an indication of displacement current (I_{dis}) [26, 27] at the onset of an applied potential. The magnitude of the displacement current is proportional to the time rate of change in the pulse electric field ($I_{dis} \propto \varepsilon \frac{dE}{dt}$) [27]. Atten [25] suggested a relationship between the magnitude of the maximum transient current and the applied voltage as $I_m \propto V^3$, while the steady state current is related as $I_{ss} \propto V^2$. In general, the charge transportation in the transient regime is more efficient compared to that in the steady regime, which could be explained by the hydraulic model proposed by Felici [28] (in Ref. [24]) for transportation of charges within dielectric liquids. According to this model, the transient regime is dominated by inertial effect of the fluid at high enough applied electric field as opposed to the viscous effect in the stationary regime. Within the transient regime, the fluid moves from the emitter electrode to the collector

and back to the emitter electrode in the form of an elongated closed loop. The backward return portion of the loop (from the collector to the emitter electrode) carries charge free liquid from the bulk while only the forward portion of the loop (from the emitter to the collector electrode) contains the charges. Due to the acceleration of the charges within the transient time, the EHD mobility (i.e. the apparent mobility considering the effect of EHD motion) is greater than the ionic/true mobility. The non-dimensional parameter that characterizes the ratio of EHD mobility to the ionic mobility is $M = \sqrt{\varepsilon/\rho}/k$ [29]; where ε, ρ and k are the permittivity, mass density and ionic mobility of the dielectric liquid, respectively. The enhancement factor (M) in the mobility in transient regime for typical dielectric liquids is between 2 to 1000 [30].

For applied DC voltages, at time greater than the relaxation time, all the charges available within the bulk of the fluid is considered to reach the collector electrode and the transient effects described above do not exist. However, in the case of an applied pulse voltage, the fluid would undergo repetitious transitional effects that depends on the pulse repetition rate. The total charge in the fluid at the application of an electric field can be considered a combination of injected and displacement currents.

The objective of this study is to investigate the use of pulsed voltage signals to enhance the performance of ion drag/injection EHD micropumps. It is expected that the additional current arising from the transient phenomena would lead to generation of higher pressure than the equivalent DC case. In this study, the effect of different pulse voltage parameters such as pulse repetition rate and duty cycle was determined with HFE

7100 as the working dielectric fluid. The fabrication of the micropump and experimental methodology is described in the next section, followed by a presentation and discussion of the results, and finally the conclusions of the study.

5.2 Microfabrication & Experimental Methodology

The micropump is composed of 100 pairs of lithographically patterned gold electrodes in series that are embedded along the bottom glass wall of a microchannel. The details of the microfabrication can be found in [21]. The pump had an asymmetric planar electrode configuration where the width of the emitter and collector electrodes were 20 and 40 μm respectively. This particular electrode geometry was found to result in a significantly higher pump performance than a symmetric configuration where the width of both the emitter and collector electrodes are equal [21]. The PDMS microchannel (26 mm long) was made out of a silicon mold and bonded to the glass substrate. A schematic of the pump is shown in Fig. 5.1 with the key dimensions.

The micropumps were tested with HFE 7100 as the working fluid under a no flow condition. A DC steady voltage was applied using a Trek 677 supply/amplifier (capacity of 2 kV, accuracy ≤ 0.1% of full scale) that was connected to the embedded emitter and collector electrode pads. An ammeter (Keithley 2636 SourceMeter, resolution of 1 fA, accuracy better than 0.02% of reading + 25 nA) was used to record the current readings at different applied voltages. Short glass tubes of 1.5 mm diameter were connected to the inlet and outlet of the micropump that functioned as the fluidic interconnections. Transparent plastic tubing of 1/16 inch diameter was subsequently connected to the glass tubes. To determine the pressure generation, the plastic tubes were positioned vertically and the micropump was filled with the working fluid using a syringe so that the fluid level could be easily detected in both the inlet and outlet columns to ensure no entrapped

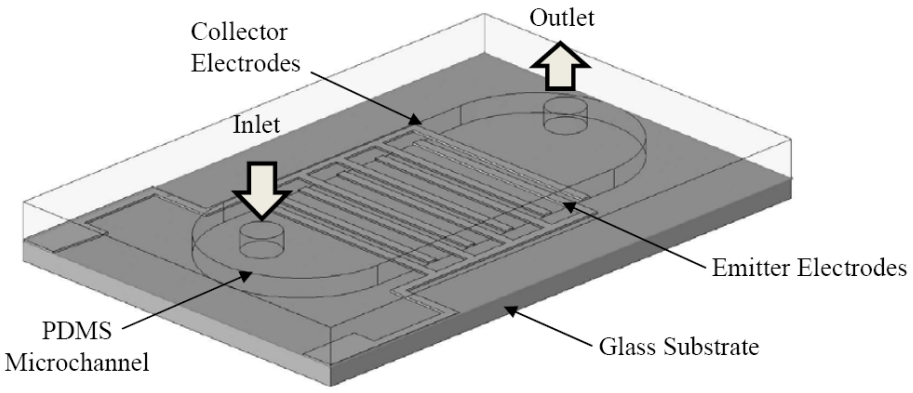

(a)

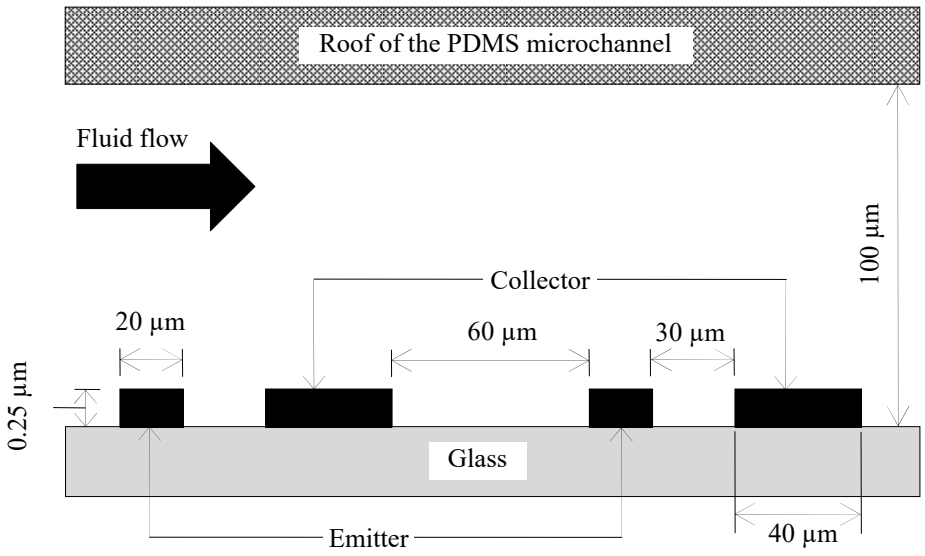

(b)

Fig. 5.1: Schematic of (a) EHD micropump and (b) cross sectional view (dimensions not to scale).

bubbles. The fluid level in both the inlet and outlet columns was checked to be equal before turning on the power supply. The fluid level in both plastic tubing readily equalized indicating that surface tension effects were not dominant in the pressure measurement. The pressure head was determined at different applied voltages by measuring the difference in the fluid level in the inlet and outlet columns using a height gage (KBC tools, resolution 0.02 mm; which corresponds to 0.3 Pa).

The pulse voltage was applied using a function generator (Tektronix AFG-3022B) with a voltage output of 10V peak to peak at a maximum frequency of 25 MHz. The voltage output from the function generator is amplified using a voltage amplifier (Trek 677B) where the maximum gain is 200V/V. The current reading was measured indirectly from the known resistance of a high voltage resistor (Ohmite, 1 MΩ) used in series with the micropump and the voltage drop across it. The voltage across the resistor was recorded using a high voltage differential probe (Tektronix P5200, accuracy ± 3%) along with an oscilloscope (Agilent InfiniiVision DSO-X 2014A, 2GSa/s maximum, equivalent uncertainty in current reading < 3 nAmps, sampled at 200 KSa/s to 5 MSa/s depending on the pulse repetition rate). The effect of the pulse repetition rate (f) and duty cycle (D_C) on the pump performance was determined.

5.3 Results and Discussion

The tests were performed using HFE-7100 as the working fluid. Negative voltages were applied to the emitter electrodes (i.e., field emission) while the collector electrodes were grounded in all the experiments performed as it was found from previous studies that field emission (in negative polarity) is advantageous over field ionization (in positive polarity) due to higher charge injection and lower threshold voltage for the onset of charge injection [12-16].

5.3.1 *Effect of DC voltage*

Experiments were initially performed to characterize the pump performance at applied DC voltages for reference, and to determine appropriate conditions for the pulsed voltage studies. A typical measurement of current over time for an applied step voltage of 800 V DC is presented in Fig. 5.2, and is similar to previous studies [24]. At the onset of the DC voltage, the current rises sharply to a maximum (I_m) at approximately 40 s and then gradually reduces to a steady value (I_{ss}) over time (~600 s). The steady state current and pressure generated at different voltages are plotted in Fig. 5.3. The data presented are an average of 5 independent realizations. The current-voltage characteristic (Fig. 5.3) shows the typical trend of discharge in a dielectric liquid, with a low slope quasi-Ohmic region and a high slope injection region [16]. The threshold voltage (V_{th}) for the onset of charge injection was estimated as the voltage where the low slope quasi-Ohmic region and the steeper injection region intersect [16], which in this case is 637 V. The static

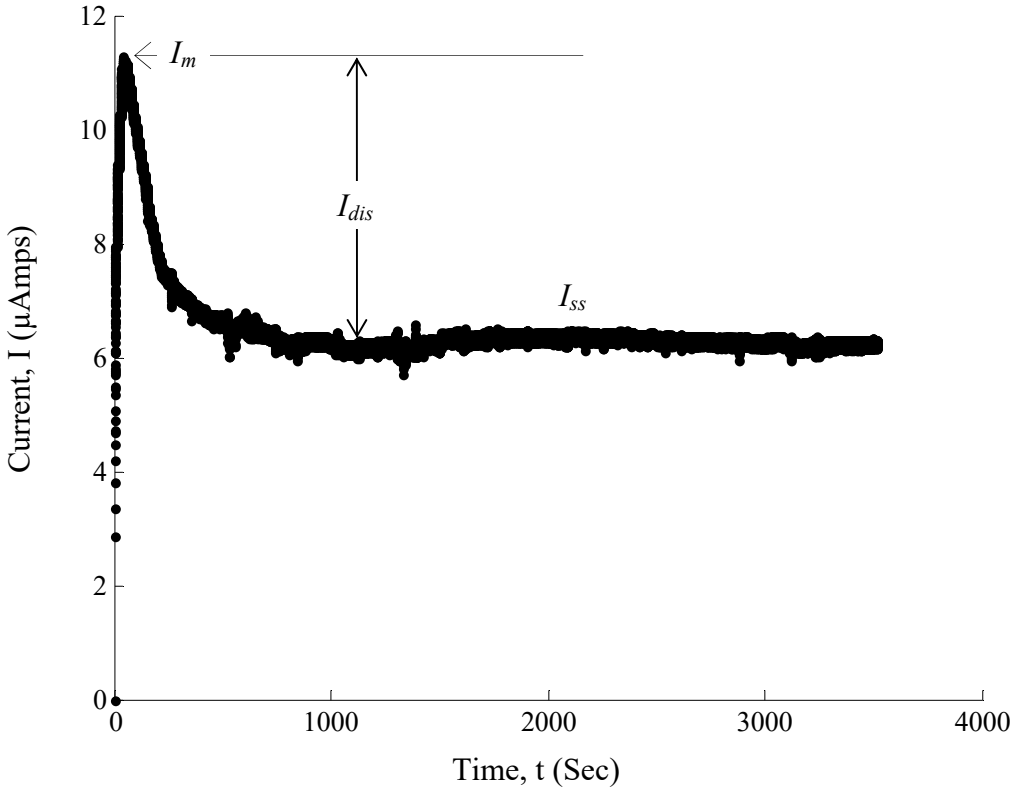

Fig. 5.2: Experimental current response to a step voltage of 800 V DC with time.

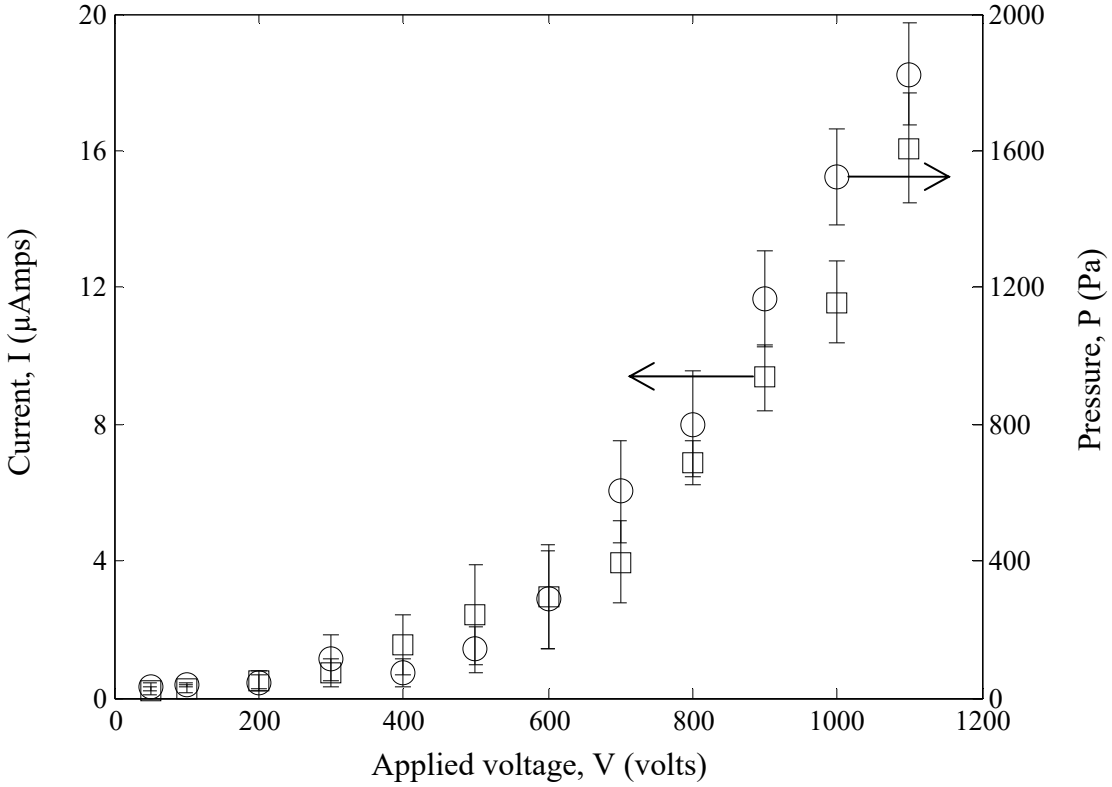

Fig. 5.3: Variation of □ current and ○ static pressure with applied DC voltage for HFE-7100 as working fluid.

pressure with applied voltage follows a similar trend to the current-voltage characteristic and indicates that the pressure generated is directly proportional to the current.

Atten and Gosse [31] showed that for an applied step voltage to the electrodes in a dielectric fluid within the injection regime, the cusp/overshoot in current (I_m in Fig. 5.2) is proportional to the magnitude of the applied voltage. Thus, the pulse voltage signals were chosen so that both the low and the high levels of the voltage signal was in the injection regime for this pump (>637 V). In this study, pulse voltages with a low level of 700 V and high levels of 800 and 900 V (pulse magnitudes of 100 and 200 V

respectively) were used to investigate the influence of the pulse voltage on the pump performance.

5.3.2 *Effect of pulse voltage*

The effect of the pulse repetition rate and duty cycle on the pump performance was examined in this study. The range for the pulse repetition rate was selected by estimating the critical pulse repetition rate (f_C) associated with the charge relaxation time (τ_C) [32] as:

$$\tau_c = \frac{\varepsilon}{\sigma} \qquad (5.1)$$

and

$$f_c = \frac{1}{2\pi\tau_c} \qquad (5.2)$$

where ε and σ are the permittivity and conductivity of the working fluid. The properties of the working fluid are presented in Table 5.1. The relaxation time for HFE 7100 was calculated as $2.15X10^{-3}$ s, which corresponds to a critical pulse repetition rate of 74 Hz. In this study (HFE 7100, f_C = 74 Hz) the pulse repetition rate was set in the range 0.005 Hz - 5000 Hz. In particular, the low f range (compared to f_C of 74 Hz) was of interest, while still spanning the moderate to high f range.

A typical time trace of current over one cycle with V_H = 800 V, V_L = 700 V, D_C = 50% at f = 0.1 Hz is shown in Fig. 5.4 at stable condition, recorded at a sampling rate of

200 KSa/s. Positive and negative peaks are present in the current trace when the voltage level is stepped up or down, respectively (Fig. 5.4 (b & c)). The current relaxes to a steady state after the transient within the corresponding half cycle. The average time to reach a steady current from the peak current is approximately $5X10^{-4}$ s, which is approximately 5 times shorter than the estimated relaxation time for HFE 7100. For a step voltage, the current at the onset of the step voltage is a combination of both injection and displacement current [26, 27, 32], where the displacement current is due to the sudden change of the voltage [27, 33]. Charging of the electrodes starts as soon as a potential is applied and continues till they attain that set voltage. During this charging process, a heterocharge layer adjacent to the electrodes builds up within the dielectric liquid and is equal to the static charges formed in the electrodes. Over time, the displacement current decreases from its initial value at the voltage onset to zero when charging is complete.

Table 5.1: Properties of HFE-7100

Property	Value
Boiling point (°C)	61 [36]
Viscosity (Kg/ms)	$3.7X10^{-4}$ [36]
Specific heat (J/KgK)	1255 [36]
Density (Kg/m^3)	1481 [36]
Volume resistivity (Ω cm)	$3.29 X 10^9$ [36]
Dielectric constant, 100 Hz – 10 MHz	7.39 [36]
Dielectric strength (0.1 in. gap)	28 kV (RMS) [36]
Ionic mobility ($m^2/V.s$)	$1.31X10^{-8}$ [37]

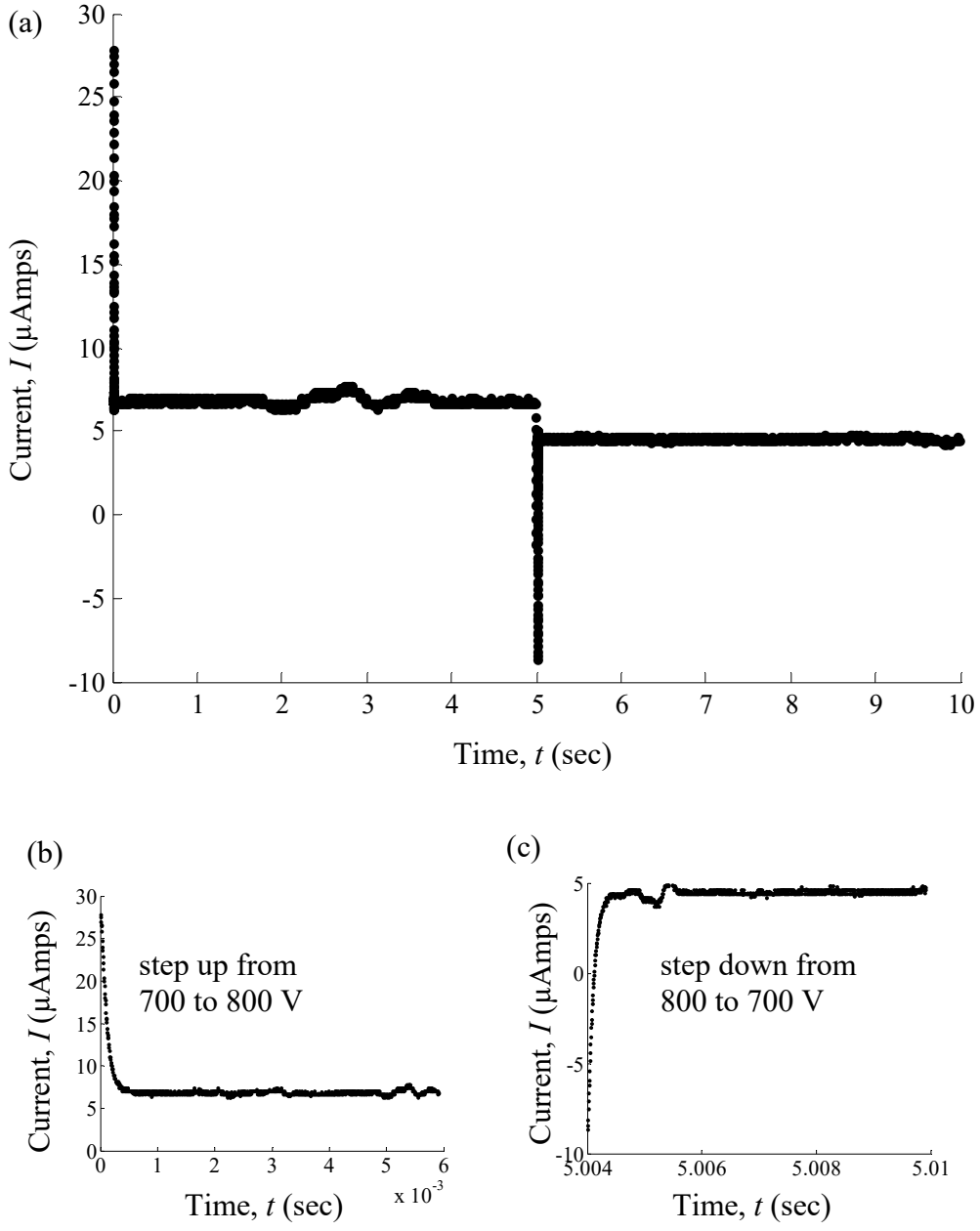

Fig. 5.4: (a) Time trace of the current of one complete cycle (sampling rate 200 KSa/sec). (b & c) zoomed in view of the transient current. D_C = 50%, V_L = 700 V and V_H = 800 V for f = 0.1 Hz.

The time trace of the total current thus shows a steady state upon completion of charging, representing only the injection current. When the applied voltage across the electrodes changes to another magnitude, the heterocharges within the liquid along with the static charges in the electrodes rearrange to attain the new set voltage. If the change in the applied voltage is from a lower level to a higher level (e.g., from 700 to 800 V, Fig. 5.4 (b)), immediate charging of the electrodes take place while in the opposite case (e.g., from 800 to 700 V, Fig. 5.4 (c)) discharge of the electrodes occur to attain the new set voltage.

The effect of the pulse repetition rate on the average of stable current (averaged over 10 min) for a pulse magnitude of 100 V (between 700 & 800 V) and 200 V (between 700 & 900 V) at 50% duty cycle is shown in Fig. 5.5. The corresponding current readings at applied DC voltages of 700, 800 and 900 V are also presented in Fig. 5.5 for comparison. The average current for the pulse voltage between 700 and 800 V in the low pulse repetition rate range ($f < 5$ Hz) remained nearly constant with a magnitude close to the average of the currents of the two DC levels, as expected. It decreased with increasing f beyond 5 Hz. For the pulse voltage between 700 and 900 V, experiments were performed only at the low f range, and the characteristic was similar to that for the pulse voltage between 700 and 800 V.

At $f < f_C$, the charge carriers introduced at the emitter electrode have sufficient time (compared to its charge relaxation time) to reach the collector electrodes. At $f > f_C$, the charges do not completely reach the collector electrode and thus the effective current reduces since the electric field is not fully established. The pulse repetition rate beyond

which there was a decrease in average current in Fig. 5.5 was approximately 10 Hz. This is below the estimated f_C of 74 Hz (based on charge relaxation time), but of a similar order of magnitude.

The corresponding static pressure generation with pulse repetition rate at 50% duty cycle is shown in Fig. 5.6. The static pressure at the DC voltage levels of 700, 800 and 900 are also presented for comparison. The static pressure at low pulse repetition rates (0.005 Hz $\leq f \leq$ 10 Hz) for the pulse magnitude of 100 V was greater than the

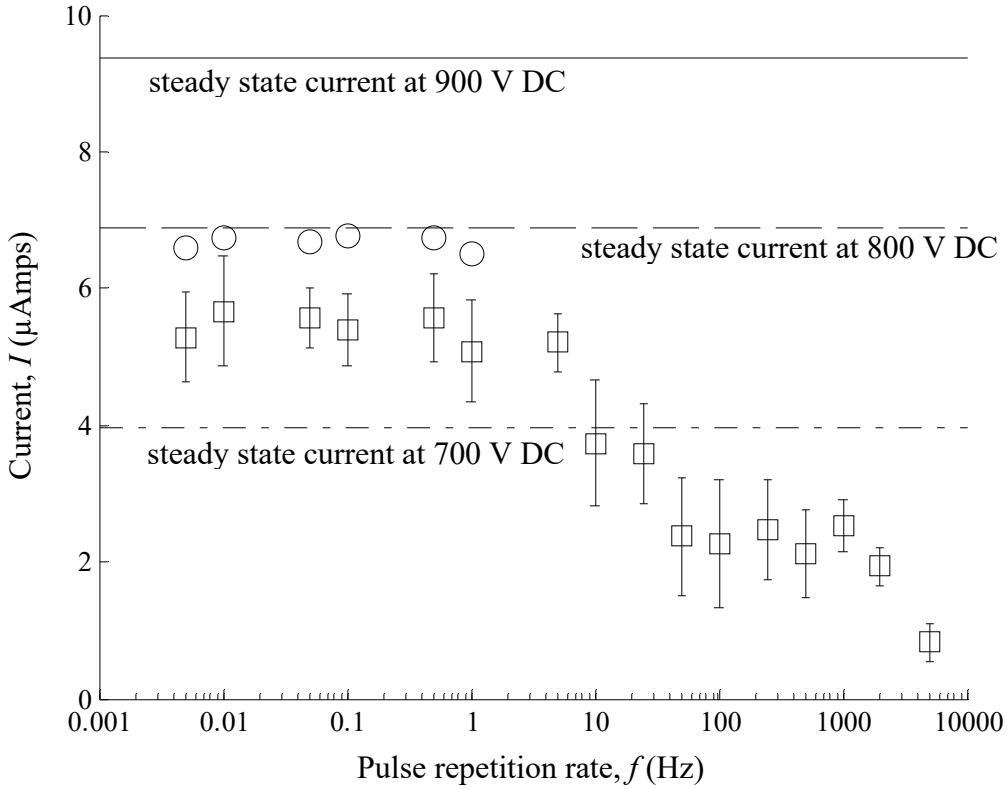

Fig. 5.5: Variation of current as a function of pulse repetition rate with D_C = 50 %, □ pulse magnitude of 100 V (V_L = 700V & V_H = 800 V) and ○ pulse magnitude of 200 V (V_L = 700V & V_H = 900 V). Current at an applied DC voltage of — - — 700 V, – – 800 V and — 900 V.

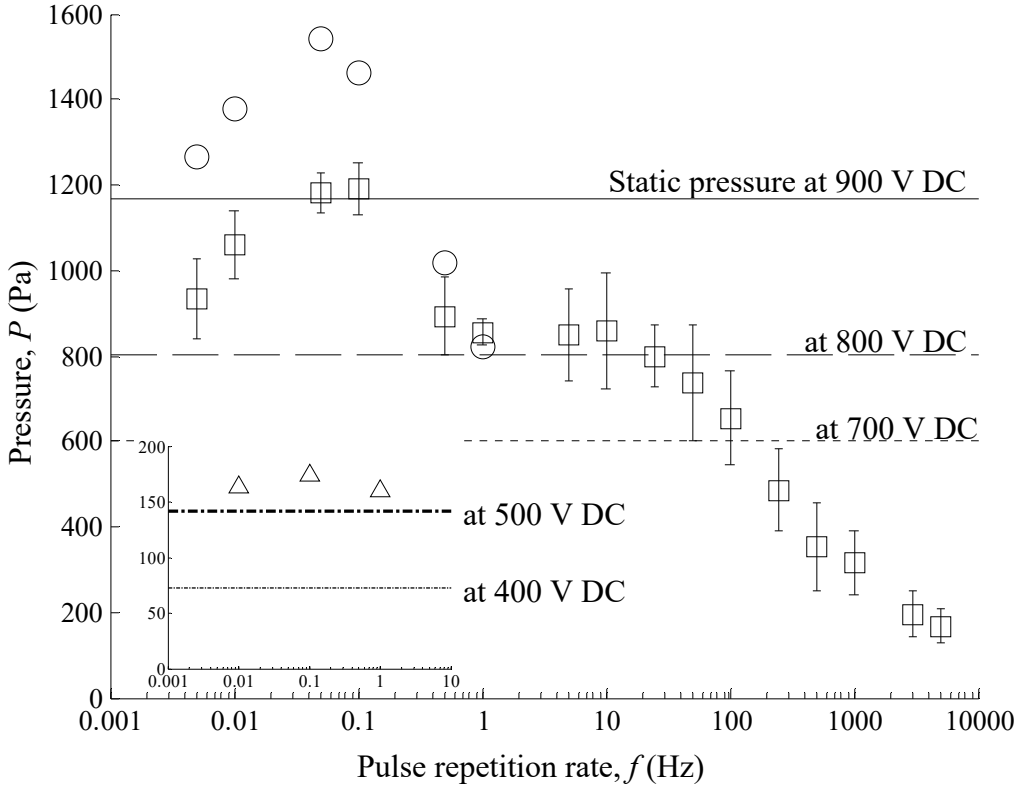

Fig. 5.6: Variation of pressure as a function of pulse repetition rate with D_C = 50 % for □ V_L = 700V & V_H = 800 V, ○ V_L = 700V & V_H = 900 V and Δ V_L = 400V & V_H = 500 V

pressure with an applied 800 V DC. Within this range of pulse repetition rates, the pressure initially increases to a maximum of 1190 Pa at 0.1 Hz and then decreased. The pressure continued to decrease for pulse repetition rates greater than 10 Hz. Similar results were obtained for the pulse magnitude of 200 V, where the static pressure was greater than at an applied 900 V DC for f < 0.1 Hz. In this case, the static pressure reached a maximum of 1540 Pa at f = 0.05 Hz. The maximum enhancement in pressure generation was found to be 70% and 75% respectively for the pulse magnitude of 100 V

and 200 V when compared to the average of the static pressure generated at the low and high DC voltage levels. The slightly greater percentile enhancement in static pressure for the pulse magnitude of 200 V compared to the pulse magnitude of 100 V could be attributed to the higher displacement current in the former due to a higher *dV/dt*. The average magnitudes of *dV/dt* at a pulse repetition rate of 0.1 Hz were 1.49 and 0.62 MV/s respectively. At the very low pulse repetition rates ($f \leq 0.05$ Hz), oscillations in the inlet and outlet liquid columns that followed the change in voltage levels were observed. The level of oscillation was approximately 140 Pa, and the average of the readings were used for these measurements.

The fluidic time scale will be greater than the relaxation time and could be the reason for the discrepancy between the pulse repetition rates (*f*) at which the current and static pressure begin to decrease. At very low Reynolds number (which would be the case here), the viscous term dominates over the momentum term. In the case of static pressure measurement, there is no/very low flow of fluid when the system reaches fluidic steady state. The time associated with viscous diffusion is defined as, $t_{diff.} = L_c^2/\nu$ [35], where L_c is the characteristic length and ν is the kinematic viscosity of the dielectric liquid. For the pump studied, the characteristic length was considered as the inter-electrode spacing between the emitter and collector electrodes, within which the viscous diffusion would take place. This length is 30 μm and the time associated with viscous diffusion was estimated at $3.6X10^{-3}$ s which corresponds to 44 Hz, compared to charge relaxation time

of $2.15X10^{-3}$ s. At applied pulse repetition rates $f < 44$ Hz, the fluid has sufficient time to reach steady state and thus would generate higher pressure.

The enhancement in the static pressure for the pulse voltage over the DC voltage case in the low pulse repetition range can be attributed to the displacement current. This was confirmed by performing experiments within the conduction regime for a pulse voltage between 400 and 500 V (both V_L and $V_H < V_{th}$) for 0.01 Hz < f < 1 Hz. The experimental results are shown in the inset in Fig. 5.6, and are similar to the pulse voltage application within the injection regime. In this conduction regime (pulse voltage between 400 and 500 V), there was an enhancement of 62% in the static pressure when compared to the average pressure at the corresponding DC levels. The ratio of the average displacement current (difference between the peak and the steady current in a half cycle) to the steady state current within a half cycle of a pulse ($R = I_{dis}/I_{avg\_steady\_pulse}$) with D_C = 50% and V_H = 800 V, V_L = 700 V is presented in Fig. 5.7. This ratio is on average 5% higher when the voltage is stepped up compared to when the voltage is stepped down. This ratio increases with pulse repetition rate and reaches a maximum value of 4.8 at 0.5 Hz and then decreases with a further increase in the pulse repetition rate. The additional charges/ions induced within the liquid due to the sudden change in the voltage magnitude enhances motion of the bulk fluid [23] and thus likely causes the higher static pressure. The presence of a maximum pressure (Fig. 5.6) is likely due to the combined effect of the displacement current (I_{dis}) and the pulse repetition rate (f). In the low pulse repetition rate range, the effect of I_{dis} is dominant over f. As the magnitude of displacement current or

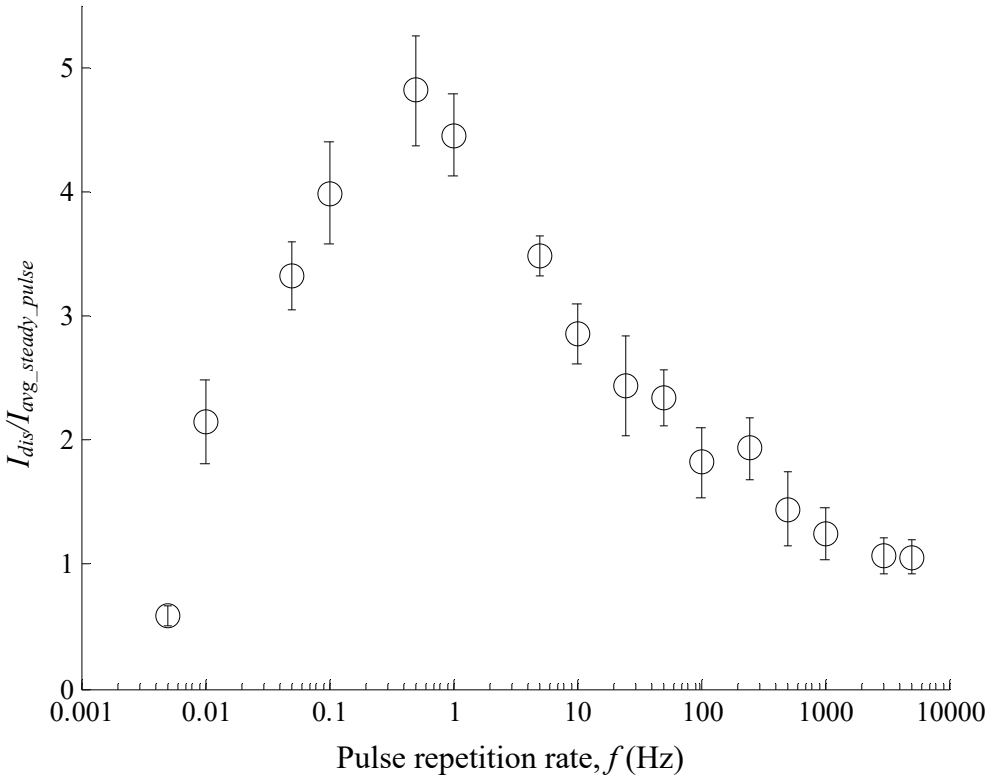

Fig. 5.7: Ratio of displacement (I_{dis}) to the average of the steady current of the half cycle of a pulse voltage ($I_{avg\_steady\_pulse}$) with D_C = 50 %, V_L = 700V and V_H = 800 V at different pulse repetition rate (f).

the charges available at the low pulse repetition rate is smaller (Fig. 5.7), the static pressure generated by the pump is smaller. At moderate pulse repetition rate the magnitude of displacement current is greater and the frequent occurrences of the sudden peaks help efficient transfer of the available charges from emitter to the collector electrodes and thus generate higher pressure. At higher pulse repetition rates, the charges do not have sufficient time to reach the collector electrodes and results in lower injection current [15, 34] and thus lower static pressure.

The effect of the duty cycle (D_C) for the pulse magnitude of 100 V (between 700 V and 800 V) at f = 0.1 Hz on average current and static pressure is shown in Fig. 5.8 and Fig. 5.9, respectively. The pulse repetition rate was set at 0.1 Hz, which corresponds to the f where a maximum pressure was generated (Fig. 5.6). There is a slight increase in the current with D_C, with the value remaining between the 700 V and 800 V DC levels. The current at 0 and 100% duty cycle is expected to correspond to those at the DC voltage levels of 700 and 800 V. The experimental range of the duty cycle was from 5% to 95%; however, the above trend is not seen in these results. The pressure is close to the low voltage value at very low D_C, and increases with an increase in D_C, reaching a maximum at D_C = 65%. It then decreases beyond this value and approaches the high voltage value with a further increase in D_C. The reasons for the change in current and pressure with duty cycle are not well understood at present, but a plausible explanation could be the net charges available at the different duty cycles.

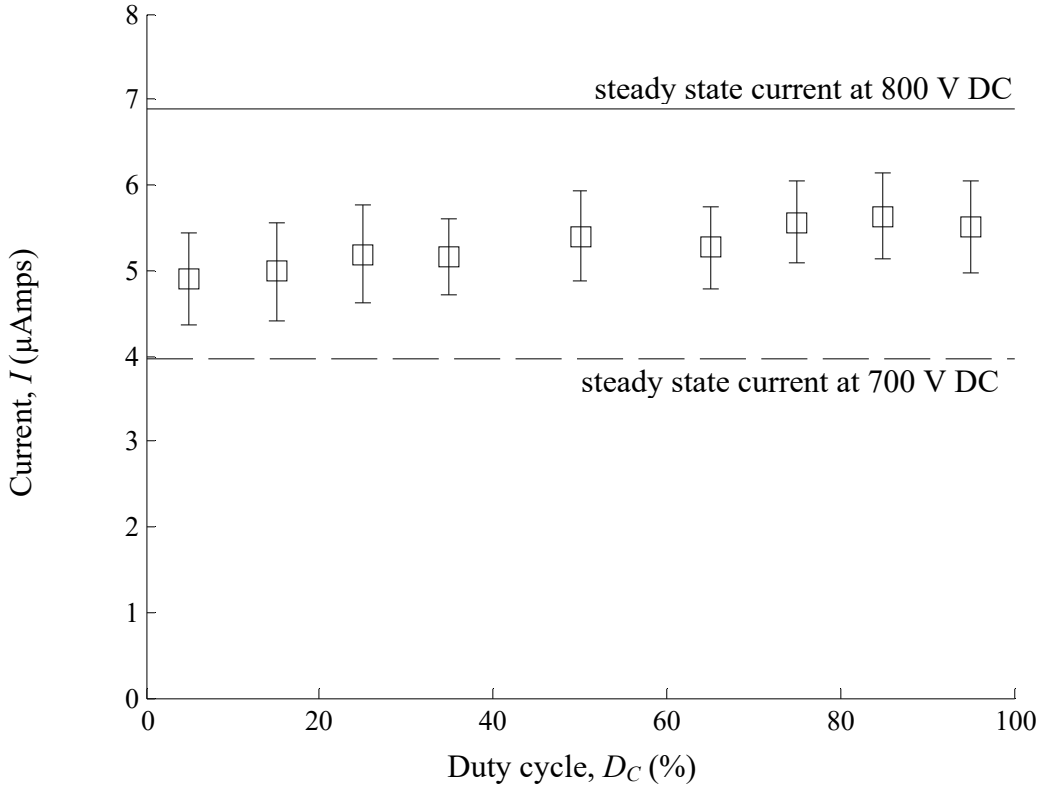

Fig. 5.8: Variation of current with duty cycle with f = 0.1 Hz, V_L = 700 V and V_H = 800 V. (Steady state current at an applied DC voltage of – – 700 V and — 800 V are also presented for comparison.).

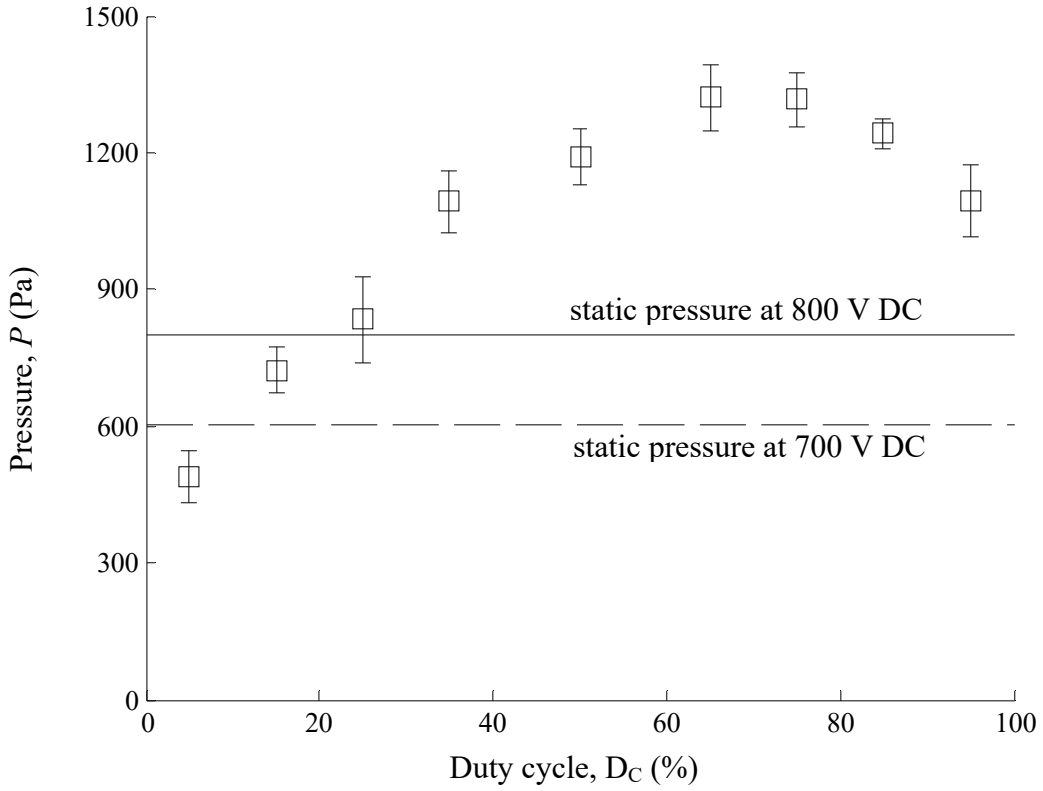

Fig. 5.9:Variation of pressure with duty cycle with f = 0.1 Hz, V_L = 700V and V_H = 800 V. (Pressure at an applied DC voltage of – – 700V and ― 800V are also presented for comparison).

5.4 Conclusion

The effect of a pulsed voltage on the performance of EHD micropumps was investigated with HFE7100 as the working fluid. The micropump consisted of 100 planar electrode pairs that were embedded along the bottom wall of a 100 μm high and 5 mm wide micro-channel, where the width of the emitter and collector electrodes was 20 and 40 μm, respectively. The micropump had an inter-electrode spacing of 30 μm. The effect of pulse repetition rate and duty cycle on the pump performance was evaluated. The static pressure generation at low pulse repetition rates and 50% duty cycle was higher compared to the corresponding high DC level of the pulse. The application of a pulse voltage within the injection regime (between 700 and 800 V) showed an optimum pulse repetition rate of f_{opt} = 0.1 Hz for a maximum static pressure generation of 1190 Pa, while for a pulse between 700 and 900 V a maximum pressure of 1540 Pa was achieved at an optimum pulse repetition rate of f_{opt} = 0.05 Hz. The maximum enhancement in the pressure was about 75% when compared to the average of the static pressure generated at the low and high DC voltage levels. Similar pressure generation characteristics were observed within the conduction regime (for a pulse between 400 and 500 V). The enhancement in the static pressure for the pulse voltage over the DC voltage case in the low pulse repetition range can be attributed to the displacement current due to the step change in voltage at the onset of a pulse. For a pulse repetition rate of 0.1 Hz, an optimum duty cycle of 65% was found to generate the maximum pressure.

5.5 References

[1] B.D. Iverson, S.V. Garimella, Recent advances in microscale pumping technologies: a review and evaluation, Microfluid. Nanofluidics 5 (2008) 145-174.

[2] H. Andersson, A. Van den Berg, Microfluidic devices for cellomics: a review, Sens. actuators B Chem. 92 (2003) 315-325.

[3] A. Noori, P.R. Selvaganapathy, J. Wilson, Microinjection in a micro fluidic format using flexible and compliant channels and electroosmotic dosage control, Lab a Chip 9 (2009) 3202-3211.

[4] V. Singhal, S.V. Garimella, A. Raman, Microscale pumping technologies for microchannel cooling systems, Appl. Mech. Rev. 57 (2004) 191-221.

[5] S.V. Garimella, V. Singhal, D. Liu, On-chip thermal management with microchannel heat sinks and integrated micropumps, Proc. IEEE 94 (2006) 1534-1548.

[6] J. Darabi, K. Ekula, Development of a chip-integrated micro cooling device, Microelectron. J. 34 (2003) 1067-1074.

[7] S. Hardt, F. Sch€onfeld, Microfluidic Technologies for Miniaturized Analysis Systems, Springer, 2007.

[8] J. Seyed-Yagoobi, Electrohydrodynamic pumping of dielectric liquids, J. Electrost. 63 (2005) 861-869.

[9] J.R. Melcher, Traveling-wave induced electroconvection, Phys. Fluids (1958-1988) 9 (1966) 1548-1555.

[10] C. Yang, D. Li, Analysis of electrokinetic effects on the liquid flow in rectangular microchannels, Coll. Surf. A Physicochem. Eng. Asp. 143 (1998) 339-353.

[11] S.-i. Jeong, J. Seyed-Yagoobi, Experimental study of electrohydrodynamic pumping through conduction phenomenon, J. Electrost. 56 (2002) 123-133.

[12] W.F. Schmidt, Electronic conduction processes in dielectric liquids, Electr. Insul., IEEE Trans. (1984) 389-418.

[13] B. Halpern, R. Gomer, Field emission in liquids, J. Chem. Phys. 51 (1969) 1031-1047.

[14] B. Halpern, R. Gomer, Field ionization in liquids, J. Chem. Phys. 51 (1969) 1048-1056.

[15] M. Butcher, A. Neuber, M.D. Cevallos, J.C. Dickens, H. Krompholz, Conduction and breakdown mechanisms transformer oil, Plasma Sci. IEEE Trans. 34 (2006) 467-475.

[16] M. Russel, P. Selvaganapathy, C. Ching, Effect of electrode surface topology on charge injection characteristics in dielectric liquids: an experimental study, J. Electrost. 72 (2014) 487-492.

[17] O.M. Stuetzer, Ion drag pressure generation, J. Appl. Phys. 30 (1959) 984-994.

[18] S.-H. Ahn, Y.-K. Kim, Fabrication and experiment of a planar micro ion drag pump, Sens. Actuators A Phys. 70 (1998) 1-5.

[19] J. Darabi, M. Rada, M. Ohadi, J. Lawler, Design, fabrication, and testing of an electrohydrodynamic ion-drag micropump, Microelectromech. Syst. J. 11 (2002) 684-690.

[20] L.-J. Yang, J.-M. Wang, Y.-L. Huang, The micro ion drag pump using indiumtin-oxide (ITO) electrodes to resist aging, Sens. Actuators A Phys. 111 (2004) 118-122.

[21] P.Z. Kazemi, P.R. Selvaganapathy, C.Y. Ching, Electrohydrodynamic micropumps with asymmetric electrode geometries for microscale electronics cooling, Dielectr. Electr. Insul., IEEE Trans. 16 (2009) 483-488.

[22] M. Russel, P.R. Selvaganapathy, C.Y. Ching, Electrohydrodynamic injection micropump with composite gold and single walled carbon nanotube electrodes, IEEE J. Microelectromech. Syst. 24 (5) (2015) 1557-1564.

[23] P. Atten, B. Malraison, S.A. Kani, Electrohydrodynamic stability of dielectric liquids subjected to ac fields, J. Electrost. 12 (1982) 477-488.

[24] R. Tobazeon, Electrohydrodynamic instabilities and electroconvection in the transient and ac regime of unipolar injection in insulating liquids: a review, J. Electrost. 15 (1984) 359-384.

[25] P. Atten, Electrohydrodynamic instability and motion induced by injected space charge in insulating liquids, Dielectr. Electr. Insul., IEEE Trans. 3 (1996) 1-17.

[26] H. Yamada, T. Sato, High-speed electro-optical measurement of prebreakdown current in dielectric liquids, Electr. Insul., IEEE Trans. (1985) 261-267.

[27] A. Watson, The displacement current from ramped voltage application to dielectric liquids, in: Electrical Insulation and Dielectric Phenomena, 1994., IEEE 1994 Annual Report., Conference on, IEEE, 1994, pp. 935-941.

[28] N. Felici, Phénomènes hydro et aérodynamiques dans la conduction des diélectriques fluides, Rev. Gen. Electr, 78 (1969) 717-734.

[29] P. Atten, R. Moreau, Stabilité électrohydrodynamique des liquides isolants soumis à une injection unipolaire, J. Mécanique, 11 (1972) 471-521.

[30] N. Felici, High-field conduction in dielectric liquids revisited, Electr. Insul., IEEE Trans. (1985) 233-238.

[31] P. Atten, J. Gosse, Transient of one-carrier injections in polar liquids, J. Chem. Phys. 51 (1969) 2804-2811.

[32] A. Ramos, Electrokinetics and Electrohydrodynamics in Microsystems, Springer, 2011.

[33] J.C. Devins, S.J. Rzad, R.J. Schwabe, Breakdown and prebreakdown phenomena in liquids, J. Appl. Phys. 52 (1981) 4531-4545.

[34] B.H. Hamadani, Electronic Charge Injection and Transport in Organic Fieldeffect Transistors, 2007. Ann Arbor, 1050, 48106-41346.

[35] A.O. El Moctar, N. Aubry, J. Batton, Electro-hydrodynamic micro-fluidic mixer, Lab a Chip 3 (2003) 273-280.

[36] M.S. El-Genk, H. Bostanci, Saturation boiling of HFE-7100 from a copper surface, simulating a microelectronic chip, Int. J. Heat Mass Transf. 46 (2003) 1841-1854.

[37] V. Benetis, Experimental and computational investigation of planar ion drag micropump geometrical design parameters, 2005.

Chapter 6

Effect of external fluid flow on discharge characteristics in a dielectric liquid with planar electrode configuration

Abstract

The effect of fluid flow, both in the co- and counter flow direction with respect to the electric field direction, on discharge characteristics in a dielectric liquid has been studied. A set of 100 interdigitated planar electrode pairs were photolithographically fabricated on a thin glass substrate which acts as the bottom wall of a 100 micron high, 5 mm wide and 50 mm long microchannel. The width of the emitter and collector gold electrodes was 20 and 40 μm respectively, with inter-electrode spacing of 120 μm. Spacing between each adjacent electrode pairs is 240 μm. A syringe pump was used to induce a flow through the microchannel. Current was recorded at different applied DC potential across the emitter and collector electrodes at different flow rates. The results showed an increase in current when flow was induced compared to the no flow case for all applied fields. At low applied electric fields, the current increased as the flow rate increased; while at the higher applied electric fields, there was an optimum flow rate for maximum current.

6.1 Introduction

Discharge characteristics in dielectric liquids have been studied for different polarities of applied field [1, 2], different flow rates for both AC [3, 4] and DC applied fields [3-7] and for gas [7] and liquids [1, 2] with macro-scale inter-electrode spacing (e.g., few mm) and for Reynolds number up to approximately 500. The dielectric fluid flow was either between coaxial cylinder electrodes [3-5] or parallel plate electrodes [2, 6] with the electric field normal to the flow. If the applied electric field is sufficient to overcome the energy barrier set by the cathode emitter electrode and the dielectric liquid, electron(s) will be released from the metal surface into the dielectric liquid to form a negative ion. Momentum interchange between the charged ions and liquid molecules enables the former to be transported through the field free regions. This momentum transfer is typically very efficient as the charged particle and the neutral liquid molecules are of similar mass. The kinetic energy gained by the liquid molecules due to the applied electric filed can induce a bulk liquid motion along the path of charge flow [2]. The mobility of the dielectric liquid, when a strong electric field is applied, is thus enhanced [1, 2]. The dielectric mobility increases compared to its true mobility as the ion velocity relative to liquid increases [1] which depends on the applied electric field [2]. Coe et. al. [2] studied the effect of hydrodynamic resistance between the emitter and collector electrodes on the discharge characteristics, and found that the current reduced by a factor of 5 when a hydraulic resistance was imposed between the electrodes. They suggested that the current could be significantly increased if a flow was induced from the emitter to

the collector electrode by means of a pump, and found an enhancement factor between 5 to 10 in current when the liquid was pumped at 0.5 m/s. For air Jaworek and Krupa [7] found for a needle-flat plate electrode configuration that the discharge current, for field ionization, increased initially and then decreased as the air velocity increased. The optimum velocity to result in the maximum current depended on the field strength. In case of field emission, the discharge current decreased as the flow velocity increased. The onset voltage to discharge and the breakdown voltage were found to generally increase as the air velocity increased, with a peak at 0.5 and 0.25 m/s respectively. The onset voltage to discharge and breakdown voltage increased by 45 and 25% respectively for air velocity of 4 m/s when compared to still air.

Miyao et al. [3] found for an AC applied field with coaxial cylinder electrode configuration and maximum Reynolds number of 167 that the current decreased with an increase in the flow velocity at lower temperature; but at high temperature the discharge behaviour was inconclusive. In the case of a DC applied field, the current increased as the flow velocity increased [3]. The results of Metwally [4] for an applied DC field with similar electrode configuration and $Re \leq 250$ were contrary to the findings by Miyao et al [3]. Metwally [4] for applied DC voltage, found that the current decreased with an increase in the flow. In case of AC voltage the current, depending on the electrode material and geometry, increased or decreased as the flow velocity increased [4]. Yuan et al. [5], also for coaxial electrode configuration, found that temperature had a great effect on the current vs. flow velocity relationship and showed that at temperature less than 40 °C the current decreased as the flow velocity increased; while it increased at temperature

above 80 °C. The reason behind is the disparity in the increase in the mobility of the positive and negative ions caused by the decrease in the viscosity at higher temperature. In a coaxial electrode configuration, the fluid flow is perpendicular to the electric field and there are no studies for the planar electrode geometry with dielectric fluid flowing parallel to the electrodes. The discharge characteristics as a function of flow velocity depend on electrode geometry and the fluid. It is important to study this for planar electrode geometries as it has practical application in electrohydrodynamic (EHD) micropumps. In a system where the configuration proposed in this study is used as a heat sink and fluid is supplied with an external pump, the external flow provided by the pump would have an effect on the charge injection and needs to be studied. The objective of this study is to investigate the discharge characteristics of dielectric liquid with planar electrode configuration as a function of fluid flow induced externally.

6.2 Experimental Facility

The schematic of the interdigitated electrodes bonded to the PDMS microchannel is shown in Fig 6.1. The module consists of two sets of electrodes: the emitter connected to the high voltage probe of the DC supply and the electrically grounded collector. The dimensions are presented in Fig 6.1 (b) and details of the microfabrication can be found in [8]. The fluid under test is a commonly used dielectric liquid, HFE 7100 from 3M. The DC field was supplied by connecting a high voltage power supply (Trek 677 with capacity of 2 kV, accuracy ≤ 0.1% of full scale) to the emitter electrodes while having the collector electors grounded. The current was measured using an ammeter (Keithley 2636 SourceMeter, resolution of 1 fA, accuracy better than 0.02% of reading + 25 nA) at different applied voltages. Experiments were performed for field emission mode (negative emitter) as it was found to generate higher discharge current compared to the field ionization mode (positive emitter) [9-11]. Experiments were performed for fluid flowing (i) from the emitter to collector electrode direction and (ii) from the collector to emitter electrode direction. The former direction of fluid flow, hereafter, will be referred as co-flow as the electric field lines are stretched from the emitter to the collector electrodes. The latter will be reffered as counter-flow. The fluid flow direction shown in Fig 6.1 (b), for example, aligns along the net electric field direction, thus presents the co-flow direction.

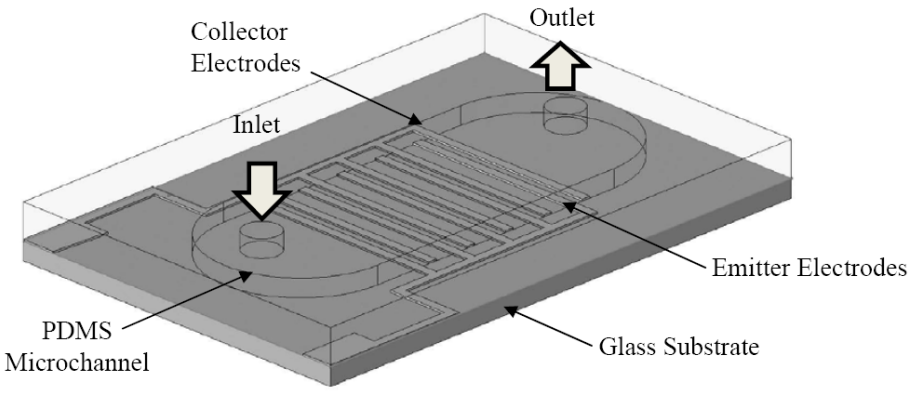

(a)

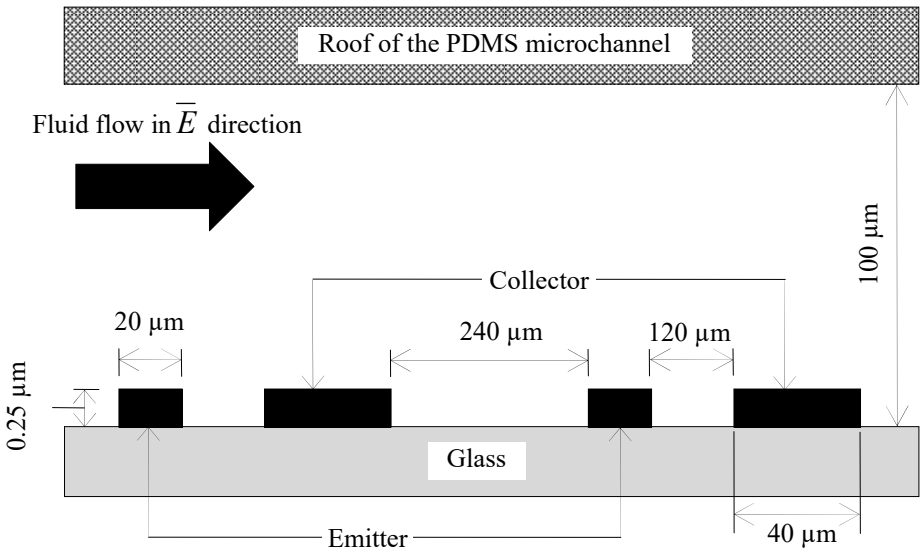

(b)

Fig. 6.1: Schematic of (a) interdigitated electrodes and (b) cross sectional view (dimensions not to scale).

6.3 Results and Discussion

The discharge current as a function of applied DC potential for static (i.e., fluid velocity = 0) and dynamic fluid condition ($Re \leq 13.1$) is presented in Fig 6.2 (a & b) for co-flow and counter-flow cases. It is obvious that there are two regimes: (i) low slope quasi-Ohmic regime, i.e. that of conduction phenomenon, where current flow is due to the dissociation and recombination of the fluid molecules and the hetero-charges formation at the electrodes; and (ii) high slope injection regime, where charges are injected into the dielectric liquid by electron tunneling. This transition from the low slope quasi-Ohmic region to the high slope injection region has been considered as the onset of charge injection [11]. The voltage at which this transition occurs is considered as the threshold voltage (V_{th}), which for no fluid flow (e.g. static) condition was found to be 900 V. The threshold voltages for co-flow conditions were smaller than that of the static condition, i.e., < 900 V (Table 6.1). For the counter-flow condition the threshold voltage was greater than that of the static condition (Table 6.2). The threshold voltage, in case of co-flow, decreased as the *Re* increased; while for counter-flow there was a peak at $Re = 1.31$. The slopes of the I-V curve for the *static condition* within the conduction and injection regimes were 0.39 and 30.26 nA/V respectively. The external flow increased the slope of I-V curves for both co- and counter flow conditions within their respective conduction and injection regimes compared to the static condition (Table 6.1 & 6.2). This slope within the conduction regime gradually increased as the flow velocity increased, while for the injection regime this slope initially increased and then decreased. For the

co-flow condition the optimum *Re* to have maximum slope within the injection regime was 5.23 while for counter flow condition it was 1.31.

Table 6.1: Threshold voltage and slope of I-V curve at different Reynolds number at *co-flow* condition

Reynolds number	Threshold voltage (V)	Slope in conduction region (nA/V)	Slope in injection region (nA/V)
0	900	0.39	30.26
1.31	768.25	0.98	52.2
2.62	830.46	1.1	77.8
5.23	837.72	1.75	79.5
7.85	849.18	4.74	73.02
10.46	816.03	5.7	57.66
13.1	738.64	6.34	41.06

Table 6.2: Threshold voltage and slope of I-V curve at different Reynolds number at *counter-flow* condition

Reynolds number	Threshold voltage (V)	Slope in conduction region (nA/V)	Slope in injection region (nA/V)
0	900	0.39	30.26
1.31	1158.62	5.9	98.78
2.62	1066.88	3.66	92.33
5.23	996.73	4.46	82.46
7.85	1043.6	5.56	90.2
10.46	943.54	4.83	58.52
13.1	924.1	5.74	45.6

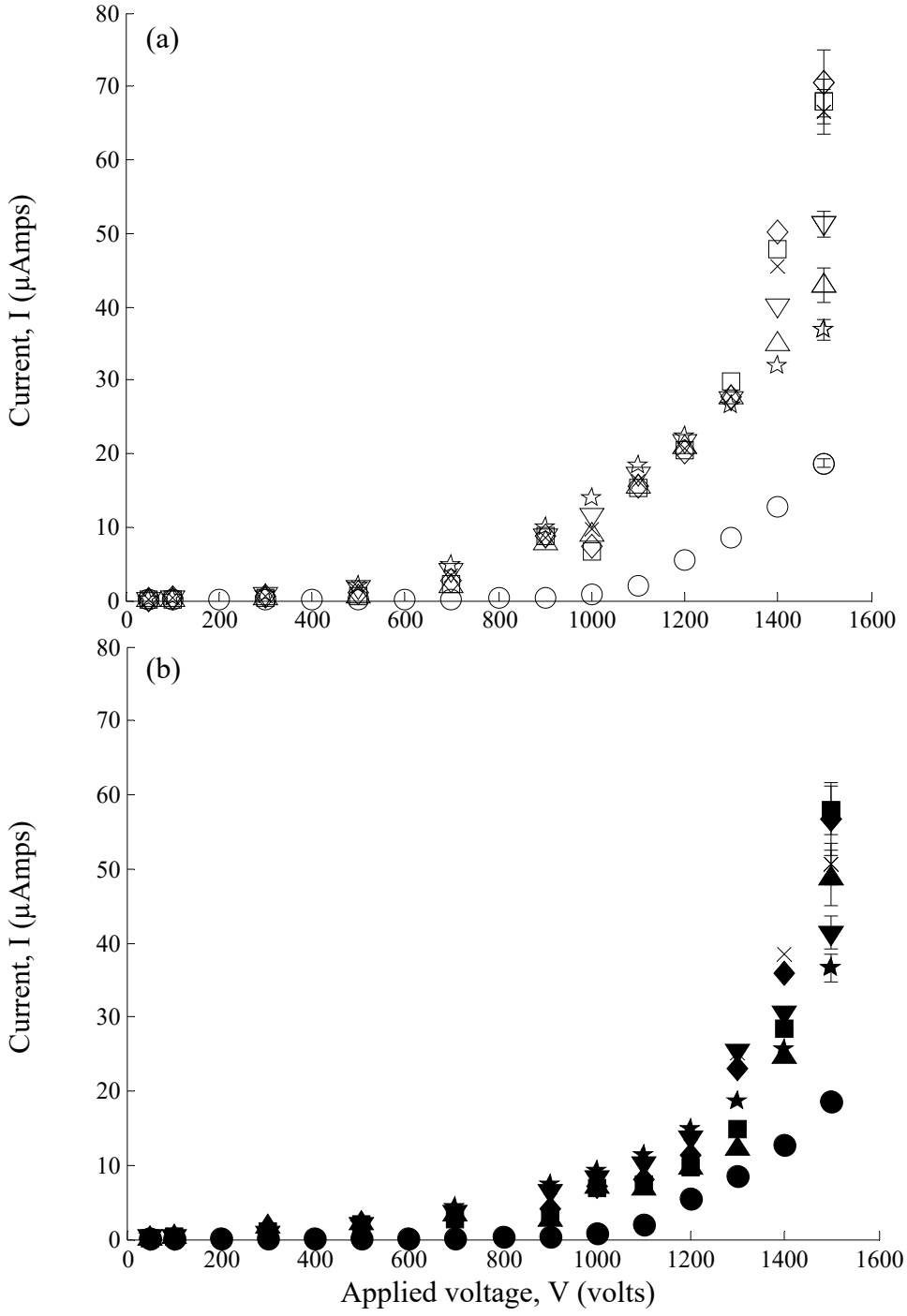

Fig. 6.2: Discharge characteristics in HFE 7100 with applied DC voltage at *Re* of: (circle) 0, (triangle) 1.31, (square) 2.61, (diamond) 5.19, (cross) 7.85, (down point triangle) 10.43 and (pentagon) 13.1. (a) Open symbols for co-flow and (b) filled symbols for counter-flow direction.

The external flow increases the current in both the conduction and injection regime, as found previously [3]. The total current density within the conduction regime can be expressed as [12]

$$j = \sigma E + qw \qquad (6.1)$$

while the total current density within the injection regime, ignoring diffusion, can be expressed as [12]

$$j = q(w + kE) \qquad (6.2)$$

The components σE, qw and qkE in equation (1) & (2) represent current due to conduction, convection and migration/ionic mobility respectively; where j is the total current density, σ the electric conductivity of the bulk liquid, q the charge density, w the fluid local velocity due to the application of electric field E and k the true ionic mobility. In this study, there is an additional external flow velocity (W) set by the external pump and equation (6.1) & (6.2) can be modified for conduction and injection regimes as

$$j = \sigma E + q(w \pm W) \qquad (6.3)$$

$$j = q(w \pm W + kE) \qquad (6.4)$$

As the liquid motion (w) set by the applied electric field (E) flows in the direction of ion motion [1], the external velocity (W) in equation (6.3) & (6.4) is positive for the co-flow case and negative for the counter-flow case. It is evident from Fig 6.2 that, within the conduction regime the total current at a given Reynolds number increase as the applied electric field increases. This is due to the increase in the conduction current component in equation (6.1) and (6.3). The current for the co-flow fluid direction was found to be

smaller than the counter-flow direction within the conduction regime and shown for 100, 300 and 500V in Fig 6.3 as an example (deduced from Fig 6.2 (a) & (b)). It was expected according to equation (6.3) that co-flow (+*W*) would result in a higher magnitude in the convection current compared to the counter flow direction (-*W*), which was not observed for the conduction regime. Within the conduction regime the total current increases with an increase in *Re* for the co-flow direction and approaches a limiting value. For counter-flow, there is an initial increase in the total current with liquid flow with a subsequent decrease and approaches a limiting value.

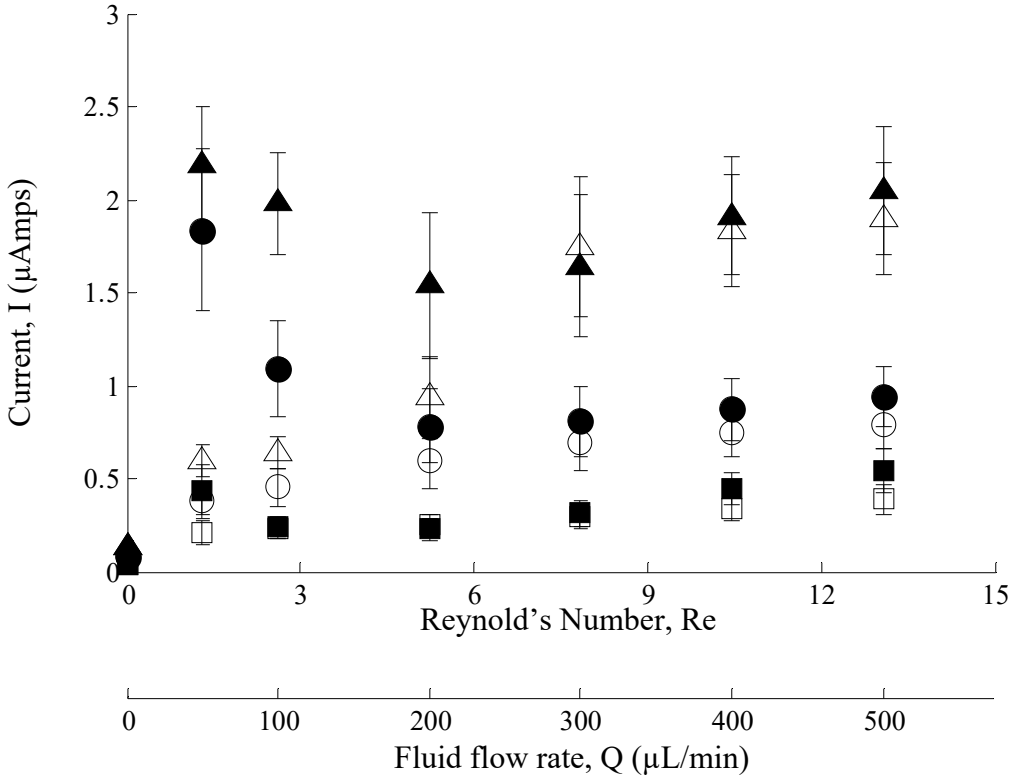

Fig. 6.3:Discharge current at different flow rates within conduction regime. (square) 100V, (circle) 300V and (triangle) 500V. Open symbols represent co-flow, filled symbols represent counter-flow.

For the injection regime ($V > V_{th}$): the migration component (qkE in equation (6.2) & (6.4)) occurs due to the motion of ions relative to the bulk fluid with velocity KE, under an applied field (E). Under the unipolar charge assumption (i.e., charge injection from one electrode), this component represents the motion of free ions due to charge injection through the metal/dielectric interface [12]. Within the injection regime the discharge current was greater for co-flow ($+W$) compared to the counter-flow ($-W$) case (Fig 6.4), as expected according to equation (6.4). At very high applied voltage (e.g., 1300, 1400 and 1500 V) there exists an optimal flow velocity to generate a maximum current as shown in Fig 6.4. The presence of optimum flow velocity within the injection regime could be an indication of the hydraulic change in flow regime from laminar to turbulent. It was suggested for unipolar injection that there exists a critical Reynolds number of 10 [13, 14] beyond which EHD instability occurs.

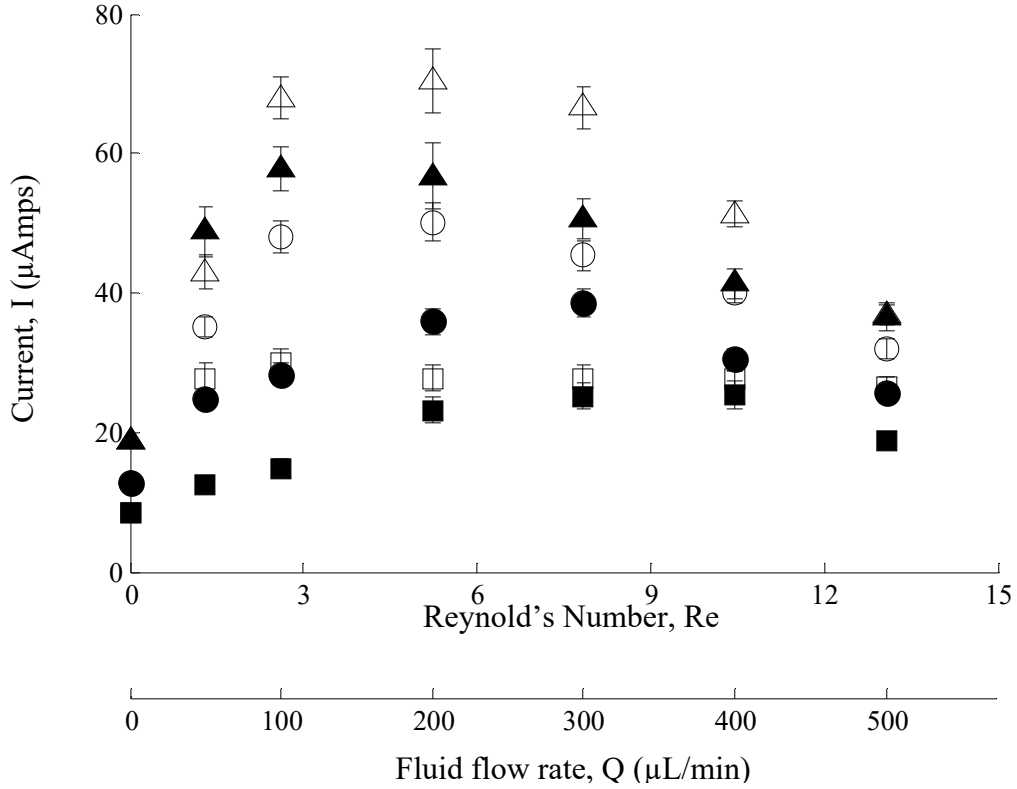

Fig. 6.4: Discharge current at different flow rates within injection regime. (square) 1300V, (circle) 1400V and (triangle) 1500V. Open symbols represent co-flow, filled symbols represent counter-flow.

6.4 Conclusions

Experiments were performed to study the effect of external fluid flow on the discharge characteristics in a dielectric liquid with an interdigitated planar electrode configuration. The experimental cell was 100 μm high, 5 mm wide and 50 mm long microchannel. The interdigitated planar electrodes consist of two sets of electrodes: the emitter and collector electrodes, which were 20 and 40 μm wide respectively, with inter-electrode spacing of 120 μm. HFE 7100 was used as the working fluid. Experiments were performed for a Reynolds number ranging from 0 to 13.1 with the fluid flowing both along and opposite to the electric field. It was found that the total current increased for any applied voltage with an external flow compared to the static case. The threshold voltage for the onset of charge injection decreased for any flow velocity case except for Re = 1.31 at counter–flow direction. In general, the total current increased as an increase in the *Re*, with an optimum *Re* to generate a maximum current at very high voltages within the injection regime.

6.5 References

1. Gray, E. and T. Lewis, *The effects of liquid motion on ion mobility measurement in hexane.* British Journal of Applied Physics, 1965. **16**(7): p. 1049.
2. Coe, G., J. Hughes, and P. Secker, *High-current injection into liquid hexane using field emitters.* British Journal of Applied Physics, 1966. **17**(7): p. 885.
3. Miyao, H., M. Higaki, and Y. Kamata, *Influence of AC and DC fields on streaming electrification of transformer oil.* Electrical Insulation, IEEE Transactions on, 1988. **23**(1): p. 129-135.
4. Metwally, I., *Flow electrification of transformer oil effects of mixed fields.* Dielectrics and Electrical Insulation, IEEE Transactions on, 1998. **5**(4): p. 518-526.
5. Yuan, G., et al. *The effect of DC field on streaming electrification in converter transformer*. in *Strategic Technology (IFOST), 2011 6th International Forum on*. 2011: IEEE.
6. Leblanc, P., et al. *Impact of an DC electric field on the charge accumulation at the pressboard/oil interface*. in *Dielectric Liquids (ICDL), 2014 IEEE 18th International Conference on*. 2014: IEEE.
7. Jaworek, A. and A. Krupa, *Corona discharge from a multipoint electrode in flowing air.* Journal of electrostatics, 1996. **38**(3): p. 187-197.
8. Kazemi, P.Z., P.R. Selvaganapathy, and C.Y. Ching, *Electrohydrodynamic micropumps with asymmetric electrode geometries for microscale electronics*

cooling. IEEE Transactions on Dielectrics and Electrical Insulation, 2009. **16**(2): p. 483-488.

9. Schmidt, W., *Electronic conduction processes in dielectric liquids.* IEEE transactions on electrical insulation, 1984. **5**(EI-19): p. 389-418.
10. Butcher, M., et al., *Conduction and breakdown mechanisms in transformer oil.* IEEE transactions on plasma science, 2006. **34**(2): p. 467.
11. Russel, M., P. Selvaganapathy, and C. Ching, *Effect of electrode surface topology on charge injection characteristics in dielectric liquids: An experimental study.* Journal of electrostatics, 2014. **72**(6): p. 487-492.
12. Chang, J.-S., A.J. Kelly, and J.M. Crowley, *Handbook of electrostatic processes*. 1995: CRC Press.
13. Lacroix, J., P. Atten, and E. Hopfinger, *Electro-convection in a dielectric liquid layer subjected to unipolar injection.* Journal of Fluid Mechanics, 1975. **69**(03): p. 539-563.
14. McCluskey, F. and P. Atten, *Modifications to the wake of a wire across Poiseuille flow due to a unipolar space charge.* Journal of Fluid Mechanics, 1988. **197**: p. 81-104.

Chapter 7

Summary and Conclusions

7.1 Summary and Conclusions

In this thesis, methods of enhancing the performance of ion drag electrohydrodynamic (EHD) micropumps have been investigated. An approach to reduce the energy barrier between the metal electrode and dielectric liquid has been adopted to inject charges at lower applied electric voltage. This was performed either by modifying the electrode surface topology or by adding a doping agent to the dielectric liquid. Another approach investigated was to use a pulsed voltage to exploit the displacement current due to the sudden change in voltage levels.

A fundamental study of the discharge characteristics in HFE 7100 as dielectric liquid was performed for different electrode surface topology while keeping the nominal inter-electrode spacing the same. A copper rod was used as the electrode and its surface was modified by chemical etching or by depositing single walled carbon nanotubes (SWCNT) to generate electrodes with different sharpness and roughness. Experiments were performed for both field emission and field ionization and better performance was observed for the former mode. Sharpness of the electrode surface was dominant over its roughness on enhancing the charge injection. Presence of sharp features generated much higher current at very low applied voltages. A significant reduction in the threshold voltage for the onset of charge injection (factor of ~ 5) was observed with SWCNT

deposited electrodes. This methodology of developing electrodes with nano features was then applied to an ion drag EHD micropump where SWCNT was deposited on the emitter electrodes while keeping the collector electrodes smooth. Two pumps with inter-electrode spacing of 120 and 40 μm were tested. The threshold voltage for these pumps reduced by a factor of 3 and 1.4 respectively, compared to the corresponding pump with smooth electrodes. Pump performance in terms of static pressure, flow rate and input power was improved. In particular, the enhancement factors in static pressure and flow rate at no back pressure condition were 5 and 3 respectively for the pump with inter-electrode spacing of 120 μm. The highest static pressure generated by the pump with inter-electrode spacing of 40 μm is 4.7 kPa at an applied voltage of 900 V. In an attempt to reduce the energy barrier between the electrodes and the dielectric, a redox doping agent, Ferrocene was diffused into the working fluid HFE 7100. Doping Ferrocene increases the charge availability within the base liquid by giving an electron via redox reaction while retaining its molecular structure without decomposition. Different levels of doping was tested and a generic trend of performance improvement was observed as the level increased. The onset of charge injection reduced as the doping increased. A maximum static pressure of 6.7 kPa was generated at 700 V with 0.2% Ferrocene, which is over an order of magnitude increase compared to no doping. The generation of 6.7 kPa of static pressure is the highest pressure generated to date. A flow rate at no back pressure condition of 0.47 mL/min at 700 V was achieved with 0.05% doping agent, an enhancement of a factor of 9 compared to no doping. It was found from the pump curves

that, the overall pump performance at different back pressure conditions was significantly better when the doping agent was added.

The effect of pulsed voltage, within the conduction and injection regime of the micropump, was studied. The ion drag EHD micropump under study performed significantly better at very low pulse repetition rates. An optimum pulse repetition rate to generate maximum pressure was found for different pulse levels of voltages. The maximum pressure at that pulse repetition rate was significantly greater compared to the average of the associated DC level static pressure. For example the static pressure was enhanced by about 70% for pulse between 700 and 800 V at the optimum pulse repetition rate of 0.1 Hz. Duty cycle was found to have an effect on the static pressure as well. For the aforementioned pulse level an enhancement of about 88% in static pressure was observed at the optimum duty cycle of 65%.

An experimental study on the effect of external flow on charge injection was studied at different flow rate ($0 \leq Re \leq 13.1$) and applied DC voltage. This study is of interest for applications where an external pump is used to flow dielectric liquid through a microchannel with embedded electrodes deposited on the floor of the channel. In that application the EHD micropump will act as a microchannel and a secondary pump. The threshold voltage for the onset of charge injection reduced for $Re > 0$. An increase in the current was observed when external flow was induced. Within the injection regime a maximum current at an optimum flow rate was observed.

7.2 Research Contributions

The contributions of this thesis can be summarized as:

1. A fundamental study of surface topology of the electrode on the discharge characteristics in a dielectric liquid was performed. Surfaces were created by polishing, chemically etching and by depositing SWCNT on the smooth or etched surfaces and were characterized. An enhancement in the discharge characteristics for electrodes with sharp features was observed. The threshold voltage for the onset of charge injection was significantly reduced. This is the first ever experimental study of discharge characteristics of sharp asperities performed in dielectric liquid.
2. The surface topology study was applied to an ion drag EHD micropump. SWCNT was deposited on gold electrodes to generate surface with sharp asperity. Use of such 3D electrode in a micropump is unique and improvement of previous studies such as micro-pillars or 3D bumps. This deposition technique is also easier compared to previous microfabrication methods to create 3D features and produces higher static pressure than those reported previously.
3. The effect of doping agent in dielectric liquid was studied to improve ion drag EHD performance further. A redox dopant, Ferrocene, was diffused into the dielectric liquid to enhance the injection strength and EHD mobility. Three different doping levels were studied and better pump performance was

observed for higher doping level. The static pressure generated in this study superseded all previously reported values.

4. The effect of pulsed voltage on charge injection and pump performance was studied to exploit the displacement current due to the sudden change in the voltage levels. Experiments were performed for both conduction and injection regimes. A range of pulse repetition rate and duty cycle was found to generate higher static pressure compared to average of the DC voltage levels.
5. The effect of external flow on discharge characteristics has been studied for Reynods number ranging from 0 to 13.1. An increase in current and a decrease in threshold voltage was observed for external flow. Within the injection regime an optimum flow rate to produce maximum current was observed.

7.3 Recommendations for Future Work

In this study several ways to enhance the pump performance had been studied. Additional experiments to study the surface topology with other sharp features such as multi-walled carbon nanotube (MWCNT) or graphene can be performed. The effect of combining the parameters studied in this thesis, e.g., modified surface topology, addition of doping agent into the dielectric liquid and application of pulsed voltage is expected to enhance the pump performance further and needs to be experimentally confirmed. An integrated cooling system incorporating the micopumps developed in this thesis to a heat

sink/exchanger to study the overall system performance will be helpful to validate their practical application.